Dissertation zur Erlangung des Doktorgrades

der Fakultät für Chemie und Pharmazie

der Ludwig-Maximilians-Universität München

Investigation of the roles of cyclic AMP dependent regulation of the hyperpolarization-activated cyclic nucleotide-gated type 4 channel in neuronal circuits

Jennifer Katherine Kass

aus

New Westminster, Canada

2021

Erklärung

Diese Dissertation wurde im Sinne von § 7 der Promotionsordnung vom 28. November 2011

von Herrn Prof. Dr. Martin Biel betreut.

Eidesstattliche Versicherung

Die Dissertation wurde eigenständig und ohne unerlaubte Hilfsmittel erarbeitet.

München, den 02.12.2021.   _____

                                                                    Jennifer Kass

Dissertation eingereicht am 02.12.2021

1. Gutachter: Prof. Dr. Martin Biel

2. Gutachterin: Prof. Dr. Susanne Koch

Mündliche Prüfung am 17.01.2022

1 Introduction

Heartbeats, muscle twitches and lightning fast thoughts are all products of bioelectricity and require membrane proteins called ion channels. The basic function of an ion channel can be distilled down to, 'The hole opens. Ions go through. The hole closes' (Isacoff et al., 2013). Ion channel proteins in cellular membranes open and close in response to various electrical and chemical stimuli, allowing cells to tap into the energy stored in transmembrane ionic gradients to generate the electrical signals that serve as the basis for nerve and muscle conduction (Faber and Pereda, 2018). Studies of the key mechanisms by which these processes happen, and the pathophysiological consequences of ion channel dysfunction called 'channelopathies', remain a central focus in the field. One might wonder after years of detailed poking and prodding at what may seem like a simple process, is there anything left to learn? The answer is overwhelmingly yes. The ion channel field is vast and great progress has been made in understanding how ion channels 'gate their pores' (Isacoff et al., 2013). However, several key questions remain unsolved in the field, for example: (1) understanding the voltage sensing mechanism, which is central to understanding neuronal signaling, (2) the transformation from cartoon models to a three dimensional understanding of the molecular nature of ion channels, (3) how the multicomponent protein complexes of ion channels are assembled and delivered to the right place in cells, and (4) how ion channels function in neuronal circuits.

Cryo-electron microscopy (EM) has triggered a recent revolution in ion channel research as cryo-EM can capture the full range of a protein's conformational states and produce structures at near atomic resolution (Lau et al., 2018). Cryo-EM has been used in probing questions one and two, as it has been used in recent studies to investigate the voltage sensing modes in K_V and Na_V channels (Lee and MacKinnon, 2017; Tao and MacKinnon; 2019, Jiang et al., 2021). Additionally, cryo-EM structures can provide visualization of bound small-molecule ligands which has had a profound impact on drug discovery, in investigating the mechanism of action of drugs, and by aiding in the development of new compounds (Van Drie and Tong, 2020). In regards to question number three, several point mutations in K_V and Na_V channels that are associated with epilepsy have been shown to be linked to trafficking defects resulting in degradation of the channel early in the trafficking process (Vacher and Trimmer, 2012; Balse and Boycott, 2018). Continued pursuit of these questions is indispensable for developing new methods to manipulate channel function, for both fundamental research, and for the development of new drugs to treat channelopathies.

1.1   Hyperpolarization activated cyclic nucleotide gated channels

Of particular interest in the present work is question number four, and the family of ion channels regulating pacemaker activity in neurons, the hyperpolarization-activated cyclic nucleotide-gated (HCN) channels.   The first characterizations of the hyperpolarization activated current in the heart were reported in the late 1970's (Noma et al., 1976; Brown et al., 1979a; Brown et al., 1979b) and in neurons in the early 1980's (DiFrancesco, 1981; Halliwell et al., 1982). However, it wasn't until nearly twenty years later when HCN channels were cloned and identified as the molecular correlate of the hyperpolarization activated current (Ludwig et al., 1998; Santoro et al., 1998; Gauss et al., 1998).

HCN channels conduct a mixed Na^+/K^+ current which is termed I_h in neurons (Halliwell et al., 1982), and I_f in heart sinoatrial node cells (Brown et al., 1979).   Unlike most cellular conductances which are activated by membrane depolarization, I_h is activated by membrane hyperpolarization at potentials negative to -55 mV.   This is near the resting membrane potential (RMP) of most neurons and therefore channels are partially open at rest.   The ratio of Na^+ to K^+ permeability of HCN channels (P_{Na}:P_K) ranges between 1:3 to 1:5 with values of the reversal potential ranging between -25 to -40 mV under physiological conditions (Tian and Shipston, 2000; Aponte et al., 2006).   As a result, I_h is an inwardly directed current mainly carried by Na^+ at rest, and therefore depolarizes the membrane (Biel et al., 2009).   Voltage dependent activation and deactivation of I_h, actively opposes deviations away from the RMP, which can be attributed to the reversal potential of I_h falling close to the base of its activation curve.   In an effect called the depolarizing voltage sag, the activation of HCN channels at hyperpolarized membrane potentials causes a depolarizing inward current, driving the membrane potential towards the reversal potential of I_h and close to the initial value of the RMP (Mayer and Westbrook, 1983).   Because of these properties, I_h is important for the determination of the resting membrane potential and provides a mechanism to limit both hyperpolarizing and depolarizing currents in neurons.   Consequently, I_h is involved in dampening both excitatory and inhibitory stimuli arriving at the neuron (Atherton et al., 2010).

Another key feature of I_h is that its activation is dually regulated by cyclic nucleotides in addition to voltage.   Membrane hyperpolarization is sufficient and necessary for channel activation, however its activation is also facilitated by the cyclic nucleotides 3',5'-cyclic adenosine monophosphate (cAMP) and 3',5'-cyclic guanosine monophosphate (cGMP). Neurotransmitters and hormones which increase cAMP levels facilitate the activation of I_h by shifting the half-maximal activation ($V_{0.5}$) values to more positive values and accelerate the kinetics of channel opening (Tokimasa and Akasu, 1990; DiFrancesco and Tortora, 1991).

The acceleration of channel opening can be attributed to the depolarizing shift in the $V_{0.5}$ (Wainger et al., 2001). Conversely, a decrease in cAMP levels shifts $V_{0.5}$ values to more negative voltages. HCN4 channels show the slowest activation kinetics, and the highest sensitivity to cAMP compared to the other HCN channel isoforms (HCN1-4) (Schweizer et al., 2010). cAMP binds HCN channels directly via the cAMP nucleotide binding domain (CNBD) located on the cytosolic C-terminus (COOH) of HCN channels (DiFrancesco and Tortora, 1991). This is in contrast to other ion channels which are regulated by cAMP through protein kinase A (PKA) mediated phosphorylation such as the $K_V4.2$, $K_V2.1$ and the calcium activated BK channels (Kim and Park, 2008). However, it has been shown that HCN2 is also directly phosphorylated by the cGMP-dependent protein kinase II (cGKII), and shifts the $V_{0.5}$ to more negative voltages counteracting the stimulatory action of cyclic nucleotides conferred by the CNBD (Hammelmann et al., 2011).

1.2 HCN channel structure

HCN channels, together with cyclic nucleotide-gated (CNG) and the Eag-like K^+ channels, form the subgroup of cyclic nucleotide-gated cation channels within the large superfamily of the pore-loop cation channels. There are four isoforms in the HCN channel family (HCN1-4). HCN channels are composed as tetramers and can occur as homo- or heterotetramers. Each monomeric subunit consists of three structural domains: the cytosolic N-terminus, the transmembrane core, and the cytosolic C-terminus, shown in Figure 1. The transmembrane core consists of six transmembrane α-helical segments (S1-S6). The S4 segment functions as the voltage sensor and has nine arginine or lysine residues spaced at every third position (Vaca et al., 2000). Positively charged S4 segments are found in all members of the voltage dependent pore-loop cation super family (Catterall et al., 2010). It has been thought that the inward movement of S4 leads to the opening of HCN channels, which is in contrast to other ion channel families activated by depolarization such as the K_V and Ca_V channel families where the inward movement of S4 leads to channel closing (Männikkö et al., 2002). However, it remains unclear how the inward S4 movement opens HCN channels in response to hyperpolarization. A recent study examined whether two conserved residues in the HCN channel family E356 and N370, which are located at the interface between S4 and S5 in the cryo-EM hHCN1 structure, are important in S4 movement. The authors suggest that the main S4 movement is required but not sufficient to open the gate (Wu et al., 2021). The authors propose that S4 moves in two steps and that channel opening is favoured by the second S4 movement (Wu et al., 2021). HCN channels also do not show

voltage dependent inactivation, which is also in contrast to other ion channel families such as the Ca$_V$ channel family and Na$_V$ channel family.
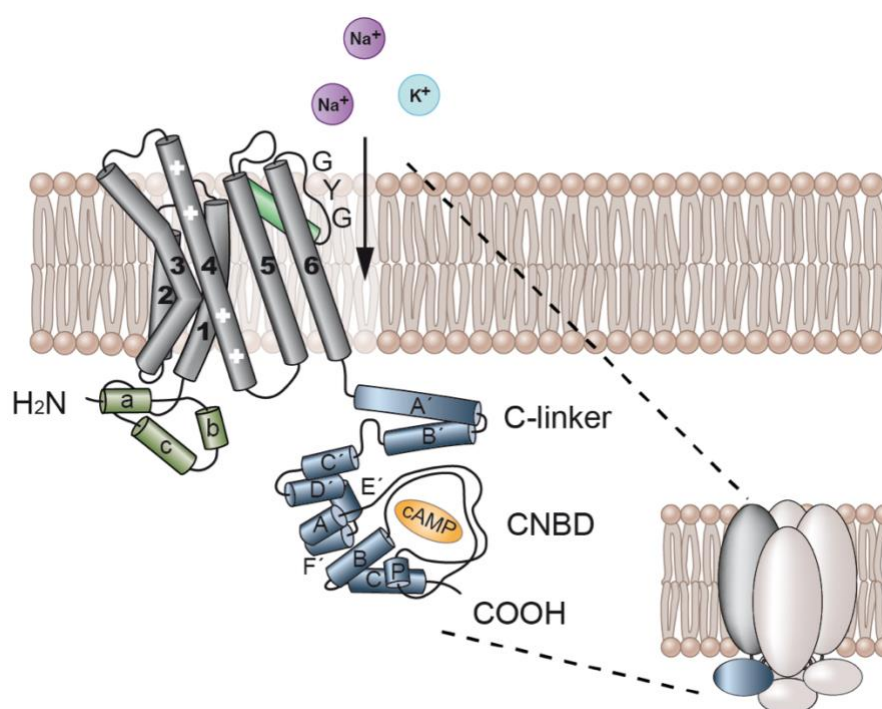

Figure 1. The structure of HCN channels. HCN channels are composed as tetramers (homo- or heterotetramers). Each monomer consists of six α-helical transmembrane segments S1-S6 (grey) and the intracellular N- and C-termini. Helices S1-S4 form the voltage-sensing domain containing the voltage sensor S4, which carries positively charged arginine or lysine residues (+) at every third position. S5, S6 and the pore helix (green) form the channel pore, which contains the selectivity filter GYG. The C-terminal region (blue) is composed of the C-linker which consists of six α-helices (A'-F'), and the CNBD, which consists of three α-helices (A-C) with a β-roll between the A- and B- helices. Binding of cAMP induces a conformational change which facilitates channel opening. The image is adapted from Hennis et al., 2021.

The pore region consists of the pore helix, S5 and S6, and contains the selectivity filter carrying the glycine-tyrosine-glycine (GYG) motif. The GYG motif is also found in highly selective K$^+$ channels (the K$_V$ channel family) and forms the selectivity filter specific for K$^+$ (Doyle et al., 1998). This was a particularly surprising discovery given that HCN channels carry an inward Na$^+$ current under physiological conditions, although the channels show higher permeability to K$^+$ over Na$^+$. This conundrum was recently solved in 2017, through single-particle cryo-EM comparing the selectivity filter of the human HCN1 channel, with the selectivity filter of the prokaryotic KcsA channel. It was found that the selectivity for K$^+$ arises from the precise geometry of the selectivity filter of the GYG motif, in which K$^+$ ions are coordinated by carbonyl oxygen atoms forming four binding sites (Lee and MacKinnon, 2017). However, in HCN channels, the tyrosine side chain in the GYG motif is re-orientated 180°. This causes the carbonyl oxygen atoms which form two of the binding sites for coordinating K$^+$, to no longer be in the ion binding pathway (Lee and MacKinnon, 2017). Thus, the

differences in ion selectivity can be explained by the differences in the orientation of amino acids (aa) in the GYG motif between HCN channels and K_V channels, explaining permeability to Na^+.

The cytosolic COOH-terminal channel domain is composed of the C-linker and the CNBD (Figure 1). The C-linker is 80 aa long, and connects the CNBD which is ~120 aa long, with the S6 segment. The C-linker is composed of six -helices (A'-F') (Figure 1). The CNBD is evolutionarily conserved with CNG channels, and is composed of a highly conserved α-helix, followed by an eight-stranded β-roll, a short B-helix, and a long C-helix (Zagotta et al., 2003).

1.3   Regulation of HCN channels via the N- and C- termini

Regulation of HCN channels by cAMP is mediated through the CNBD. The cAMP binding pocket in the CNBD is formed by several aa residues at the interface of the β-roll and C-helix. In the HCN2 channel, R591 and T592, within the β-roll, are responsible for the high affinity binding of cAMP, and these arginine and threonine residues are highly conserved in the HCN channel family (Zhou and Siegelbaum, 2007). Additionally, it has been found in CNG channels that three aa in the C-linker region, I439V, D481A and D494S, are major determinants of the affinity of the channel for cAMP, and therefore channel gating (Zong et al., 1998).

Regulation of HCN channels also occurs via the distal C-terminus. Tetratricopeptide repeat-containing Rab8b interacting protein (TRIP8b) is a brain specific auxiliary subunit of HCN channels, which can differentially regulate the gating, surface expression and trafficking of HCN channels in a subtype-specific manner (Santoro et al., 2004; Zobeiri et al., 2018). TRIP8b contains a ~350 aa tetratricopepide repeat (TPR) protein binding domain, which interacts with the SNL (serine-asparagine-leucine) tripeptide in the C-terminus of HCN1, -2, and 4 (Santoro et al., 2004). It has been found that this interaction site is necessary and sufficient to enable TRIP8b to inhibit channel activation and downregulate channel surface expression (Santoro et al., 2011). It has also been found that TRIP8b also interacts through a second interaction site, in which a conserved middle region of TRIP8b interacts at the border region of the C-linker and the CNBD in HCN1 channels (Lewis et al., 2009). This interaction site stabilizes the C-terminal domain of TRIP8b, allowing for the optimal interaction between HCN1 and TRIP8b (Santoro et al., 2011). An 80 aa fragment within the core of TRIP8b has

also been found to be sufficient to inhibit the action of cyclic nucleotides to facilitate HCN1 channel opening (Santoro et al., 2011).

Less is known about regulation of HCN channels via the N-terminus. A recent study examining the role of the N-terminal HCN channel domain, suggests that the N-terminal region serves to transmit the conformational change induced by cAMP binding to the transmembrane voltage sensing domain (Porro et al., 2019). It has also been found from HCN1 channels in photoreceptors, that the N-terminus contains a 20 aa region containing a leucine-based endoplasmic reticulum export motif, which can redirect a membrane reporter from outer segments to the plasma membrane of the inner segments of photoreceptors (Pan et al., 2015).

1.4 Distribution of HCN4 and HCN2 channels in the central nervous system

Expression of the HCN2 channel is abundant in the CNS while the HCN4 channel is expressed in specific subsets of regions. Western blot analysis has previously shown that HCN2 is expressed in the somatosensory cortex (SSC) and in several thalamic nuclei: the posterior thalamic nucleus (POm), the ventrobasal complex (VB) the dorsal lateral geniculate nucleus (dLGN) and centromedial (CM) thalamus. In contrast, HCN4 was detected in the VB and PO. This result has also been confirmed in immunohistochemical staining, in which HCN2 was highly expressed in the SSC and thalamus, while HCN4 was only highly expressed in the thalamus (Zobeiri et al., 2018). In addition, it has been shown in independent studies that in thalamocortical (TC) neurons, HCN4 has a dendritic staining pattern while HCN2 is expressed in the somata and dendrites (Zobeiri et al., 2018; Hammelmann et al., 2019). In line with these results, another study examining the expression of HCN channels in the mouse brain using the RNAscope® fluorescent multiplex assay, also identified HCN4 mRNA in vesicular glutamate transporter type 2 (VGlut2)-positive excitatory neurons which was always co-expressed with HCN2 mRNA in the thalamus, except for the reticular thalamic nucleus (nRT) which did not express HCN4 mRNA (Oyrer et al., 2019). Giant cholinergic interneurons in the striatum also co-expressed high levels of HCN4 mRNA and HCN2 mRNA. HCN4 mRNA was also highly expressed in the medial and lateral habenula while HCN2 mRNA was not expressed (Oyrer et al., 2019). In contrast, the cortex, amygdala and hippocampus expressed low levels of HCN4 mRNA, while HCN2 was highly expressed. (Oyrer et al., 2019).

1.5   Roles of I_h in the central nervous system

The unique biophysical features of I_h are essential in regulating excitability in neurons. HCN channels are partially open at rest and are important in setting the resting membrane potential. Therefore, HCN channels provide negative feedback as they can counteract both membrane depolarization and hyperpolarization. Consequently, I_h is involved in numerous neurophysiological functions in the CNS including dendritic integration (Harnett et al., 2015), synaptic transmission (Park et al., 2011), motor learning and spatial working memory (Nolan et al., 2003), and notably in the sustained rhythmic neural oscillations in TC networks and hippocampal dependent networks (McCormick and Bal, 1997; Biel et al., 2009). These oscillations arise from the synchronized activity of neurons and are thought to have a key role in information processing in neuronal networks (McCormick and Bal, 1997).

1.6   The thalamus and the thalamocortical network

The thalamus is divided into the dorsal thalamus (referred to simply as the thalamus), and the ventral thalamus (also known as the sub thalamus). The VB complex of the thalamus is comprised of two first-order nuclei, which are responsible for relaying somatosensory signals to the cortex: the ventral posteromedial nucleus (VPM) containing afferents from the face and neck, and the ventral posterolateral nucleus (VPL) which contains afferents from the rest of the body (O'Reilly et al., 2021). The VPL and VPM receive their peripheral inputs through various pathways (i.e. the lemniscal, extralemniscal and paralemniscal pathways) (Haidarliu et al., 2008). Other thalamic nuclei such as the nucleus submedius and ventromedial nucleus also receive somatic input, notably for nociception and sensorimotor integration (Monconduit et al., 1999).
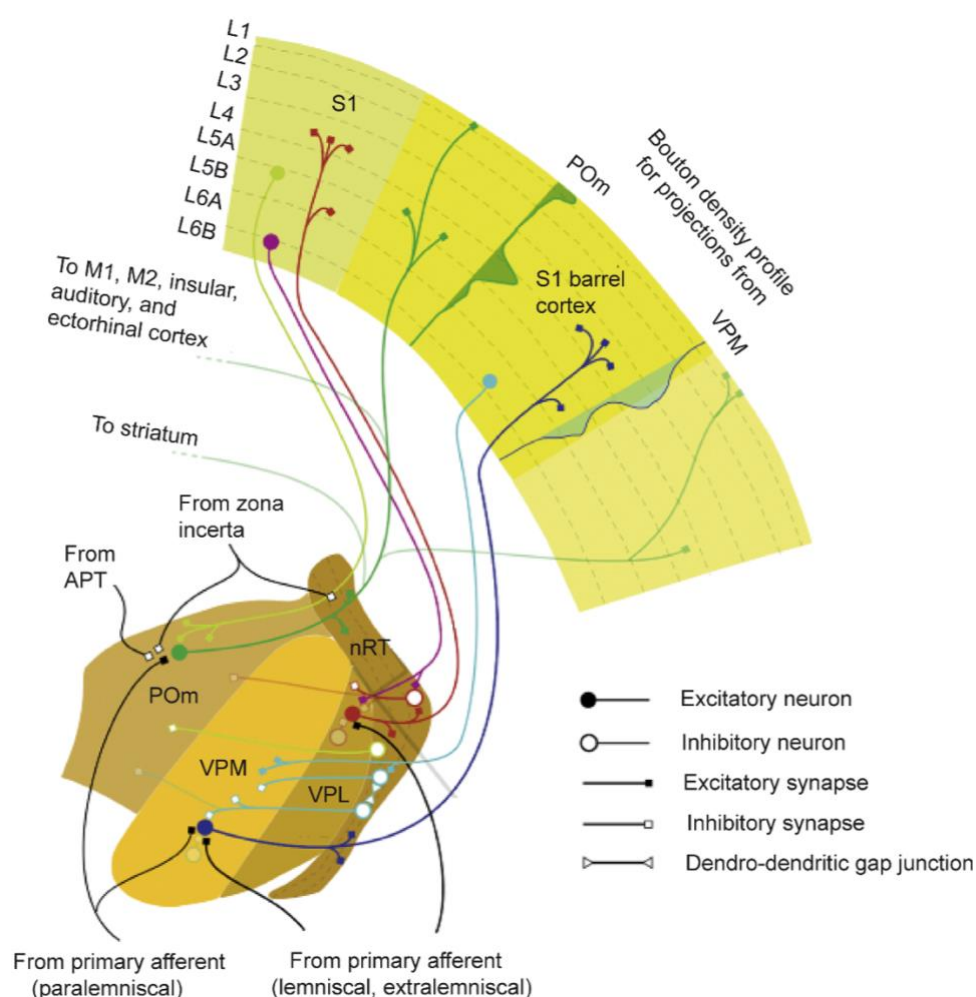
Figure 2. Overview of the key features and primary pathways of the somatosensory TC circuit in rodents. The rodent VB is composed mainly of excitatory TC neurons which primarily innervate layer 4 (L4) and to some extent L2-3 and L5b-6, of the primary somatosensory cortex (S1). Additionally, it projects to the inhibitory nRT of the ventral thalamus. TC signals are amplified and further processed in complex cortical microcircuitry, and are also fed back directly to the thalamus via monosynaptic pathways. Cortical L5 and L6 pyramidal cells close the TC loop by projecting to their initial first order nuclei, the VPL or VPM, and the associated higher order nuclei, namely the POm for the somatosensory system. These also project to the nRT, which in turn generates inhibitory postsynaptic potentials (IPSPs) in the same nuclei (i.e. VPL, VPM, POm). The POm also receives inhibiton from extrareticular sources including the zona incerta and the anterior pretectal nucleus (APT), and excitation from the paralemniscal pathway. The image is adapted from O'Reilly et al., 2021.

For simplicity, the TC circuit is composed of three key loci. The first, is glutamatergic corticothalamic pyramidal neurons (CPN) in layers V/VI of the cortex, which project to both the nRT and to TC neurons. The second is glutamatergic TC neurons which project to CPN and nRT neurons. The third, is γ-aminobutyric acid (GABA)-ergic nRT neurons which project to TC neurons and also synapse with other neurons within the nRT (Cain et al., 2015). A more detailed overview of the TC somatosensory loop in rodents is given in Figure 2.

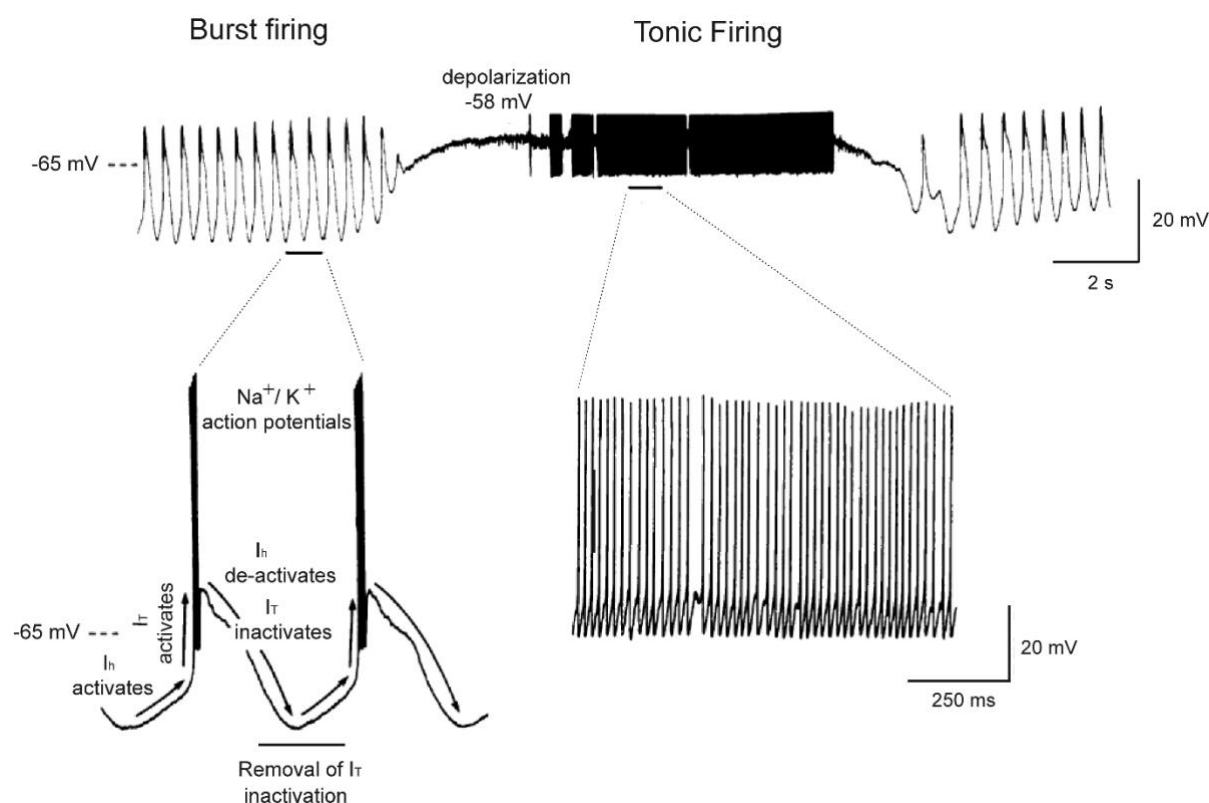### 1.6.1 Burst and tonic firing in the TC circuit

Figure 3. The mechanism of firing modes of TC neurons. *(Upper)* Example of a cat TC neuron in the dLGN at a RMP of -65 mV firing in the burst firing mode. A depolarizing current injection to -58 mV, switched the neuron to the tonic firing mode of action potential generation. Subsequent removal of the depolarization switched the neuron back to burst firing. *(Lower)* Expanded traces of the oscillatory activity and mechanism of the currents which largely mediate it. Activation of I_h at hyperpolarized potentials, subsequently activates the low threshold Ca^{2+} current (I_T) and depolarizes the membrane towards the threshold for a burst of Na^+ and K^+- dependent action potentials. The depolarization de-activates I_h. Repolarization of the membrane from I_T inactivation is followed by a hyperpolarizing overshoot, which in turn removes the inactivation of I_T and again activates I_h, which then depolarizes the membrane towards the threshold for another low threshold Ca^{2+} spike. The image is adapted from McCormick and Pape, 1990a.

In the TC network, neural oscillations are produced during sleep (vigilance) stages, sensory processing, and during seizures. I_h has a main role in the generation and maintenance of the delta frequency rhythm which is generated in single TC neurons (Steriade et al., 1994). The discovery first made by Jahnsen and Llinas in 1984 that TC neurons fire in two main firing modes termed the tonic (or transmission) mode and the burst mode, and also the involvement of a low threshold Ca^{2+} conductance (Jahnsen and Llinas, 1984a, b), lead to the understanding of the roles of I_h in these oscillations, and the mechanisms involved in the thalamic gating of sensory information (Steriade et al., 1987; McCormick and Pape, 1990a; McCormick and Bal, 1997). During the awake state and in rapid eye movement (REM) sleep, TC neurons are depolarized by afferent connections and gated from the thalamus to the

cortex, and neurons fire in the tonic firing mode which is characterized by single Na^+ channel spikes (McCormick and Bal, 1997). In the burst firing mode, which is seen during non REM (NREM) sleep or during epileptic discharges, neurons show a monotonous repetitive firing pattern at hyperpolarized potentials, and is considered to decrease the transfer of sensory information to the cortex. The burst firing mode is due to the close interaction of I_h with T-type voltage gated calcium channels (VGCCs) which conduct a current termed I_T (McCormick and Pape, 1990a; Steriade et al., 1993; Llinás and Steriade, 2006). The following model has been proposed as shown in Figure 3. Activation of I_h at hyperpolarized potentials more negative than -65 mV, depolarizes the membrane activating I_T and generates a low threshold Ca^{2+} spike (rebound burst firing), typically followed by a series of Na^+ spikes. I_T is inactivated at depolarized potentials, which terminates the low threshold Ca^{2+} spike, and I_h is also deactivated. The resulting hyperpolarizing overshoot removes the inactivation of I_T, activates I_h, and the cycle repeats thus sustaining rhythmic burst firing (McCormick and Pape, 1990a; McCormick and Hugenard 1992).

Burst firing in TC neurons is a characteristic feature accompanying the spike and wave discharges (SWDs) observed in electroencephalography (EEG) recordings during absence seizures (Danober et al., 1998). It is thought that during absence seizures, CPN and TC neurons are locked in a self-propagating oscillatory loop, at least partially due to the hyperpolarizing rhythmic and synchronizing drive (Seidenbecher and Pape, 2001). Burst firing itself is not a pathophysiological marker per se, however during absence seizures there is inappropriate switching from tonic firing to oscillatory burst firing, that is believed to play a role in the impairment of consciousness by interrupting incoming sensory information (Pinault and O'Brien, 2005).

1.6.2   Roles of HCN channels in the TC circuit

Studies from HCN2 knock out (KO) mice have shown that HCN2 constitutes the majority of I_h from TC neurons, with HCN4 being the other predominant component of I_h. In HCN2 KO mice, I_h in TC neurons was reduced approximately 80% and this was also associated with an approximate 12 mV hyperpolarizing shift in the RMP (Ludwig et al., 2003). TC neurons from HCN2 KO mice were also more susceptible to fire in the burst firing mode, and HCN2 KO mice exhibited spontaneous absence seizures indicated by SWDs in EEG recordings (Ludwig et al., 2003), thus demonstrating a key role of HCN2 channels in the TC circuit.

1.7   Roles of cAMP dependent regulation of I_h in the CNS

cAMP dependent regulation (CDR) of I_h has been shown to have a direct influence on several neuronal processes. These include effects on the RMP (Raes et al., 1997), firing of action potentials (Wang et al., 2002), in the transmission of inflammatory pain (Herrmann et al., 2017), the regulation of spatial periodicity of grid cells in the medial entorhinal cortex (Heys et al., 2012), in the control of working memory (Thuault et al, 2013), and in the coincidence detection of sound (Yamada et al., 2005). CDR of I_h has also been proposed to be involved in regulating thalamic network activity, and may be a mechanism in which neurotransmitters regulate the transition of firing modes, and therefore the activity state of the thalamus (McCormick and Pape, 1990b; McCormick, 1992). Neurotransmitter mediated alterations in the voltage dependence of I_h by serotonin (5-HT) and noradrenaline (NA), have previously been observed (McCormick and Pape, 1990b), and has been proposed to occur through coupling of $G_{\alpha s}/G_{\alpha i}$ to adenylyl cyclase and the corresponding increases or decreases in cAMP levels, respectively (McCormick, 1992; Heine et al., 2001; Frère and Lüthi, 2004).

Using an HCN2 knock-in mouse model expressing a mutant HCN2 channel with normal voltage dependent gating but unable to bind cAMP (HCN2EA), it has been shown in our lab that CDR of HCN2 is important in regulating the transition from burst to tonic firing in VB neurons (Hammelmann et al., 2019). In addition, HCN2EA mice showed altered NREM sleep, generalized absence seizures, and VB specific deletion of HCN2 but not HCN4 also induced these seizures (Hammelmann et al., 2019). TC neurons predominantly express HCN2 and HCN4, and while HCN2 channels were highly expressed in several thalamic nuclei of HCN2EA mice, expression of HCN4 was restricted to the VB thalamus (Hammelmann et al., 2019). These findings demonstrated that CDR of HCN2, is important for normal function of thalamic oscillations and preventing the appearance of absence seizures, but that the HCN4 channel is not involved in the mechanism of absence seizures. Less is known about the specific roles of HCN4 in the TC circuit, and was of interest to investigate in the current work.

1.8   Serotonin in the CNS

The neurotransmitter 5-HT is widely distributed in the CNS and is involved in a vast number of physiological functions including hormone secretion, sleep and circadian rhythm, motor control, immune system functioning, nociception, food intake, energy balance and social interactions (Bacqué-Cazenave et al., 2020). In addition, 5-HT also contributes to higher brain

functions, such as in cognition and regulating mood and emotions, where it has a role in synaptic plasticity (Jenkins et al., 2016).

There are fourteen 5-HT receptors, organized into seven sub-classes. They are metabotropic G-protein-coupled receptors (GPCRs) and modulate an intracellular second messenger system, which includes a direct effect of increasing or decreasing cAMP levels (Pithadia and Jain, 2009). The $5HT_1$ and $5\text{-}HT_5$ receptors are coupled to $G_{\alpha i}$, the $5HT_2$ receptors are coupled to $G_{\alpha q/11}$, and the $5HT_4$, $5HT_6$ and $5HT_7$ receptors are coupled to $G_{\alpha s}$. The only exception is the $5\text{-}HT_3$ receptor which is a ligand gated ion channel. The roles of the $5\text{-}HT_5$ receptors are largely unknown. The effects of the activation of 5-HT subtypes on cAMP levels, the localization of the receptors, and physiological roles and disorders associated with receptor dysfunction, are summarized in Table 1 in the Appendix.

1.8.1   Localization of 5-HT receptors

In several brain regions 5-HT is released diffusely through volume transmission and has been suggested to act as a neuromodulator, rather than a classical neurotransmitter (Ciranna, 2006). Serotonergic axons innervating the thalamus originate from the medial and lateral divisions of the dorsal raphe nuclei (DRN) and median raphe nuclei (MRN) (Figure 4). The distribution of fibers is not uniform, with the preferential targets being the midline and intralaminar nuclei, or the higher order nuclei, and the rest of the dorsal thalamus including the VPL and VPM, receiving sparse input (Varela et al., 2014). Less is known about serotonergic afferents to the thalamus, and the physiological effects on 5-HT in the thalamus, although effects of 5-HT on the thalamus have been implicated in several processes including the sleep-wake cycle, feeding behaviour, reward, motivation and stress (Petrovich, 2021; Ye and Zhang, 2021).
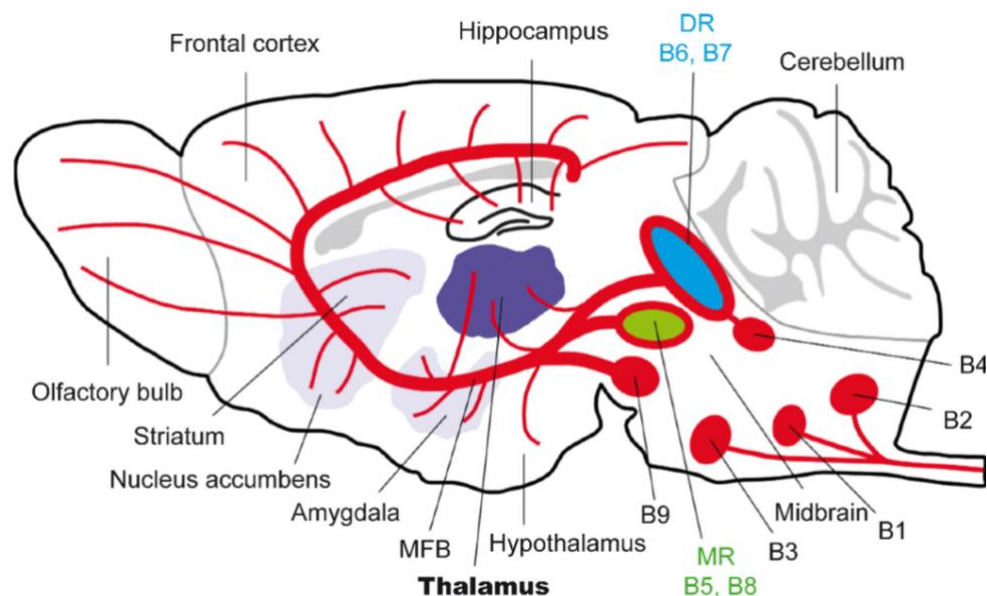
Figure 4. Main neuroanatomical structures which receive afferent 5-HT projections in the rodent brain. 5-HT neurons are clustered into nine nuclei numbered B1-9 (depicted in red) on a rostrocaudal axis. The more rostral raphe nuclei contain the DRN (B6 and B7; depicted in blue) and the MRN (B5 and B8: depicted in green) which project to several different but overlapping brain areas including the thalamus (dark purple). The more caudal nuclei (B1-B3) in the medulla project to the spinal cord and the periphery. MFB; medial frontal bundle. The image is adapted from Lesch and Waider, 2012.

1.8.2 Serotonergic regulation of I_h

Conflicting results have been reported as to whether serotonin exerts a hyperpolarizing or depolarizing effect on I_h in the thalamus. It was first reported by McCormick and Pape in 1990, that 5-HT along with NA, modulates thalamic burst firing by enhancing I_h, and that this enhancement of I_h is mediated by increases in intracellular cAMP (Pape and McCormick, 1990b). Application of NA in the absence of antagonists resulted in a slow depolarization and decrease in input conductance, which was blocked by the α_1 adrenergic receptor antagonist prazosin. Application of 5-HT (300 uM) to cat or guinea pig dLGN and medial geniculate neurons at its RMP (-60 to -68 mV) resulted in an increase in membrane conductance, and a small 1-3 mV depolarization in the I_h activation curve, resulting in the dampening or abolishment of rhythmic burst firing (Pape and McCormick, 1990b).

In 2002, Moncton and McCormick examined the effect of 5-HT on various thalamic nuclei including the lateral posterior, lateral dorsal, pulvinar, mediodorsal, central medial, ventral anterior, central lateral, VB, and medial geniculate nuclei. They found that the predominant action of 5-HT was hyperpolarization and inhibition of the tonic firing mode. Hyperpolarization of TC neurons was mediated via two mechanisms. The first mechanism

was via direct action through an increase in K^+ conductance mediated by the $5\text{-}HT_{1A}$ receptor, supported by the finding that the hyperpolarization persisted in the presence of tetrodotoxin (TTX), which blocks Na_V channels, and the block of GABAergic synaptic transmission (Moncton and McCormick, 2002). The response was antagonized by the $5\text{-}HT_{1A}$ antagonist WAY100635 and mimicked by the application of the $5\text{-}HT_{1A}$ agonist 8-OH DPAT (Moncton and McCormick, 2002). The second mechanism was via an indirect mechanism, through activation of local GABAergic interneurons. In slices where GABA receptors were not blocked by the $GABA_A$ antagonist bicuculline and the $GABA_B$ antagonist CGP35348, 5-HT increased the frequency and amplitude of IPSPs in TC neurons (Moncton and McCormick, 2002). These studies demonstrate that the effect of 5-HT on I_h in TC neurons is undoubtedly complex, but did not conclusively demonstrate that 5-HT exerts its effect on I_h through the CDR property of HCN channel.

1.9   Aim of the Study

HCN channels are key regulators of neuronal excitability and play a crucial role in the physiology of complex behaviours. Although great efforts are being made to study the role of HCN channels in central nervous systems, major questions remain unanswered regarding their function in neuronal networks, their modulation, and their impact on our behaviour. A key feature of HCN channels is the modulation by cAMP. For a long time, it has not been possible to dissect this modulation *in vivo* from voltage dependent modulation, due to lack of specifically blocking the binding of cyclic nucleotides to HCN channels. Using genetically modified mouse models in which the binding of cAMP to the channel is abolished, this modulation can be studied for the first time on a cellular level, and its consequences for systemic processes and impact on behaviour can be examined.

The present work aimed to investigate roles of HCN4 in the thalamus. The cellular expression of HCN4, the biophysical properties of I_h, and the properties of firing patterns are examined using a variety of biochemical and electrophysiological methods to resolve how CDR of HCN4 affects the TC network at the cellular and systemic level. As HCN4 is the isoform most sensitive to cAMP, TC neurons unable to bind cAMP to HCN4 are predicted to be less responsive in the presence of neurotransmitters coupled to $G_{\alpha s}/G_{\alpha i}$ to adenylyl cyclase and the corresponding increases or decreases in cAMP levels. To support this hypothesis, the serotonergic system was invoked, in which activation of certain serotonin receptors causes intracellular cAMP concentration to increase or decrease.

While it has long been known that I_h in the thalamus consists predominantly of HCN2 and HCN4, it is not known if HCN4 has cellular roles distinct from HCN2. In a second step, differences in the modulation of HCN2 and HCN4 by cyclic nucleotides have been dissected using EEG recordings and behavioural experiments (open field test, light-dark test, social interaction and visual discrimination).

2   Methods

2.1   Chemicals and Solutions

All chemicals used to make solutions were obtained from Bio-Rad, Merck, Sigma-Adrich or VWR unless stated otherwise. The quality was either "pro analysi" or "for molecular biology". Highly pure and deionized water (18 MΩ – 18.2 MΩ) from the Milli-Q Plus System (Merck Millipore) was used to make all solutions. Solutions for long-term storage were sterile filtered.

2.2   Animals

All procedures concerning animals conform to the German animal protection laws and were approved by the local authority (ROB - Regierung von Oberbayern), and in line with the approved guidelines of the German laws on animal welfare (Tierschutzgesetz). Mice were maintained by in-house breedings in standard cages, under a 12 h dark/12 h light cycle (lights on at 7 a.m.) with ad libitum access to food (Ssniff; regular feed: R/M-H; breeding feed: M-Z Extrudat) and water. Ambient temperature was 22°C, with 60% humidity.

HCN4FEA mice, generated as previously described (Fenske et al., 2020), express a global knock-in mutation in HCN4 channels containing two amino acid mutations in the CNBD (R669E, T670A), and one mutation in the C-linker (Y527F) (Figure 6). HCN2EA mice, expressing a global knock-in mutation in HCN2 channels in the CNBD (R591E, T592A), were generated as previously described (Hammelmann et al., 2019).
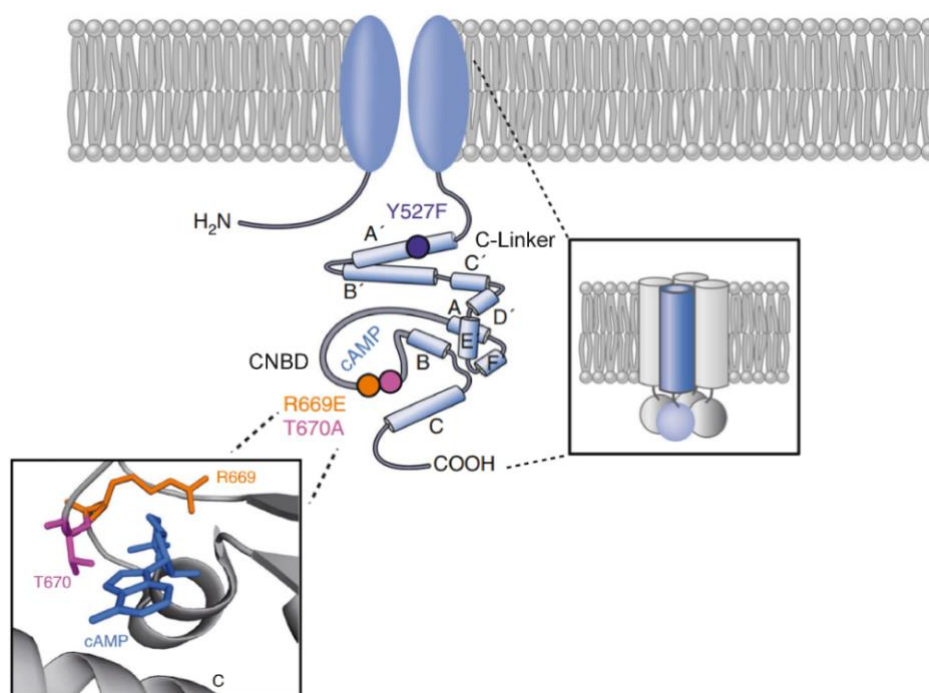
Figure 5. Schematic of the HCN4 channel depicting the 'FEA' mutation. The three introduced point mutations in the C-terminal region are depicted with coloured circles. The Y527F mutation (purple) is located in the C-linker region. The R669E (orange) and T670A (pink) mutations in the CNBD directly interact with cAMP (blue), and were introduced to completely abolish cAMP binding. (*Inset*) Interaction of residues T670 and R669 with cAMP in the CNBD. The image is adapted from Fenske et al., 2020.

2.3   Genotyping

For genotyping analysis, genomic (gDNA) was isolated from mouse ear biopsies. The isolated gDNA was amplified via polymerase chain reaction (PCR) and visualized via agarose gel electrophoresis to obtain the genotype. gDNA was isolated by poking a hole in the lid of the eppendorf tube containing the mouse ear clip tissue sample, and incubating the ear clip in 300 µL of 50 mM NaOH at 95 °C for 10 min and mixing well by vortexing. The sample was then neutralised by adding 50 µL Tris-HCl pH 8.0 and centrifuging for 6 min at 13,000 rpm and at room temperature. For PCR amplification, gene specific primers and GoTaq® DNA Polymerase (Promega) were used according to the manufacturer's instructions. PCR reactions were run in a ProFlex™ 3x32-well PCR System (Applied Biosystems, Thermo Fisher Scientific). The annealing temperature was optimised for each primer pair based on the primer melting temperature. The extension time was optimised based on the specific length of the PCR products.

Genotyping Reagents	
gDNA	2 µL
Forward primer (10 mM)	2 µL
Reverse primer (10 mM)	2 µL
dNTPs (10 mM)	0.5 µL
Green GoTaq® Reaction Buffer	5 µL
GoTaq® G2 DNA Polymerase	0.13 µL
ddH$_2$O	Add to 23 µL

PCR protocol for genotyping

Step	Temperature	Time	# cycles
Initial denaturation	95 °C	2 min	1
Denaturation	95 °C	30 s	
Annealing	59 °C	30 s	40
Extension	72 °C	40 s	
Final extension	72 °C	5 min	1
Hold	10 °C	Indefinite	1

2.4   Immunohistochemistry

Adult mice between the age of 3 – 6 months were anaesthetized with isoflurane and sacrificed.   Brains were rapidly and carefully removed, and slowly submerged into cold isobutane at a temperature between -20°C to -30°C, to remove any liquid in the brain and to deep-freeze the brain. Brains were then placed on dry ice to freeze and dry, and subsequently stored at -80°C until use. Before cryo-sectioning, brains adapted to the ambient temperature (approximately -24°C) in the cryostat (CM3050 S, Leica) and was mounted onto a cutting plate with embedding medium (Richard-Allan Scientific ™ Neg-50 ™, ThermoFisher Scientific). Three serial coronal brain slices (12 µm) cut at the level of the thalamus were fused to one microscope slide (Menzel-Gläser Superfrost® Plus, Thermo Scientific). After air drying, the slides were stored at -20°C until further use.

Immunohistochemistry was performed on 12 µm thick cryosections. The slices were stored at -20°C and thawed at room temperature before use. A liquid blocker (PAP-Pen Min - Liquid-Repellent Slide Marker Pen, Science Services) was drawn around the slices to provide

a hydrophobic barrier around the slices. The slices were then rehydrated with cold PBS for 5 min and then post-fixed by adding 4 % PFA in PBS for 5 min. The slices were washed three times with PBS and then incubated with a permeabilization and blocking buffer containing 10% ChemiBlocker ™ (Merck Millipore) and 0.3% Triton-X in PBS for 1 h. The blocking and permeabilization solution was carefully removed by pipetting. The slices were then incubated with the appropriate primary antibody (see appendix 10.2) diluted in PBS containing 5 % ChemiBlocker ™ O/N at 4°C. The next morning approximately 14 h later, slices were washed three times with PBS after removing the primary antibody solutions. The slices were then incubated with appropriate secondary antibodies (see Appendix 10.2) diluted in PBS containing 2 % ChemiBlocker™ for 1 h at room temperature. After washing two times with PBS for 5 min, the cell nuclei were stained by applying 5 µg/mL Hoechst (Thermo Fisher Scientific) for 5 min to the slices. The slices were then washed again two times with PBS for 5 min. Coverslips (Menzel-Gläser, VWR) were mounted onto the brain slices using Aqua-Poly/Mount mounting medium (Polysciences). The slides were dried and stored protected from light at room temperature until use for microscopy.

2.5   Confocal Microscopy

Images of immunohistochemically stained slices were acquired at 4600 × 4600 pixel resolution on an inverted Leica TCS-SP8 confocal laser scanning microscope, 10–40X, 1.4-NA objective and 600 Hz (Leica), and using the LASX software (Leica). For the comparison of WT and HCN4FEA littermates, slices were processed using the same protocol on the same day. The acquisition was performed with identical laser intensities and scanner settings. The intensities of the HCN fluorescence were analyzed using the plot profile tool of ImageJ software.

2.6   Western Blot

Adult mice between the age of 3 – 4 months were anaesthetized with isoflurane and sacrificed. One wildtype (WT) and one HCN4FEA mouse were sacrificed at the same time and subsequently processed together at the same time. Brains were rapidly and carefully removed, and the whole brain was cut into small pieces and homogenized into 750 µL RIPA buffer supplemented 1:25 with protease inhibitors (25X, complete™, Mini, EDTA-free Protease Inhibitor Cocktail, Sigma).

1X RIPA Buffer

5M NaCl	600 µL
10% Triton X-100	2 mL
10% Na-Deoxycholate	1 mL
10% SDS	200 µL
1M Tris pH 8.0	1 mL
ddH$_2$O	Add to 20 mL

Brains were homogenized using a mixer mill (MM400, Retsch) at 30 Hz for 2 min. Homogenized lysates were centrifuged at 10,000 x g for 30 min at 4°C, and 80 µg of the resulting supernatant was used for Western Blot analysis. PBS and 4 µL of 6X Laemmeli buffer was added to the sample for a total volume of 24 µL, and subsequently heated at 95°C for 5 min, then centrifuged briefly (~30 s).

6X Laemmeli Buffer

4X Tris-HCl pH 6.8	7 mL
Glycerol	3 mL
SDS	1 g
Bromphenol blue	1.2 mg
ddH$_2$O	Add to 20 mL

Electrophoretic separation of proteins was done by SDS-PAGE using standard methods. Briefly, protein samples and a protein ladder (PageRuler Prestained Protein Ladder, Thermo Fisher Scientific) to determine the protein size, were loaded on to a 7% polyacrylamide separating gel with a 10% stacking gel.

7% Separating gel	1 gel		10% Stacking gel	1 gel
ddH$_2$O	4.95 mL		ddH$_2$O	2.1 mL
30 % bis acrylamide	2.35 mL		30% bis-acrylamide	330 µL
1.5M Tris-HCl pH 8.8	2.50 mL		0.5M Tris-HCl pH 6.8	250 µL
10% SDS	100 µL		10% SDS	30 µL
20% APS	100 µL		20% APS	15 µL
TEMED	7 µL		TEMED	3 µL

Electrophoresis was performed in a gel apparatus (Hoefer Inc) at 100 V in SDS running buffer (10X SDS Running Buffer diluted 1:10) for 15 min followed by 150 V until finished.

10X SDS Running Buffer, pH 8.3	
Tris base	30 g
Glycine	144 g
SDS	10 g
ddH$_2$O	Add to 1L

The gel was subsequently transferred to a tank-blot system (Mini Trans blot, Biorad) onto a PVDF membrane (GE Healthcare) in cold transfer buffer at 300 mA for 1 hour.

1X Transfer Buffer	
Glycine	11.52 g
Tris base	2.42 g
ddH$_2$O	Add to 800 mL

After the transfer on to the PVDF membrane, the membrane was blocked with 5% (w/v) milk powder in TBST for 1 hour. Incubation with primary antibody was done overnight at 4°C.

10X TBS, pH 7.6	
Tris Base	12.1 g
NaCl	80.2 g
ddH$_2$O	Add to 1 L

1X TBST	
10X TBS	100 mL
Tween-20	1 mL
ddH$_2$O	Add to 1 L

Primary antibodies (see appendix 10.2) were diluted in 1% (w/v) milk powder in TBST overnight. The next morning, approximately 14 h later, the membrane was washed three times in TBST and then incubated with the appropriate secondary antibody (see appendix 10.2) in 5% (w/v) milk powder in TBST for 1 h. For detection, a luminol Reagent (SuperSignal™ West Pico PLUS Chemiluminescent Substrate, Thermo Scientific) was used according to the manufacturer's instructions. The chemiluminescence signal was detected using the Chemidoc MP Imaging system (Bio-Rad) including Image Lab software (Bio-Rad). Signals were detected with a luminescence image analyzer (ChemiDoc MP; Bio-Rad) and quantified using ImageLab software (Bio-Rad).

2.7   Co-immunoprecipitation

Co-immunoprecipitation (Co-IP) experiments were performed using 2000 µg of protein lysates (prepared as described above), with rabbit anti-HCN2, rabbit anti-HCN4 and mouse anti-TRIP8b, using Dynabeads™ Protein G magnetic beads (Thermo Fisher Scientific) according to the manufacturer's instructions. Interactions were subsequently detected with SDS-PAGE and probing with the primary antibody of interest, and with the antibody used for the pulldown.

2.8   Electrophysiology- acute thalamic slice patch recordings

2.8.1   Preparation of Brain Slices

Male and female HCN4FEA mice were used for electrophysiology experiments between the age of postnatal day (P)17-P25, with corresponding WT littermates. Mice were anaesthetized with isoflurane and sacrificed, and the brain was rapidly dissected and glued on to a slicing platform. Horizontal slices (250 µm) containing the VB thalamus were prepared on a vibratome (Leica, VT1200S) in ice-cold carbogenated (95% O$_2$, 5% CO$_2$) sucrose slicing solution.

Sucrose Slicing Solution 250 mL	
KCl	2.5 mM
NaH$_2$PO$_4$	1.25 mM
NaHCO$_3$	26 mM
CaCl$_2$	0.5 mM
MgCl$_2$	7 mM
Ascorbic Acid	1.7 mM
Sucrose	105 mM
Glucose	24.7 mM

Slices were then placed in carbogenated artificial cerebrospinal fluid (aCSF) solution at 37°C for 30 min, and subsequently at room temperature for an additional 30 minutes, until recording.

aCSF Solution 1 L	
NaCl	131 mM
KCl	2.5 mM
NaH$_2$PO$_4$	1.25 mM
NaHCO$_3$	26 mM
CaCl$_2$	2 mM
MgCl$_2$	7 mM
Ascorbic Acid	1.7 mM
Glucose	18 mM

2.8.2   Voltage clamp recordings

Brain slices were transferred to a recording chamber perfused with artificial cerebrospinal fluid (aCSF) solution and maintained at 31-33°C. TC neurons of the VB were visualized with an upright microscope (Axioskop 2 FS plus, Zeiss) equipped with a 5X objective, 40X water-immersion objective, and an infrared CCD camera (VX55, Till Photonics). Voltage and current clamp recordings were made using an EPC-10 patch-clamp amplifier (HEKA Instruments) and PatchMaster 2x90.5 software (HEKA Elektronik) was used to acquire and analyze the data. A horizontal puller (DMZ Universal Electrode Puller, Zeitz Instruments) was used to pull patch pipettes from borosilicate glass (GC150TF-10, Harvard Apparatus).

Patch pipettes were filled with an intracellular solution for both voltage clamp and current clamp recordings.

Intracellular solution	
$KMeSO_4$	140 mM
HEPES	10 mM
KCl	10 mM
EGTA	0.1 mM
Phosphocreatine	10 mM
MgATP	4 mM
NaGTP	0.5 mM

The pH of the intracellular solution was adjusted to 7.3 with 3M KOH and the osmolarity was approximately 290 mOsm/L. For experiments including cAMP, 1 µM 8-bromo (Br) cAMP (Sigma-Aldrich) was included in the pipette solution. The resistance of the pipette electrode used for measurements was 2.5–5.0 MΩ.

For measurement of I_h, slices were additionally perfused with aCSF in the recording chamber, with 2 mM $BaCl_2$, 10 mM tetraethylammonium chloride (TEA-Cl), and 0.5 µM TTX and maintained at 31°C–33°C. To determine I_h steady-state activation curves, TC neurons were clamped at a holding potential of –40 mV from which pulses of 5 s duration were applied from –140 mV to –40 mV in 10 mV increments, followed by a 1 s test pulse to –140 mV (the tail current). TC neurons were clamped at a holding potential of –40 mV from which pulses of 5 s were applied at –140 mV for 2-3 consecutive sweeps.

The effect of 5-HT was measured by applying 20 µM 5-HT (Sigma-Aldrich) to the bath aCSF solution, after recording control I_h steady-state activation curves (described above). A time course of 5-HT was then recorded by applying a single pulse at -120 mV from a holding potential of –40 mV for 3 s, every 2 min. After 12-15 min with 5-HT, I_h steady-state activation curves were recorded again and the shift in the $V_{0.5}$ was measured. The 5-HT$_7$ antagonist SB-269970 (Tocris Bioscience) was subsequently applied for 10 min in cells which remained healthy after the 5-HT time course. I_h steady-state activation curves were then recorded again and the shift in the $V_{0.5}$ value was measured.

Voltage clamp electrophysiology data was analyzed using PatchMaster software (HEKA Elektronik, Harvard Bioscience) Clampfit 10.2, and OriginPro8. Tail currents measured during the final step to -140 mV were normalized to the maximal current (I_{max}) and plotted as a function of the preceding membrane potential. The curves were fitted with a Boltzmann function: $I/I_{max} = (A1 - A2)/(1 + e^{[V-V0.5]/k}) + A2$, where $V_{0.5}$ and k represent the half-maximal voltage and Boltzmann slope factor, respectively, and A1 and A2 represent the initial and final I/I_{max} values. The current density was calculated as the steady-state current amplitude recorded at -140 mV divided by the cell capacitance. Activation time constants for the steady state current amplitude recorded at -140 mV, were fit with a two component exponential function.

2.8.3   Current-clamp recordings

To record firing patterns, slices were perfused with aCSF containing 2 mM $BaCl_2$ and maintained at 31°C–33°C. TC neurons were clamped at their RMP and 300 ms depolarizing pulses from 50 to 200 pA in 50 pA increments were applied. To test for the influence of the membrane potential on firing modes, a current injection of -50 pA or +20 pA was applied to hyperpolarize or depolarize the RMP, respectively, and firing patterns were recorded again. The voltage sag was determined by applying negative-current injections for 2.5 seconds in -10 pA increments from -20 pA to -100 pA. The voltage sag ratio was calculated by dividing the steady state of the sag measurement by the peak voltage deflection. The input resistance was determined by the maximum change in membrane potential during a 2.5 s hyperpolarizing current injection, divided by the current injected (-100 pA). A liquid junction potential of -10.23 mV was calculated using the LJPcalc Liquid Junction Potential tool (Harden and Brogioli, 2020), and reported values are not corrected for.

2.9   Quantitative real-time PCR

2.9.1   RNA extraction from thalamic tissue

For the quantitative real-time (qPCR) of 5-HT receptors, brains from mice between the ages of P20-P30, (3 HCN4FEA mice and 3 WT mice) were removed and the thalamus was carefully dissected and flash frozen in liquid nitrogen. For the qPCR of HCN channels, the thalamus was dissected from 400 µm coronal slices from adult HCN4FEA mice (4 HCN4FEA mice and 4 WT mice). RNA was subsequently extracted from the tissue samples using the RNeasy Mini Plus kit (Qiagen) according to the manufacturer's instructions. Briefly, tissue samples were homogenized in 300 µL lysis buffer (Qiagen) containing β-mercaptoethanol to

inhibit ribonucleases and centrifuged with the provided columns to eliminate gDNA. After adding 300 µL of ethanol (70%) to the flow-through, the samples were applied to RNA-binding columns and contaminating molecules were removed by washing the columns with the provided solutions. The RNA was eluted in 30 µL H_2O and concentrations were measured using a NanoDrop spectrometer.

2.9.2   First Strand cDNA synthesis and RNA extraction

The RNA extracted in the previous section (2 µg) was subsequently used for cDNA synthesis, using the RevertAid First Strand cDNA synthesis kit (ThermoFisher Scientific) according to the manufacturer's instructions. Briefly, in the first step, 0.5 µL each of Oligo dT- and random hexamer primers, were added to water and template RNA for a total volume of 12 µL. Samples were incubated at 65°C for 5 minutes then cooled at 10°C. In the second step, reaction buffer, RNase inhibitor, dNTP's, and reverse transcriptase was added to the reaction mixture, and incubated for 5 minutes at 25°C, followed by 1 h at 42°C, then 70°C for 5 min to terminate the reaction. The samples were stored at -20°C until further use.

2.9.3   qPCR protocol

qPCR was performed on a QuantStudio™ 5 Real-Time PCR System (Thermo Fisher Scientific). Reaction mixtures were pipetted in MicroAmp Fast 96-well reaction plates (Thermo Fisher Scientific), using the SYBR™ Green qPCR Master Mix (Thermo Fisher Scientific) for quantification of the PCR products, according to the following scheme in duplicate.

qPCR Reagents	
cDNA (1:4 diluted with H_2O)	2.5 µL
PowerUp™ SYBR™ Green	5 µL
Primer forward (10 µM)	0.4 µL
Primer reverse (10 µM)	0.4 µL
RNase-free water	Add to 10 µL

Annealing temperatures were calculated from the Thermofisher T_m calculator. Expression levels were analysed and normalized to the expression levels of the house keeping

gene, ALAS for the HCN channels, and GAPDH for the 5-HT receptors, using the delta delta Ct method.

qPCR protocol for 5-HT receptors

Step	Temperature	Time	# cycles
Initial denaturation	50 °C [*]	2 min	1
DNA polymerase activation	95 °C [*]	5 min	1
Denaturation	95 °C [*]	3 s	
Annealing			
-5HT1A	62.6°C		
-5HT1B	61°C		
-5HT3A	61.8°C	10 s	40
-5HT6	70.2°C		
-5HT7	63.5°C		
-GAPDH	62°C		
Extension	60 °C	30 s	
	95 °C	15 s	1
Melt curve acquisition	60 °C	1 min	1
	95 °C Ramp + 0.3 °C/s	15 s	1

qPCR protocol for HCN channels

Step	Temperature	Time	# cycles
Initial denaturation	50°C	2 min	1
DNA polymerase activation	95°C	5 min	1
Denaturation	95°C	3 s	
Annealing	58°C	10 s	40
Extension	60 °C	30 s	
	95 °C	15 s	1
Melt curve acquisition	60 °C	1 min	1
	95 °C Ramp + 0.3 °C/s	15 s	1

2.10   Behaviour experiments

Behavioural experiments were performed with adult male HCN4FEA and HCN2EA mice between the ages of 3-6 months. HCN4FEA mice and HCN2EA were age-matched with their respective WT littermates. Parameters of all tests were tracked using a computer-assisted data acquisition system (VideoMot TSE). The experiments were performed and analysed blindly with respect to genotype.

2.10.1   Open Field Test

The open field test measures anxiety like behaviours and locomotion in mice. This paradigm is based on the notion that mice will naturally prefer to be near a protective wall rather than exposed to danger out in the open (Seibenhener and Wooten, 2015). The open field box consisted of a square white box (40 x 40 x 40 cm) made of acrylic glass. Each mouse was placed in the box for 20 min. The inner region (50% of the base) was defined in the computer-assisted data acquisition system software before each experiment. Overall activity, notably in the inner region, and locomotion of the mice in the box was measured and recorded at 5 min and 20 min. After each trial, the box was cleaned with bacillol solution, and allowed to air dry before placing the next mouse in the box.

2.10.2   Light-Dark Transition Test

The light-dark transition test (LDT) is based on the natural aversion of mice to brightly lit areas and their exploratory behaviour in a novel environment (Takao and Miyakawa, 2006). Briefly, the apparatus (50 x 50 x 50 cm) contained a dark chamber which consisted of one third of the box and a brightly lit chamber which consisted of the other two thirds. Mice were placed in to the dark chamber, and were allowed to freely move between the two areas over a 10 min period. The duration and number of entries into the bright space are indicators of bright space anxiety in mice (Takao and Miyakawa, 2006). After each trial, the box was cleaned with bacillol solution, and allowed to air dry before placing the next mouse in the chamber.

2.10.3   Social Interaction Test

The social interaction aspect of social behaviour is a measurement to assess the social behaviour phenotype in mice (Kim et al., 2019). WT or HCN4FEA mice were placed into a cage for 15 min to adapt to the cage environment prior to the measurement period of training; short-term memory (STM) or long-term memory (LTM). After adapting to the cage

environment, during the training period, a juvenile social interaction partner (6-8 week old male mouse) was placed into the center of the cage with a protective wire-cage barrier around the juvenile mouse, for 5 min while the movement of the mouse was tracked. In the short term memory (STM) period, 1 h later the mouse was placed in the same cage for 10 min to adapt to the cage environment again, and the same juvenile interaction partner with the protective barrier, was subsequently placed in the cage. In the long term memory (LTM) period, after 24 h the mouse was placed into the same cage for 10 min to adapt to the cage environment again, and the same juvenile interaction partner was subsequently placed in the cage for 5 min. The number of interactions with the juvenile mouse were measured and the speed of the mouse was measured.

2.10.4   Visual discrimination test

The visual discrimination test is a test for discriminating visual stimuli, which is processed by the geniculate pathway of the dLGN in the thalamus. The test was performed as previously described (Hammelmann et al., 2019). Briefly, mice were trained to discriminate between conditioned stimulus (CS^+) and non-conditioned stimulus (CS^-) images. The CS^+ was connected to a hidden platform at the open side of a trapezoid-shaped swimming pool. Each mouse was given 3 blocks of 10 training units per day over 4 consecutive days. A single training unit consisted of no more than 5 trials for swimming consecutively into the wrong arm. A training unit was terminated when a mouse crossed the choice line and climbed onto the platform. To avoid the effect of positional learning, the side of the CS^+ image and the platform was changed after each trial using a Gellerman schedule (LRLLRLRR; L = left, R = right). To assess the visual discrimination capacity, the mean probability of a correct choice per day was analysed.

2.11   Telemetric EEG recordings

To measure EEG and electromyogram (EMG) activity, a telemetric EEG transmitter (F20-EET, Data Science International) was implanted. The head of the mouse was fixed in a stereotactic apparatus and the temperature was maintained at 37°C via a rectal feedback system. A 1.5 cm incision was made to open the scalp, and a second incision was made between the scapulae along the longitudinal axis. A small pocket was opened for the transmitter and two electrodes for the EMG transmitter were sutured into the shoulder muscle. Two small holes were drilled into the skull (0.7 in diameter (using the following coordinates: A/P -2.0; 1.8 (from bregma; recording electrode) and A/P, -1,0; M/L, -0.5 (from lambda;

reference electrode). After suturing and disinfection, mice were given a two-week recovery period before *in vivo* EEG recordings.

Cortical EEG and EMG traces of freely moving mice were recorded using A.R.T. software (Data Science International) and were videotaped. The vigilance states (wake, NREM sleep and REM sleep) were scored using Neuroscore 3.2.1 (Data Science International). Data was converted using Discrete Fourier Transform (DFT) in Neuroscore. For the analysis of sleep and wake, transitions between vigilance stages were excluded and the mean length of every sleep and wake period was calculated using Microsoft Excel. A brief awakening during NREM sleep was defined as an interruption of the sleep period by a 2-4 s wake interval in which the mouse turns or moves before falling back into NREM sleep. The number of transitions between vigilance states was calculated in Microsoft Excel. For the analysis of the transition from NREM sleep to wake, data was selected for period of at least 30 s NREM sleep followed by a period of at least 30 s wake. For every 2 s period, the mean theta power (4-8 Hz) was calculated and normalized to the total NREM theta power. All data was plotted using GraphPad Prism 5.

2.12   Statistics

Data plotting and statistical analysis were performed using GraphPad Prism 5 and OriginPro8.   All values are presented as mean ± SEM for the indicated number *n* of experiments. *P* values were calculated using either a paired t test, two sample t test, or 1- or 2-way analysis of variance (ANOVA) with Bonferroni's post hoc test. *$P < 0.05$, **$P < 0.01$, and ***$P < 0.001$ were considered statistically significant.

3   Results

In order to investigate the neuronal consequences of CDR of HCN4, a global knock-in mouse model containing three amino acid mutations in the C-terminal region of HCN4 (R669E, T670A and Y527F) was used (Figure 5). The R669 and T670 residues located in the CNBD are highly conserved in the HCN channel family and the CNG channel family, and mutation of R669 to glutamate/glutamine and T670 to alanine completely abolishes channel activation by cAMP (Liu et al., 1998; Chen et al., 2001). These residues have been shown to directly interact with the phosphate group of cAMP in high resolution structures of the CNBD (Zagotta et al., 2003; Lee et al., 2017). Previous studies have shown that eliminating the cAMP binding capability of HCN4 is associated with embryonic lethality, due to essential I_f modulation by cAMP during embryonic development (Harzheim et al., 2008). To circumvent the complete loss of HCN4 activity during embryonic development, the third Y527F mutation in the C-linker region was introduced (Fenske et al., 2020). Here, the term HCN4FEA is used to refer to homozygous mice which carry the three mutations on both *Hcn4* alleles.

3.1   Co-expression of HCN2 and HCN4 in the thalamus

I examined the expression patterns of HCN2 and HCN4 in the VB complex using immunohistochemical staining (Figure 6A, B). In both WT and HCN4FEA a strong signal for HCN2 was detected around the somata and also in the dendrites, while HCN4 expression was only enriched in the dendrites (Figure 6A, B). Quantification of the intensity of the expression confirmed that HCN2 is expressed in the dendrites, and is significantly higher around the somata, indicating that HCN2 expression is somatic and dendritic (Figure 6, upper panel). HCN4 expression was not significantly different between the somata and dendrites, which indicates that HCN4 expression is predominantly dendritic (Figure 6C, lower panel).
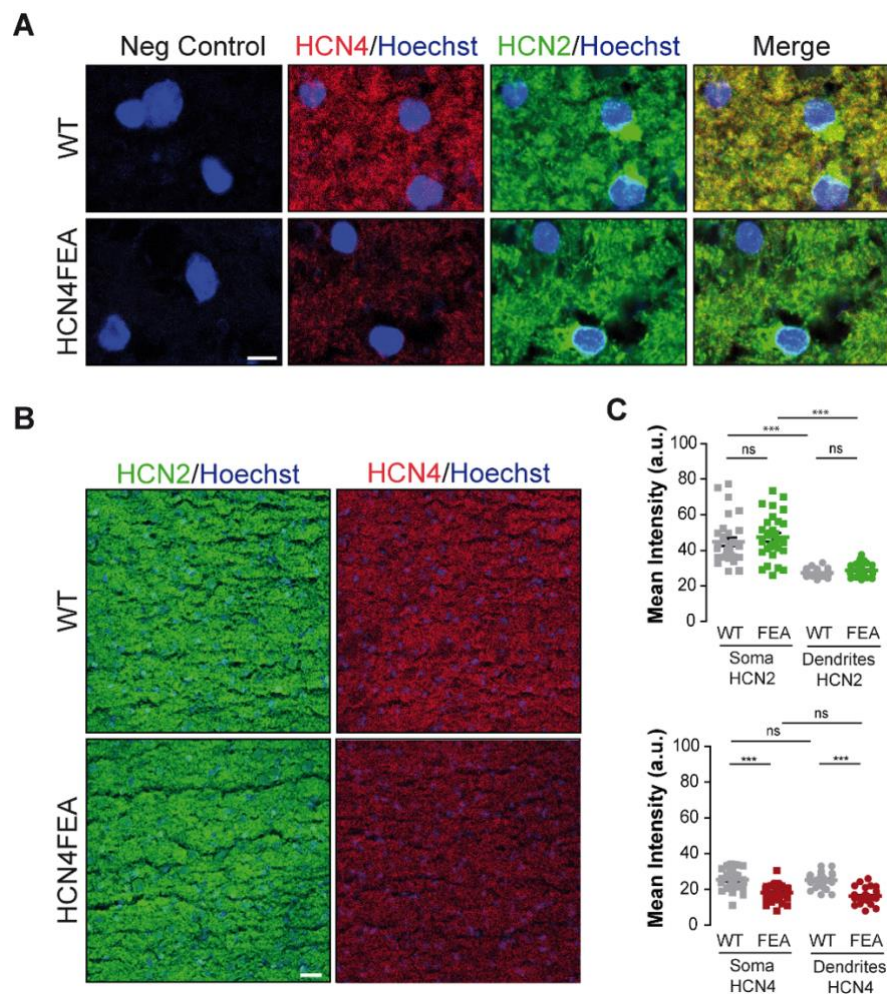
Figure 6. HCN4 channel co-expression with HCN2 in the VB thalamus. Distribution of HCN2 and HCN4 in the VB thalamus of WT and HCN4FEA mice. **(A)** Hoechst staining was performed to identify the nuclei and is depicted in blue. The negative control (first column) depicts staining without the primary antibodies; staining of HCN4 is depicted in red (rb anti-HCN4, second column); HCN2 is depicted in green (rb anti-HCN2, third column); merged images are depicted in the fourth column. Scale bar indicates 4 µm. **(B)** Overlay of anti-HCN2 (green) with hoechst, and anti-HCN4 (red) with hoechst, in the whole VB region. Scale bar indicates 30 µM. **(C)** *Upper,* quantification of the mean intensity of HCN2 fluorescence in images from WT and HCN4FEA soma and dendrites (WT: grey squares, soma [n=30], grey circles, dendrites [n=30], HCN4FEA: green squares, soma [n=30], green circles, dendrites [n=30], P<0.0001 in one-way ANOVA with Bonferroni's post hoc test). *Lower*, quantification of the mean intensity of HCN4 fluorescence in images from WT and HCN4FEA soma and dendrites (WT: grey squares, soma [n=30], grey circles, dendrites [n=30], HCN4FEA: red squares, soma [n=30], red circles, dendrites [n=30], P<0.0001 in one-way ANOVA test with Bonferroni's post hoc test).

While there was no difference in HCN2 expression levels between WT and HCN4FEA, HCN4 expression was consistently lower in HCN4FEA compared to WT (Figure 6C, lower panel). The cause of the lower HCN4 expression in HCN4FEA staining could not be determined. Further investigation of the expression levels of the HCN subtypes from qPCR from the whole thalamus did not show a difference between WT and HCN4FEA for all of the HCN channel subtypes (Figure 7). The qPCR further confirmed higher expression of HCN2 in the thalamus of WT mice, and detected low levels of HCN1 and HCN3 (Figure 7) which did not reach significance.
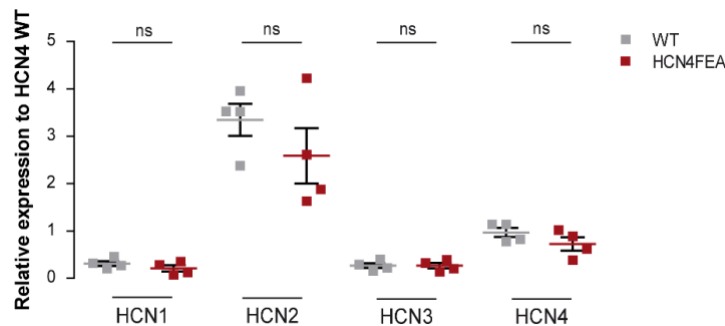
Figure 7. Lack of cAMP modulation of HCN4 does not alter expression levels of HCN isoforms in the thalamus of WT and HCN4FEA mice. Expression levels of HCN isoforms detected from the whole thalamus, of WT (grey squares, *n*=4) and HCN4FEA (red squares, *n*=4) mice, using qPCR. The analysis was performed using the delta-delta-Ct method. ns, not significant in two sample t test. Data provided by Manuela Brümmer.

Consistent with the results from the qPCR, protein expression patterns from Western blot analysis of the membrane fraction from whole brain lysates also did not show a difference in HCN4 or HCN2 levels between WT and HCN4FEA (Figure 8). It is widely known that the auxiliary HCN channel subunit TRIP8b specifically interacts with all four HCN channel subtypes through a conserved sequence in the C-terminal tail, and directly affects trafficking of HCN channels and cell surface expression at the membrane (Santoro et al., 2004). An increase in TRIP8b levels in HCN4FEA compared to WT would explain the reduced expression observed in HCN4FEA. However, Western blot analysis revealed that the expression levels of TRIP8b was also not different in HCN4FEA compared to WT (Figure 8).
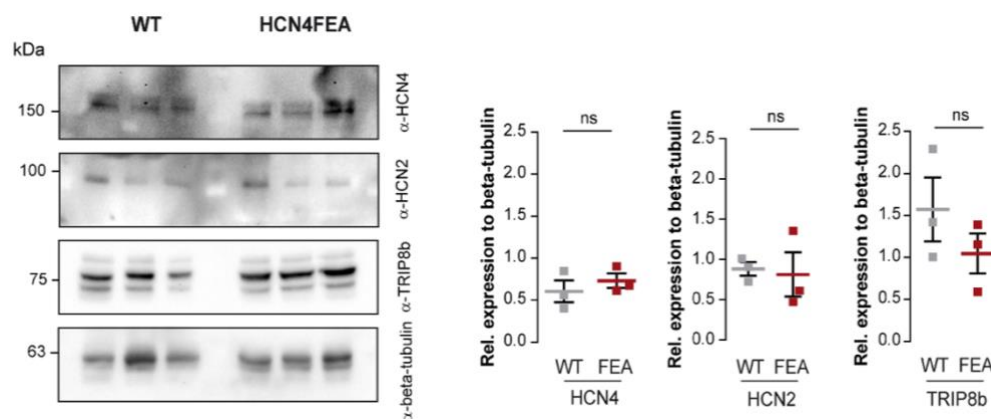

Figure 8. Expression of HCN channels in the brain. Western blot analysis (left) of whole brain lysates of WT (*n*=3) and HCN4FEA (*n*=3) mice, probed for rb anti-HCN4, rb anti-HCN2, ms anti-TRIP8b, and a loading control ms anti- beta-tubulin, and the relative expression levels (right) of HCN4, HCN2 and TRIP8b in relation to beta-tubulin. ns, not signficant in two sample t test.

It is known that HCN2 and HCN4 channel subunits interact and form heterotetrameric channels (Much et al., 2003). To ensure that the HCN4FEA mutation did not disturb channel architecture, co-IP was performed from brain lysates to pulldown and probe for HCN2 and

HCN4. Co-IP confirmed the presence of HCN2/HCN4 and HCN2/HCN4FEA hetero-tetrameric channels, indicating that channel architecture is not impacted by the HCN4FEA mutation (Figure 9A).

In addition, co-IP was performed for HCN4 and TRIP8b, to test if there is a difference in the interaction with TRIP8b with HCN4, that could explain the reduced levels of HCN4FEA observed. However, in the co-IP a difference was not detected in the interaction between HCN4 and TRIP8b between WT and HCN4FEA (Figure 9B). Furthermore, immunohistochemical staining was performed to examine the expression pattern of TRIP8b with HCN4, HCN2 and HCN1. The expression of TRIP8b with the HCN subtypes was also not different between WT and HCN4FEA in which both somatic and dendritic expression was observed (Figure 10).
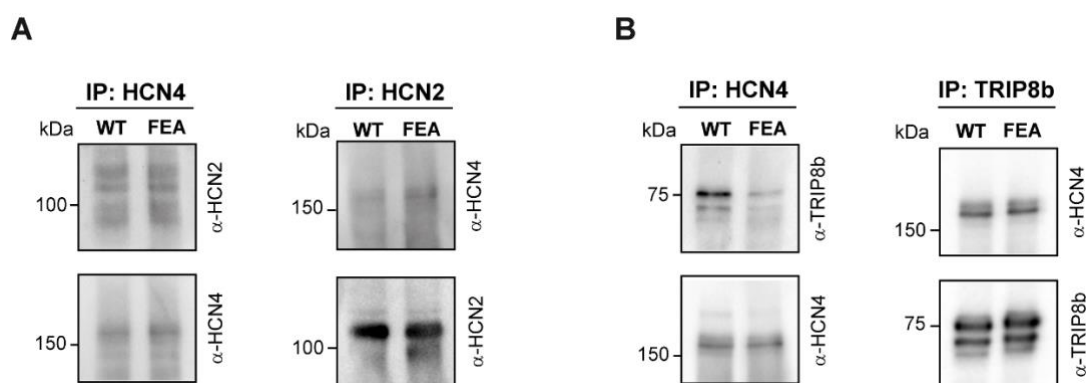

Figure 9. Interaction of HCN channels in the brain. Co-immunoprecipitations of whole brain lysates from WT (left lanes) and HCN4FEA (right lanes) mice. The 'IP' indicates the antibody used for the co-immuniprecipation, and the right-side label indicates the antibody used for probing. **(A)** Lysates were precipitated with rb anti-HCN4 (left) and rb anti-HCN2 (right). (**B**) Lysates were precipitated with rb anti-HCN4 (left) and ms anti-TRIP8b (right).
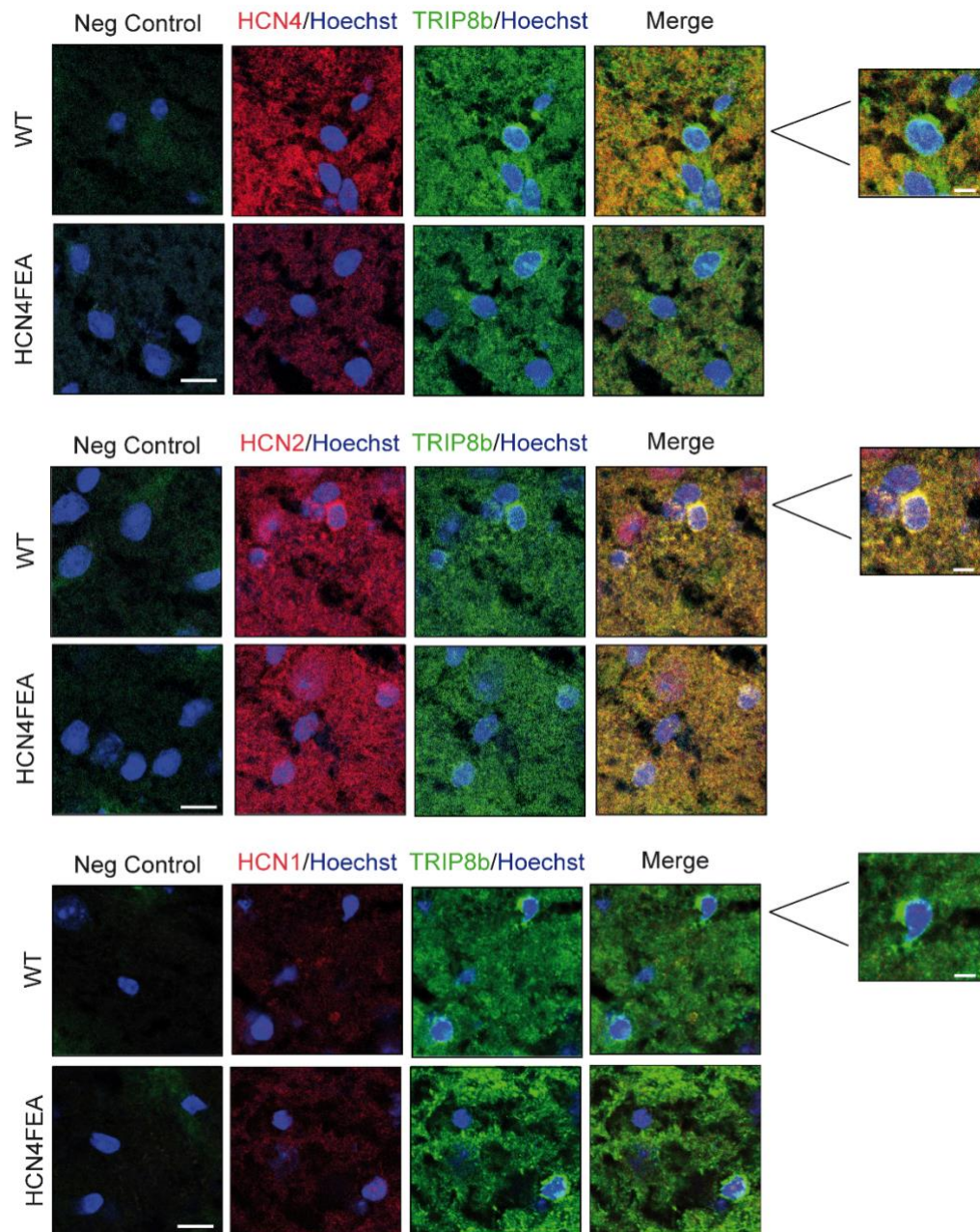
Figure 10. HCN channel co-expression with TRIP8b in the VB. Immunohistochemical staining of HCN channel isoforms and TRIP8b, in the VB of WT and HCN4FEA mice. Hoechst staining was performed to identify the nuclei and is depicted in blue. The negative control (first column) depicts staining without the primary antibody; staining of HCN channel isoforms is depicted in red (rb anti-HCN1, –HCN2 and –HCN4, third column) staining of TRIP8b (ms anti-TRIP8b) is depicted in green (third column); merged images are depicted in the fourth column, with an enlarged view of single nuclei shown in the insets (far right). Scale bars indicate 10 μm, and the scale bars in the insets indicate 4 μm.

3.2 Characterization of HCN4FEA-mediated I_h in the VB complex

To determine the contribution of CDR of HCN4 in the thalamus, I_h was characterized from TC neurons in the VB region from acute thalamic slice preparations of HCN4FEA and WT mice. Figure 11 shows representative traces of steady-state whole-cell activation currents from TC neurons of WT and HCN4FEA mice in the presence and absence of 1 µM 8-Br cAMP in the intracellular recording solution, which is in the range of reported cAMP affinities of I_h in neurons (Biel et al., 2009). Steady-state activation curves were recorded to determine the $V_{0.5}$ values of I_h. The shape of the current traces of WT and HCN4FEA in the absence of cAMP was similar between WT and HCN4FEA (Figure 11, upper traces).
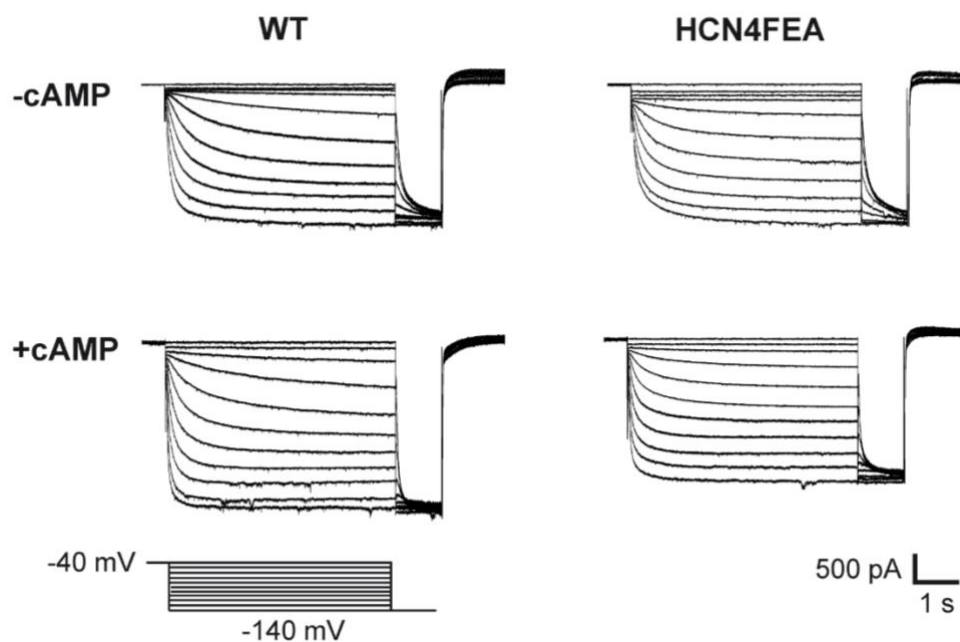

Figure 11. Impaired cAMP dependent regulation of I_h in TC neurons expressing HCN4FEA. Representative I_h traces from TC WT (*left*) and HCN4FEA (*right*) neurons in the VB, in the presence (*upper*) and absence (*lower*) of 1 µM 8-Br cAMP. Below, is the voltage protocol used to evoke the current traces, peak tail currents resulted from a 1 s voltage step to -140 mV from a 5 s voltage step (-140 mV to -40 mV; in 10 mV increments).

WT TC neurons displayed a significant shift in the $V_{0.5}$ in the presence of cAMP (Figure 12A, B; $V_{0.5}$: WT -cAMP, -88.39 ± 1.55 mV; WT +cAMP, -74.08 ± 1.05 mV), while in HCN4FEA TC neurons the voltage dependence of activation was still modulated by cAMP although to a lesser extent (Figure 12A, B; $V_{0.5}$: HCN4FEA –cAMP, -90.18 ± 0.67 mV; HCN4FEA +cAMP -79.64 ± 1.25 mV). Slope factors of the half maximal activation curves in the presence and absence of cAMP were similar between WT and HCN4FEA (Figure 12C; WT -cAMP, 9.64 ± 0.46 mV; WT +cAMP, 12.75 ± 1.21 mV; HCN4FEA –cAMP, 9.59 ± 0.64 mV; 11.72 ± 1.28 mV).

As mentioned, HCN2 is highly expressed in the VB region and this result reflects the presence of residual I_h modulation by cAMP, and the ability of HCN2 to still bind cAMP in HCN4FEA.
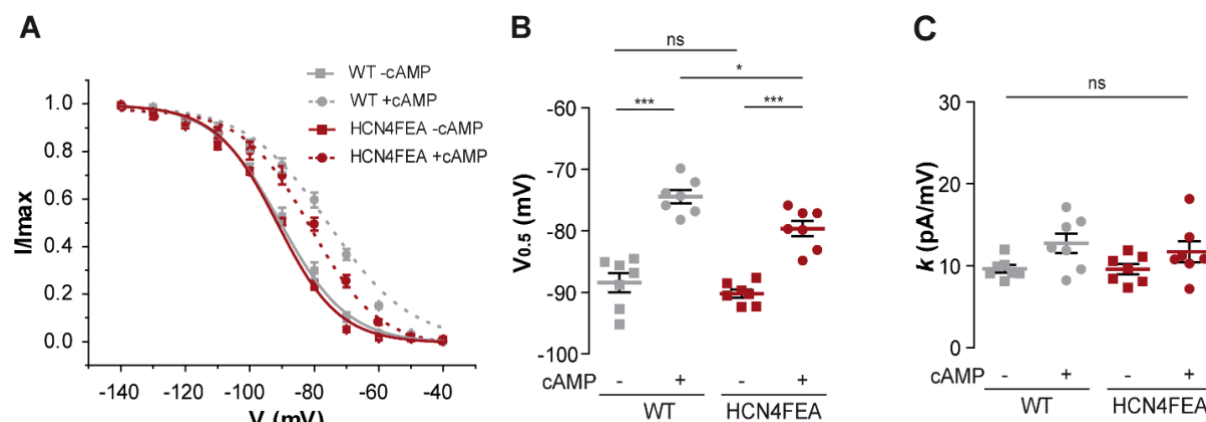

Figure 12. The voltage dependence of activation of I_h shows impaired cAMP dependent modulation in TC neurons expressing HCN4FEA (A) Normalized current-voltage relationships of I_h in TC neurons in the VB of WT and HCN4FEA mice in the absence (-cAMP) and presence (+cAMP) of 1 µM 8-Br cAMP. WT –cAMP, solid grey line [n=7]; WT +cAMP, dashed grey line [n=7]; HCN4FEA –cAMP, solid red line [n=7]; HCN4FEA +cAMP, dashed red line [n=7]. **(B)** Half maximal activation values shown in **(A)**, P<0.0001 in one-way ANOVA with Bonferroni's post hoc test. **(C)** Slope factors (k) of the half maximal activation curves shown in **(A)**, P=0.0793 in one-way ANOVA with Bonferroni's post hoc test.

This effect on the modulation of I_h by cAMP was also reflected in the activation time constants. The slow (tau slow) activation time constant was similar between WT and HCN4FEA TC neurons in the absence of cAMP, and was significantly faster in WT neurons in the presence of cAMP (Figure 13A; tau slow at -140 mV: WT -cAMP, 602.80 ± 31.84 ms; WT +cAMP, 441.24 ± 41.06 ms; HCN4FEA –cAMP, 751.67 ± 87.73 ms; HCN4FEA +cAMP, 575.18 ± 47.47 ms).
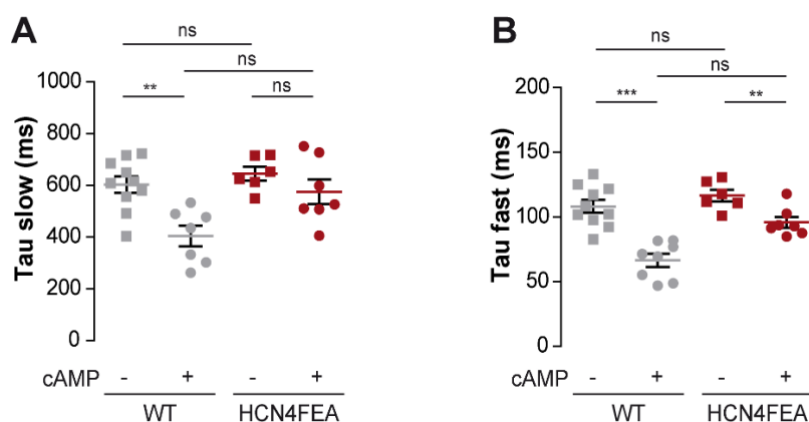

Figure 13. Activation time constants of HCN4FEA TC neurons in the VB. (A) Tau, slow component and **(B)** Tau, fast component, of TC neurons in the VB. Currents resulted from a 5 s voltage step to -140 mV from a holding potential of -40 mV. (WT -cAMP, [n=10]; WT +cAMP, [n=8]; HCN4FEA -cAMP, [n=6]; HCN4FEA +cAMP, [n=7]. P= 0.001 (tau slow) and P<0.0001 (tau fast) in one-way ANOVA with Bonferroni's post hoc test.

The fast (tau fast) activation time constant was also similar between WT and HCN4FEA TC neurons in the absence of cAMP. Intracellular cAMP significantly accelerated the activation kinetics of the tau fast component in WT and HCN4FEA neurons, although the activation kinetics were accelerated to a lesser extent in HCN4FEA (Figure 13B; tau fast at -140 mV: WT -cAMP, 108.31 ± 5.02 ms; WT +cAMP, 66.52 ± 5.07 ms; HCN4FEA –cAMP, 116.61 ± 4.54 ms; HCN4FEA +cAMP, 95.88 ± 4.24 ms).

Consistent with the effect of residual cAMP modulation by HCN2 on the $V_{0.5}$ and fast activation time constants in the VB, this effect was also reflected in the RMP. The RMP was similar between WT and HCN4FEA in the absence of cAMP. In WT TC neurons, the RMP was significantly depolarized in the presence of cAMP, while in HCN4FEA neurons, the RMP was also depolarized in the presence of cAMP, although to a lesser extent (Figure 14; WT -cAMP, -73.25 ± 0.95 mV; WT +cAMP, -60.1 ± 0.64 mV; HCN4FEA –cAMP, -72.00 ± 0.81 mV; HCN4FEA +cAMP, -66.00 ± 0.78 mV).
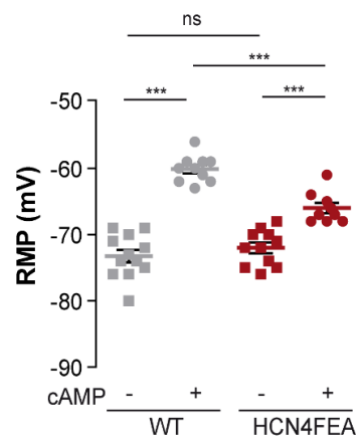

Figure 14. The resting membrane potential of HCN4FEA TC neurons in the VB. (WT -cAMP, [*n*=12]; WT +cAMP, [*n*=10]; HCN4FEA -cAMP, [*n*=11]; HCN4FEA +cAMP, [*n*=9] *P*< 0.0001 in one-way ANOVA with Bonferroni's post hoc test.

Furthermore, in agreement with the similar expression levels of TRIP8b in WT and HCN4FEA, steady-state I_h current density was also similar between WT and HCN4FEA in the absence and presence of cAMP (Figure 15; current density at -140 mV: WT -cAMP, -11.05 ± 1.08 pA/pF; WT +cAMP, -11.21 ± 1.87 pA/pF; HCN4FEA –cAMP, -7.80 ± 0.88 pA/pF; -10.87 ± 1.11 pA/pF). This indicates that the loss of cAMP binding in HCN4FEA does not affect current density and maximal activation of I_h.
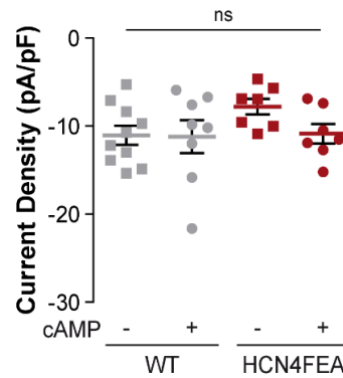
Figure 15. I_h density of HCN4FEA TC neurons in the VB. Currents resulted from a 5 s voltage step to -140 mV from a holding potential of -40 mV (WT -cAMP, [n=10]; WT +cAMP, [n=8]; HCN4FEA -cAMP, [n=7]; HCN4FEA +cAMP, [n=7], P=0.2598 in one-way ANOVA with Bonferroni's post hoc test.

3.2.1 Attenuated firing in HCN4FEA TC neurons in the VB complex

The firing properties of WT and HCN4FEA TC neurons were examined from whole-cell current clamp recordings. Current injections of +50 pA, +100 pA, +150 pA and +200 pA were applied at the RMP. In the absence of cAMP, WT TC neurons responded with a mix of high frequency burst firing with constant frequency (Figure 16A first trace, D) and tonic firing which increased in frequency in the range of 50 pA to 200 pA (Figure 16A first trace, B). In the presence of cAMP, the RMP was depolarized and WT neurons responded only with tonic firing (Figure 16A second trace) that also increased in frequency between 50 pA to 200 pA of injected current (Figure 16B). In contrast, in the absence of cAMP, HCN4FEA TC neurons responded with burst firing in which the frequency and number of burst spikes were reduced compared to WT TC neurons although not significant (Figure 16A third trace, E). Additionally, 4/11 neurons HCN4FEA TC neurons also responded with burst and tonic firing, likely reflecting cAMP modulation of HCN2, although with significantly attenuated frequency compared to WT (Figure 16B). In the presence of cAMP, HCN4FEA TC neurons again showed burst firing which did not switch to tonic firing (Figure 16A fourth trace), although 4/9 neurons only showed tonic firing but with significantly reduced frequency compared to WT TC neurons in the presence of cAMP (Figure 16B).
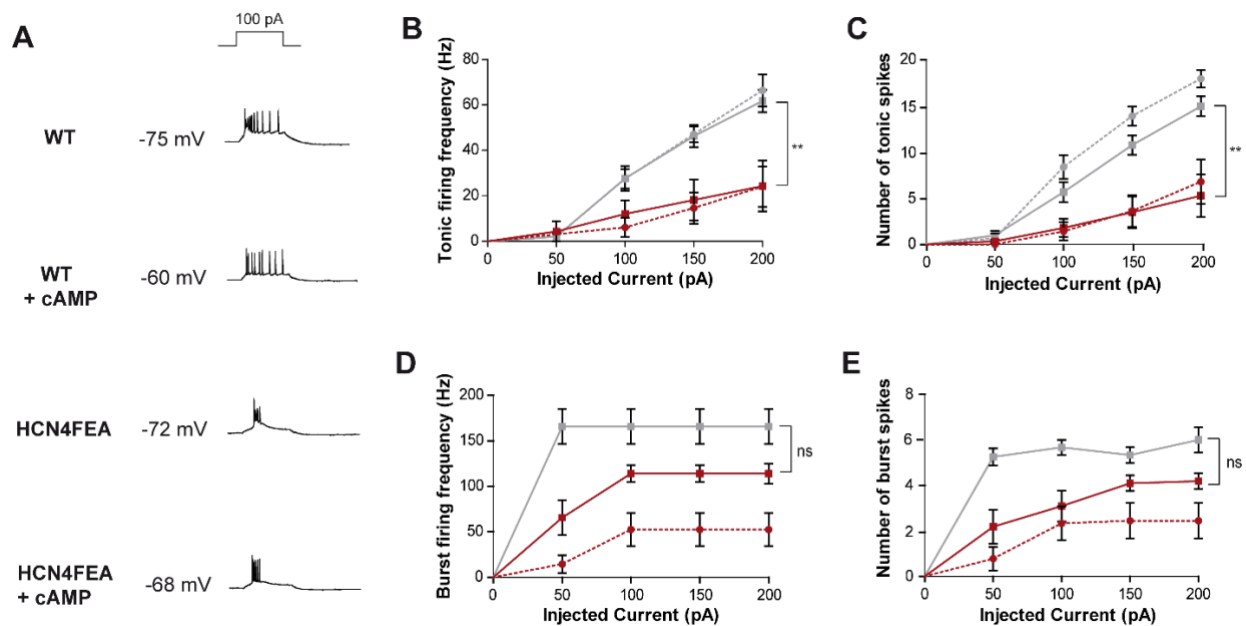
Figure 16. Impaired cAMP dependent regulation of the HCN4 channel alters firing properties of TC neurons in the VB. (A) Representative firing patterns of WT and HCN4FEA TC neurons in the VB recorded at the RMP, at a 100 pA current injection. **(B-D)** TC neurons were measured at 50 pA, 100 pA, 150 pA and 200 pA (WT -cAMP, grey squares [*n*=12]; WT -cAMP, grey circles [*n*=10]; HCN4FEA -cAMP, red squares [*n*=11]; HCN4FEA +cAMP, red circles [*n*=9]. A two-way ANOVA was compared between WT -cAMP and HCN4FEA –cAMP across all frequencies. ns, not significant. **(B)** Tonic firing frequency (*P*=0.0018 in two-way ANOVA test with Bonferroni's post hoc test). **(C)** Number of tonic spikes, (*P*=0.0030 in two-way ANOVA test with Bonferroni's post hoc test). **(D)** Burst firing frequency (*P*=0.2761 in two-way ANOVA with Bonferroni's post hoc test). Note: WT +cAMP neurons did not show burst firing at its RMP. (**E**) Number of burst spikes, (*P*=0.2563 in two-way ANOVA test with Bonferroni's post hoc test).

Additionally, the effect of the RMP on firing properties of TC neurons was examined by first either hyperpolarizing or depolarizing the RMP, and then recording the firing pattern again with current injections of +50 pA, +100 pA, +150 pA and +200 pA. A -50 pA current injection was applied to hyperpolarize the RMP, and a +20 pA current injection to depolarize the RMP. When -50 pA was injected to first hyperpolarize the RMP before firing, in both the presence and absence of cAMP, WT TC neurons showed only burst firing (Figure 17, left panel). In HCN4FEA TC neurons there was no change in burst firing (Figure 16, left panel). When +20 pA was injected to depolarize the RMP, in both the absence and presence of cAMP the frequency of tonic firing increased in WT neurons (Figure 16 upper panels). In contrast, HCN4FEA neurons showed a mixed response, with 5/9 neurons showing burst firing which did not switch to tonic firing even with a stronger depolarizing current injection. While 4/9 TC neurons only showed tonic firing, although with significantly attenuated frequency compared to WT TC neurons in the presence of cAMP (Figure 17 lower panels, 16B).
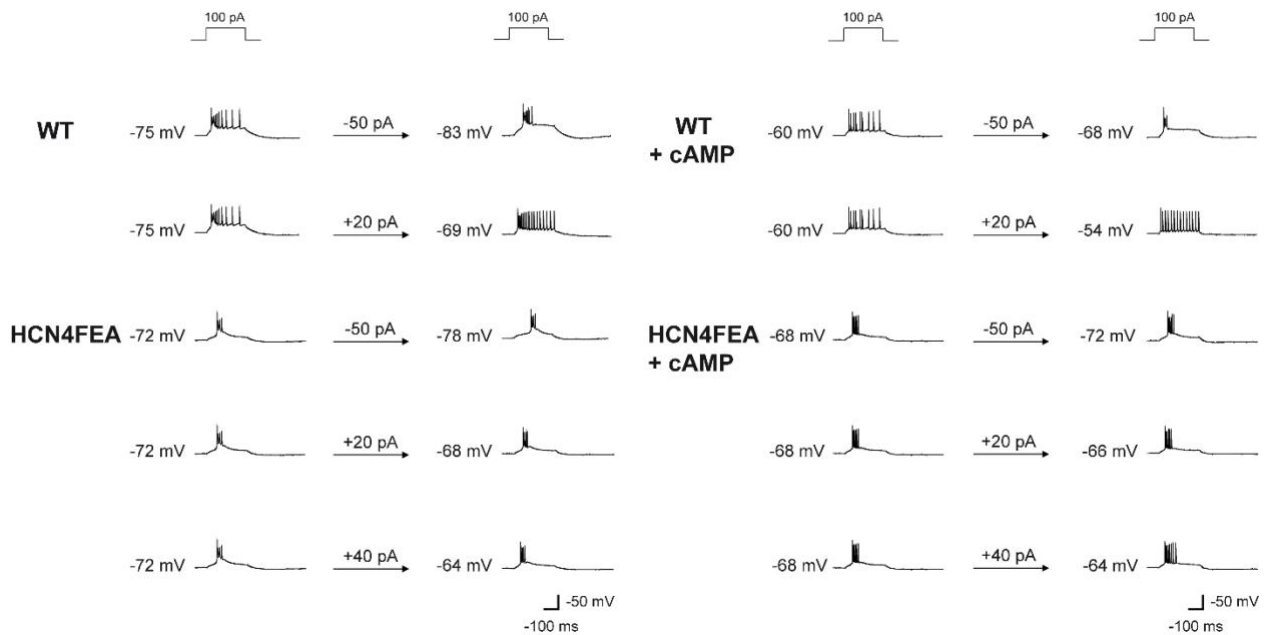
Figure 17. The effect of the RMP on firing properties of WT and HCN4FEA TC neurons in the VB. Representative traces of WT and HCN4FEA TC neurons in the absence (*left panel*) and presence (+cAMP, *right panel*) of 1 µM 8-Br cAMP at 100 pA current injections for 300 ms. Currents were measured at the RMP (*left current trace*), and either a -50 pA or +20 pA current injection was also added to the protocol to hyperpolarize or depolarize, respectively, the RMP (*right current trace*).

3.2.2   Impaired rebound burst firing in TC neurons in the VB complex

The voltage sag is characterized by a prominent and slow time-dependent inward rectification in response to membrane hyperpolarization, and is a characteristic feature of I_h (Tanaka et al., 2003). HCN4FEA neurons tended to show a smaller, less pronounced voltage sag compared to WT neurons, (i.e. the ratio between the peak and steady-state voltage was closer to 1), although this difference was not significant (Figure 18A, B). The input resistance was also not different between WT and HCN4FEA neurons (Figure 18C). However, consequences of impaired CDR of the HCN4 channel were detected in rebound burst firing, as a significantly greater magnitude of current injection was required to reach the burst firing threshold in HCN4FEA neurons compared to WT (Figure 18D; WT –cAMP, -37.27 ± 1.94 pA; HCN4FEA –cAMP, -58.18 ± 5.53 pA). HCN4FEA neurons also produced fewer action potentials per burst compared to WT (Figure 18E; WT –cAMP, 6.45 ± 0.47; HCN4FEA –cAMP, 4.36 ± 0.39). Taken together, these findings support a key role of CDR of HCN4 in regulating the transition between burst to tonic firing, the frequency of burst and tonic firing, and the current threshold for burst firing, in TC neurons in the VB.
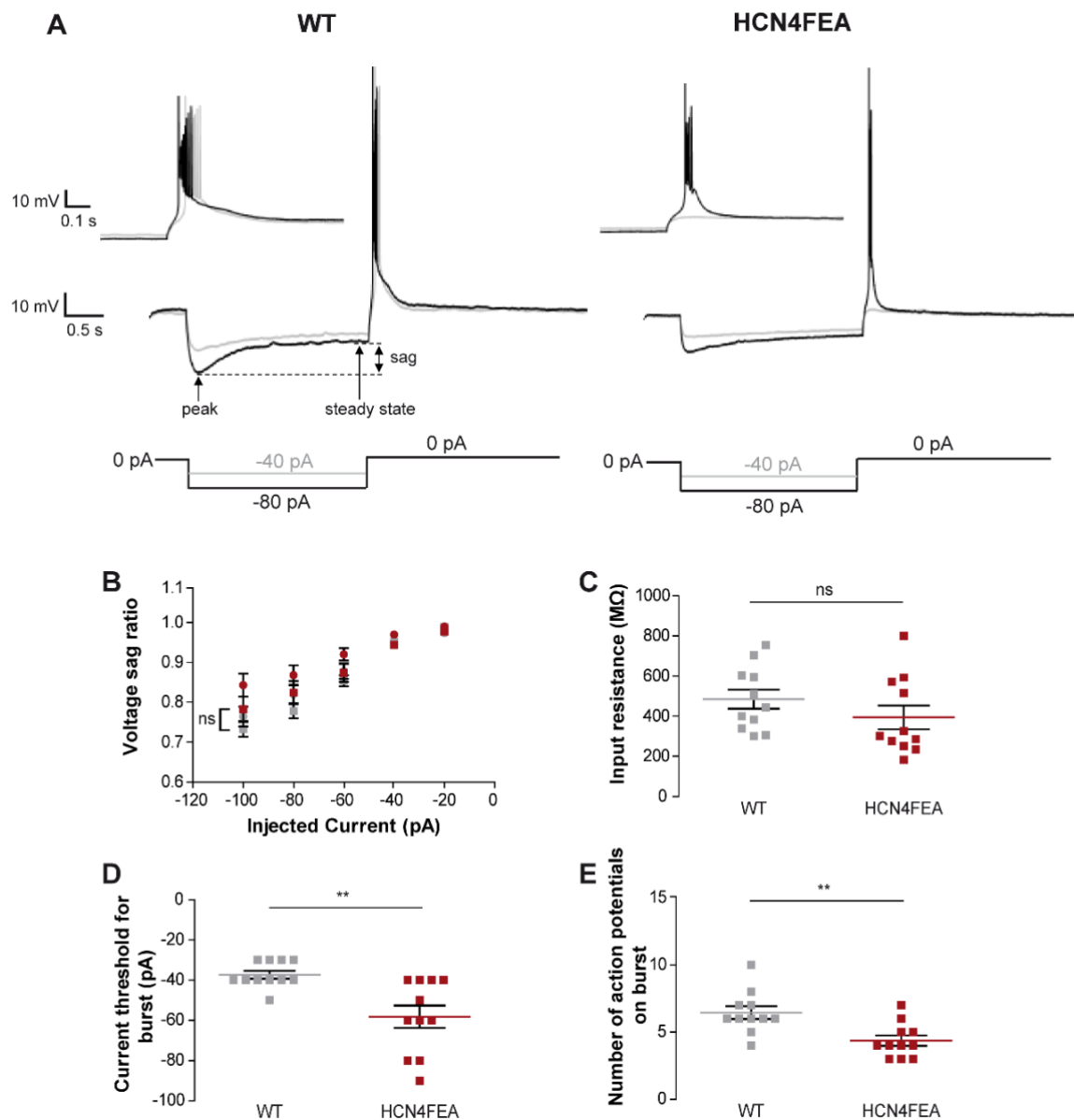
Figure 18. HCN4FEA TC neurons display suppressed burst firing. (A) Representative current clamp traces of WT (*left panel*) and HCN4FEA (*right panel*) VB neurons in the absence of cAMP, in response to 2.5 s hyperpolarizing current injections at -80 pA (black) and -40 pA (grey). The same recordings at a higher time resolution are shown in (**A**, *insets*). **(B)** The voltage sag was determined by applying negative-current injections for 2.5 s in 20 pA increments from −100 to −20 pA. The voltage sag ratio was calculated by dividing the steady state of the sag measurement by the peak voltage deflection (WT -cAMP, grey squares [*n*=11]; WT +cAMP, grey squares [*n*=10]; HCN4FEA -cAMP, red squares [*n*=11]; HCN4FEA +cAMP, red circles [*n*=9], *P*=0.3477 in two-way ANOVA test between WT -cAMP and HCN4FEA -cAMP). **(C)** Mean data for input resistance (WT -cAMP, [*n*=11]; HCN4FEA -cAMP, [*n*=11]; *P*=0.2452 in two sample t test). **(D)** Mean data for the magnitude of current injection required for threshold burst-firing (WT -cAMP, [*n*=11]; HCN4FEA -cAMP, [*n*=11]; *P*=0.0019 in two sample t test) **(E)** The number of action potentials per burst at threshold (WT -cAMP, [*n*=11]; HCN4FEA -cAMP, [*n*=11]; *P*=0.0028 in two sample t test). **(B, C)** ns, not significant.

3.3   HCN4FEA mice show impaired sensitivity to 5-HT

The effects of 5-HT and NA on I_h in the thalamus have previously been investigated (McCormick and Pape, 1990). Both neurotransmitters are coupled to $G_{\alpha s}/G_{\alpha i}$ cAMP signalling, and have been proposed to regulate thalamic network activity (McCormick, 1992; Frère and Lüthi, 2004). I investigated the effect of 5-HT on I_h by applying 20 µM 5-HT to the bath solution for 12-15 min, and recording steady-state activation curves. The amplitude of the current at maximal activation at -140 mV was not different between WT with 5-HT or HCN4FEA with 5-HT, observed from the current traces and the time course of 5-HT treatment (Figure 19).
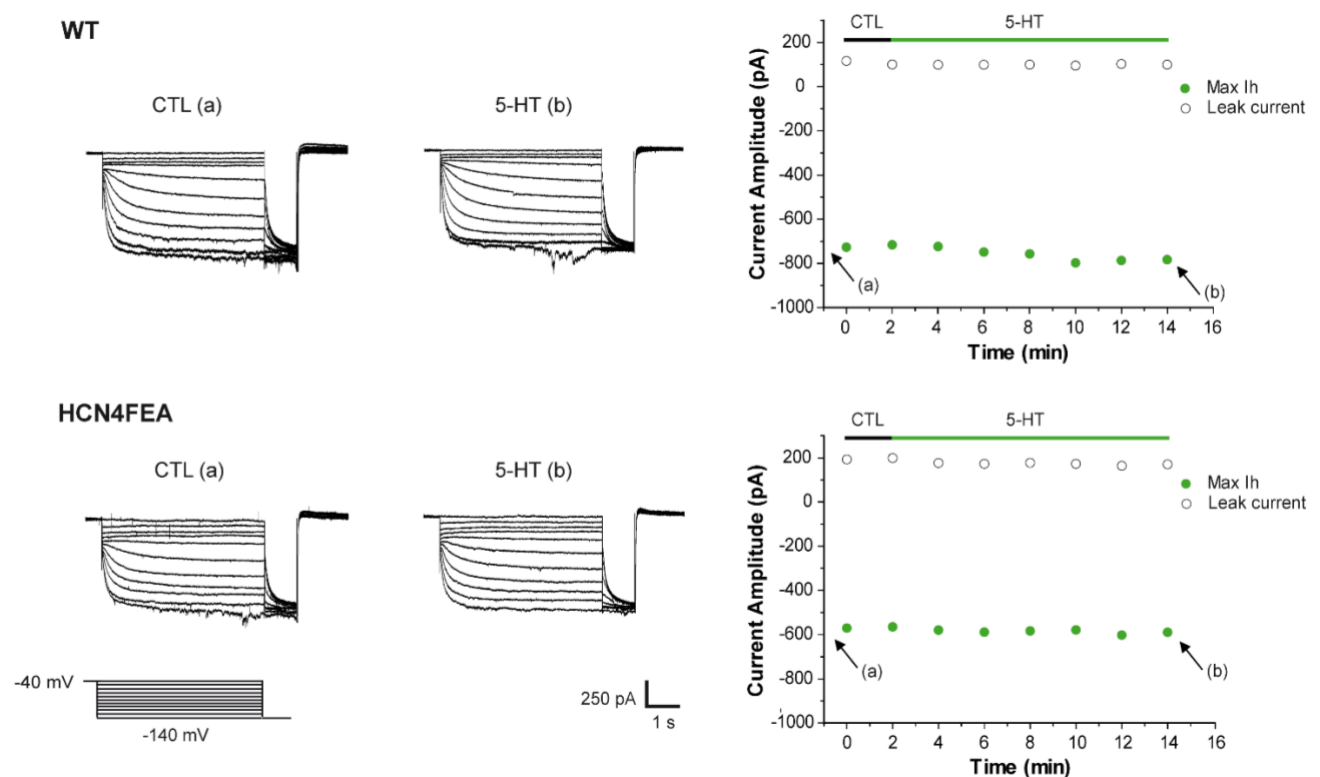

Figure 19. Time course of 5-HT treatment of WT and HCN4FEA TC neurons. Representative I_h traces from TC WT (*upper*) and HCN4FEA (*lower*) neurons in the VB, before (*left,* a) and after (*right,* b) 20 µM 5-HT. Below, is the voltage protocol used to evoke the current traces, peak tail currents resulted from a 1 s voltage step to -140 mV from a 5 s voltage step (-140 mV to -40 mV; in 10 mV increments). The time course of 5-HT application (right) was monitored by a 3 s voltage step to -120 mV, and plotted with the leak current to monitor the health of the cell.

In WT TC neurons the $V_{0.5}$ showed two groups of responses. A small hyperpolarizing shift in response to 5-HT was observed in 57% of cells (Figure 20 upper left; $V_{0.5}$: WT control, -92.74 ± 1.69 mV; WT 5-HT, -94.57 ± 1.30 mV), and a larger shift to depolarized voltages was observed in 43% of cells (Figure 20 upper right $V_{0.5}$: WT control, -89.01 ± 3.49 mV; 5-HT, -84.23 ± 3.69 mV). In contrast, in HCN4FEA TC neurons, the $V_{0.5}$ only showed a small

hyperpolarizing shift (Figure 20 lower left; $V_{0.5}$: HCN4FEA control, -87.14 ± 1.97 mV; 5-HT, -90.05 ± 2.71 mV). It is possible that HCN4FEA TC neurons may show a depolarizing shift due to residual cAMP modulation from HCN2. However, none of the HCN4FEA cells recorded from showed a depolarizing shift and all cells showed a small hyperpolarizing shift.
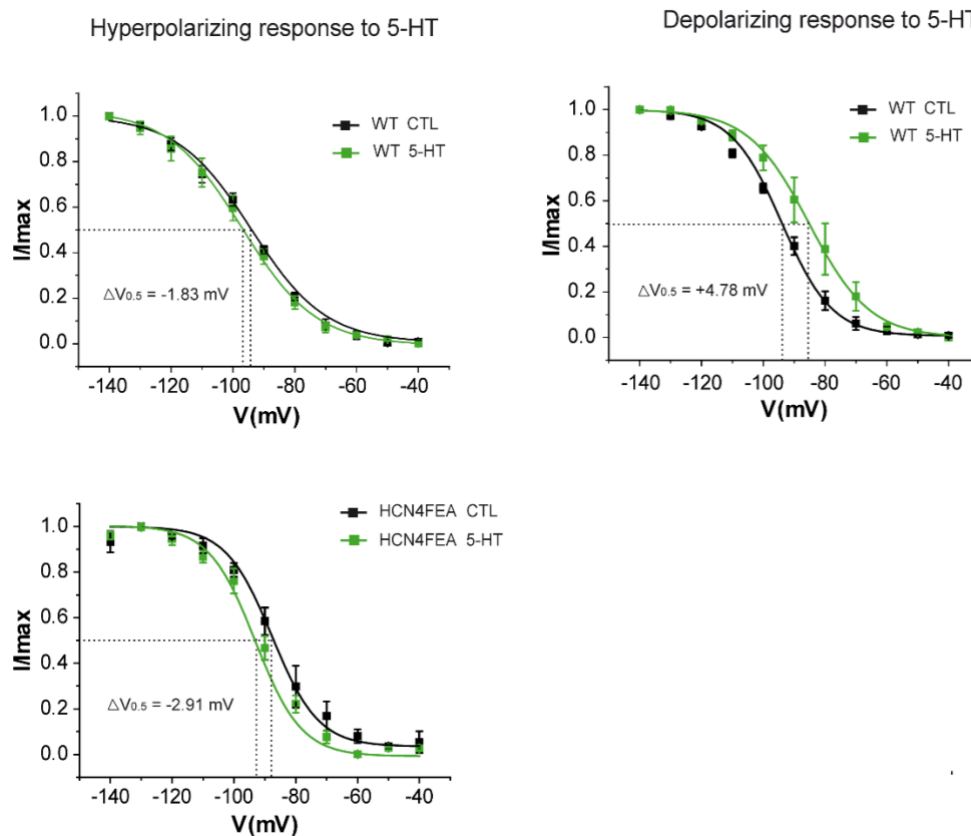

Figure 20. Impaired serotonergic modulation of I_h in HCN4FEA TC neurons. The voltage dependence of activation of I_h shows a depolarizing shift in the presence of 5-HT in WT but not HCN4FEA TC neurons**.** Normalized current-voltage relationships of I_h in TC neurons in the VB of WT (*upper*) and HCN4FEA (*lower*) mice, after treatment with 20 μM 5-HT (green).   The control is shown in the black.   WT hyperpolarizing response [*n*=4], *P*=0.2515 in paired t test*;* WT depolarizing response [*n*=3], *P*=0.1693 in paired t test; HCN4FEA [*n*=5], *P*=0.0752 in paired t test*.*

However, there was no significant difference in the $V_{0.5}$ in WT or HCN4FEA TC neurons before and after 5-HT treatment. There was also no significant difference observed in the RMP (Figure 21B), the tau slow (Figure 21C) and tau fast values (Figure 21D), before and after 5-HT treatment. Although there were no significant differences in the $V_{0.5}$, RMP, and tau values, it must be noted that responses to 5-HT were variable and the shifts of these parameters in response to 5-HT were small.
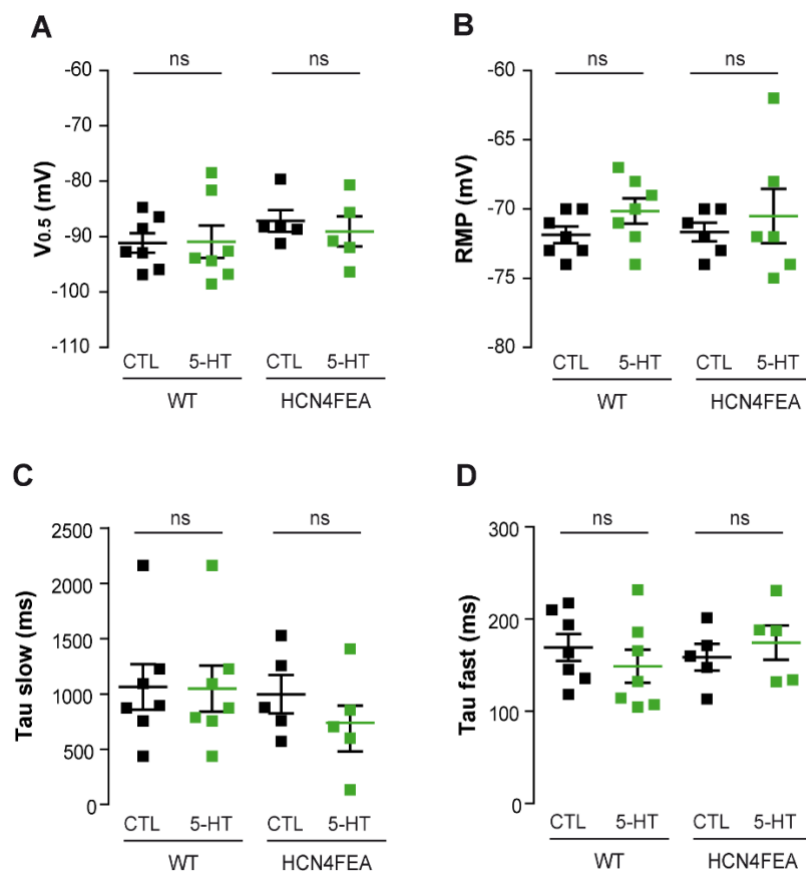
Figure 21. Biophysical properties of WT and HCN4FEA TC neurons in response to 5-HT treatment. The parameters in **(A-D)** were measured in WT and HCN4FEA TC neurons in the control (black) and after treatment with 20 µM 5-HT (green), WT [$n=7$]; HCN4FEA [$n=5$]. **(A)** $V_{0.5}$, WT, $P=0.8924$, HCN4FEA, $P=0.0752$ in paired t test. **(B)** RMP, WT, $P=0.1578$, HCN4FEA, $P=0.5407$ in paired t test. **(C)** Tau slow WT, $P=0.3559$, HCN4FEA, $P=0.0875$ in paired t test. **(D)** Tau fast: WT, $P=0.1839$, HCN4FEA, $P=0.4252$ in paired t test.

I examined the expression of 5-HT receptors and α-adrenergic receptors coupled to $G_{\alpha s}/G_{\alpha i}$ cAMP signalling. I examined the expression of the 5-HT1$_A$, 5-HT1$_B$, 5-HT$_6$ and the 5-HT$_7$ receptors from WT and HCN4FEA mouse thalamus, as these receptors are thought to be the main subtypes expressed in the thalamus (Shukla et al., 2014). The 5-HT$_3$ receptor thought to be expressed at very low levels in the thalamus (Shukla et al., 2014), was included as a control. qPCR revealed that expression of the 5-HT$_7$ receptor was reduced in HCN4FEA mice (Figure 22A). The 5-HT$_6$ receptor is the other 5-HT receptor coupled to $G_{\alpha s}$, but was expressed at very low levels (Figure 22A). The 5-HT1$_A$ and 5-HT1$_B$ receptors were expressed at lower levels compared to the 5-HT$_7$ receptor, but approximately equal levels (Figure 22A). Examination of the α-adrenergic receptors showed that expression of the adrenergic α2B receptor was also reduced in HCN4FEA mice, although was the lowest expressed receptor (Figure 22B).
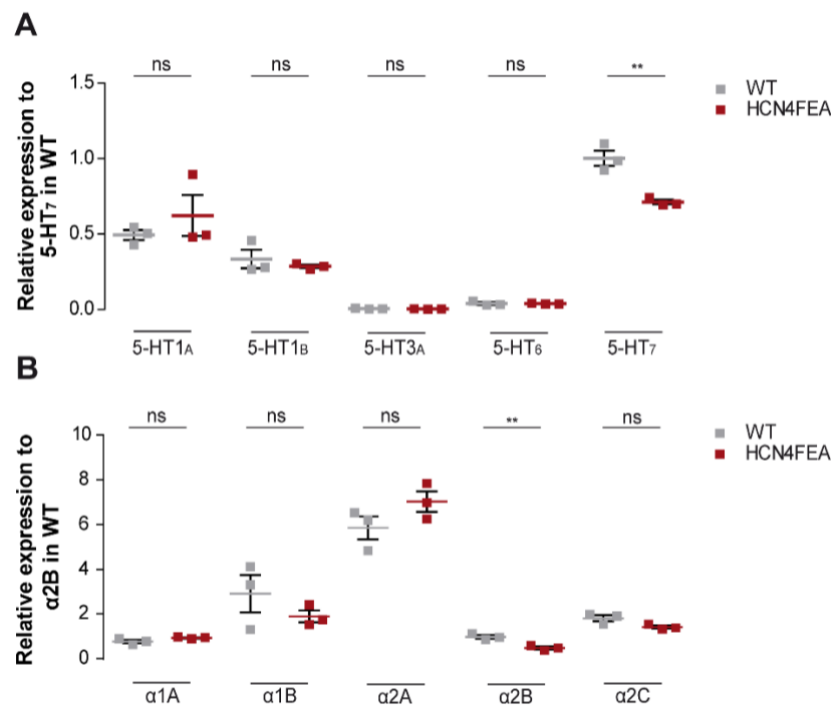
Figure 22. HCN4FEA mice show decreased expression of the 5-HT$_7$ receptor and α2B adrenergic receptor in the thalamus. The whole thalamus was dissected from age P30-P40 WT(grey squares, n=3) and HCN4FEA (red squares, n=3) mice, and expression was detected using qPCR. The analysis was performed using the delta-delta-Ct method. **(A)** Relative expression levels of selected 5-HT receptor transcripts. 5HT$_7$, P=0.0055 in two sample t test. ns, not significant. **(B)** Relative expression levels of α-adrenergic receptor transcripts. α2B, P=0.0071 in two sample t test. ns, not significant.

The depolarizing shift in the $V_{0.5}$ observed after 5-HT treatment in WT neurons (Figure 20, upper right) is consistent with the activation of 5-HT$_7$ receptors and the ability of HCN4 to bind cAMP. The small hyperpolarizing shift in the $V_{0.5}$ in WT neurons (Figure 20, upper left) is consistent with the activation of 5HT$_{1A}$ and 5HT$_{1B}$ receptors. However, as the 5HT$_7$, 5HT$_{1A}$ and 5HT$_{1B}$ receptors may be activated simultaneously, the larger depolarizing shift attributed to the activation of the 5HT$_7$ receptor likely masks the hyperpolarizing shift from activation of the 5HT$_{1A}$ and 5HT$_{1B}$ receptors which is likely why the hyperpolarizing shift in WT neurons is small. The small hyperpolarizing shift observed in HCN4FEA neurons (Figure 20, lower left) is also consistent with the inability of cAMP to bind to HCN4 and probable activation of the 5HT$_{1A}$ and 5HT$_{1B}$ receptors.

Given the predominant expression of 5-HT$_7$ in the thalamus and the decreased expression observed in HCN4FEA, I attempted to further investigated the effect of 5-HT on I$_h$ by applying 20 µM 5-HT to the bath solution for 15 min and recording steady-state activation curves and subsequently adding a specific blocker for 5-HT$_7$ receptors, SB-269970 for 10 min. This was to determine the contribution of 5-HT$_7$ receptor and confirm if the depolarizing shifts in the $V_{0.5}$ was indeed due to the activation of 5-HT$_7$ receptor and the corresponding increases in cAMP levels. In my preliminary results, in WT TC neurons the $V_{0.5}$ again showed two

responses in the presence of 5-HT. The first, a shift to depolarized voltages in response to 5-HT which was reversible after the addition of SB-269970 although the slope of the curve changed (Figure 23 right; $V_{0.5}$: WT control, -86.35 mV ± 1.28 mV; 5-HT, 81.70 ± 1.60 mV; SB-269970, -87.68 ± 0.82 mV). This result confirmed that the depolarizing shift was indeed due to activation of the 5-HT$_7$ receptor, and subsequent activation of $G_{\alpha s.}$ Secondly, I also observed a small shift to hyperpolarized voltages, which was not shifted after the addition of SB-269970 (Figure 23 left; $V_{0.5}$: WT control, -93.35 ± 3.81 mV; 5-HT, 95.58 ± 1.70 mV; SB-269970, -95.40 ± 0.41 mV). This is consistent with predominant activation of 5-HT1$_A$ and/or 5-HT1$_B$ receptors. However, I could not obtain a recording from an HCN4FEA TC neuron with SB-269970. Off target effects of SB-269970 were also not examined for in this experiment.
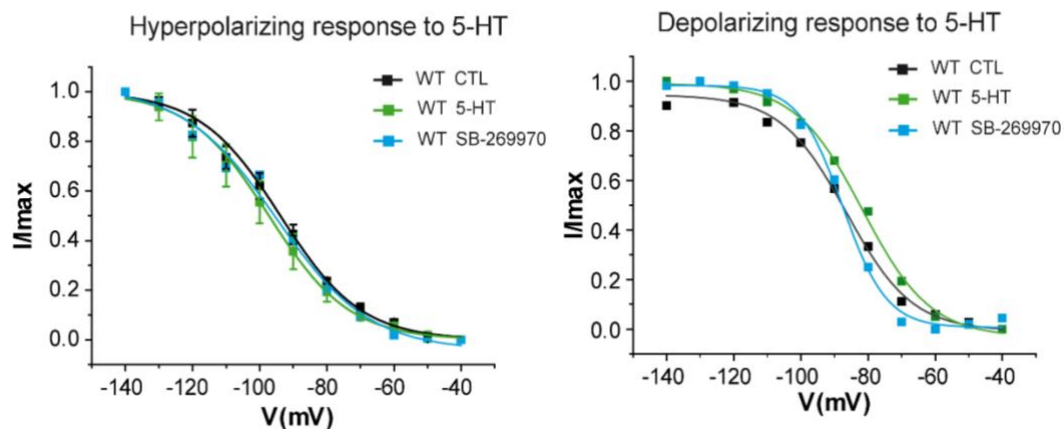

Figure 23. Contribution of the 5-HT$_7$ receptor to the shift in $V_{0.5}$ of I_h in response to 5-HT. Normalized current-voltage relationships of I_h in TC neurons in the VB of WT after treatment with 20 µM 5-HT (green) and subsequently 10 µM SB-269970 (blue). The control is shown in the black. Data from the same neurons for the control, and after 5-HT treatment, are shown. WT hyperpolarizing response [*n*=2]; WT depolarizing response [*n*=1].

3.4 HCN4FEA mice show an impaired EEG profile

The specific roles of HCN4 in the regulation of vigilance states has not been previously discovered. HCN4FEA mice did not show spike-wave-discharges (SWD) in telemetric EEG recordings, the hallmark of generalized seizures of the absence-epilepsy type, indicating that CDR of HCN4 does not contribute in generating absence seizures (data not shown). In order to determine the roles of HCN4 in the vigilance states, and the consequences of altered thalamic network activity in HCN4FEA mice, telemetric EEG recordings were performed. There was no difference in the NREM, REM, or wake power spectra (Figure 24). Although there appeared to be an increase in the delta range (0.5-4 Hz) in HCN4FEA mice, it cannot be concluded that it is a real increase, because it may be very likely due to movement artifacts.
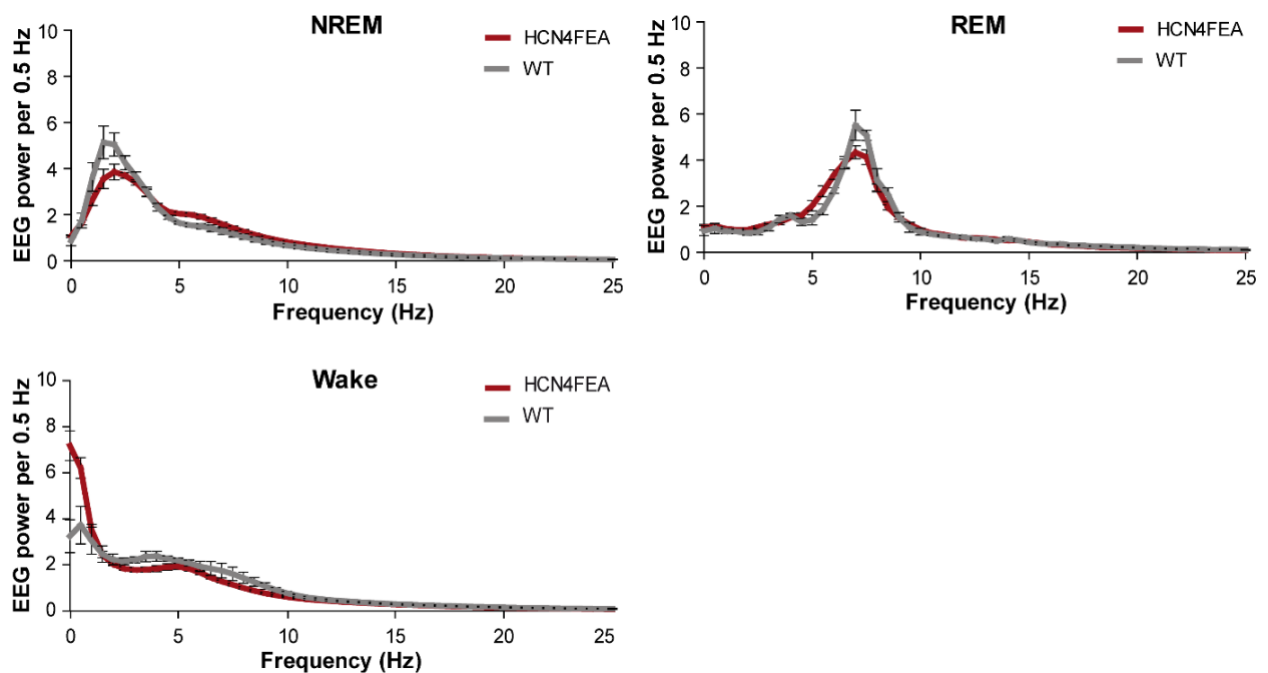
Figure 24. Power spectra of HCN4FEA mice. Power spectra of NREM (*upper left*) and REM (upper right) sleep, and the wake state (*lower left*) in WT (grey squares, *n*=5) and HCN4FEA (red squares, *n*=6) mice. Data provided by Manuela Brümmer.

Both WT and HCN4FEA mice were entrained to a 12 h light/12 h dark cycle, and showed a sleep-wake pattern characteristic of nocturnal animals which have their active period during the dark phase and their main resting period during the light phase. In the dark phase they spend approximately 70% of their time asleep (NREM and REM sleep). The transitions between NREM, REM and the wake state were examined, which revealed that HCN4FEA mice showed a significantly fewer number of transitions from NREM to the wake state during a 24 hour period (Figure 25A). Closer analysis of the NREM to wake transition in the theta power range, revealed that at time zero when the mouse awakens, in WT mice there is a decrease (Figure 25B), as arousal is accompanied by a power shift from high frequency to low frequency (Akerstedt et al., 2002). However, in HCN4FEA mice, the frequency remains high even after waking (Figure 25B). This result is also in line with the significantly reduced frequency of tonic firing observed in TC neurons in the presence of cAMP (Figure 16B), and the reduced number of burst spikes and reduced current threshold for rebound burst firing observed (18D, E). However, a difference was not observed between WT and HCN4FEA mice with respect to the total time spent in the NREM state, or the other vigilance states during the light and dark phases (Figure 25C). There was also no difference in the number of brief awakenings during a 24 h period (Figure 25D).
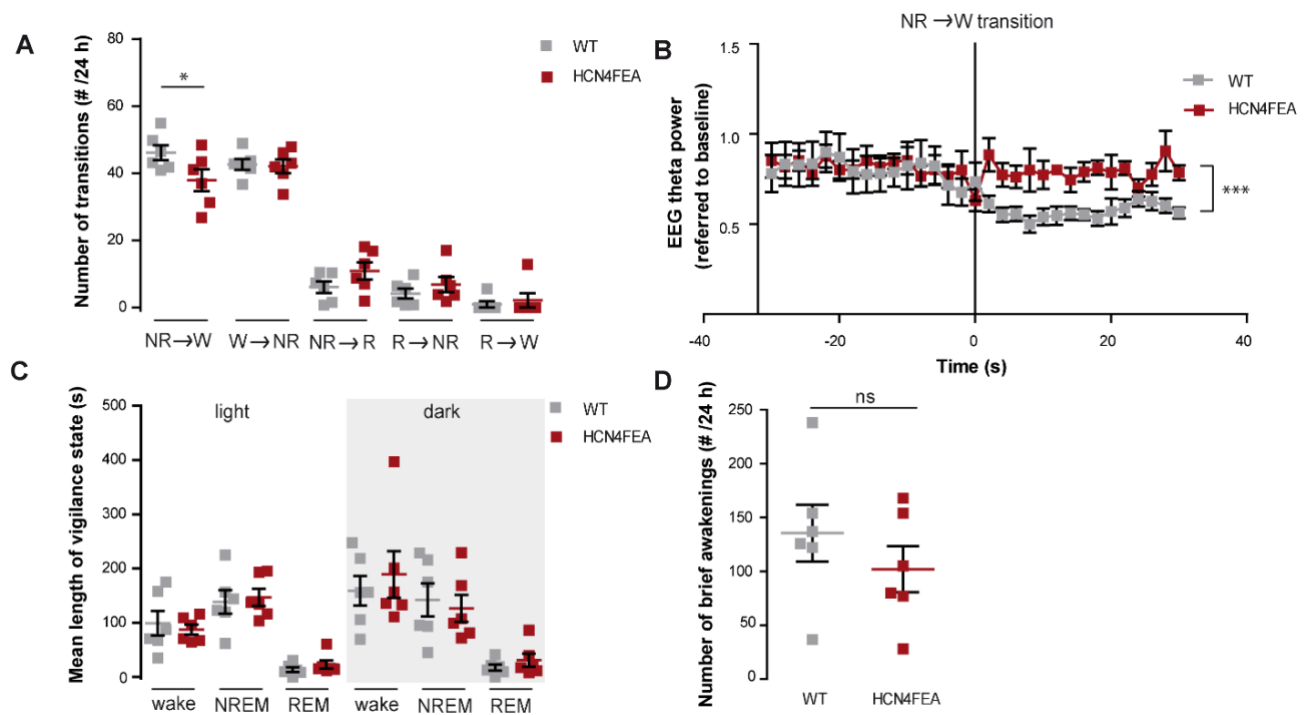
Figure 25. HCN4FEA mice show a reduced number of transitions from the NREM to wake state. The vigilance states, and the transition between vigilance states, of WT and HCN4FEA mice. (WT, grey squares n=5 mice; HCN4FEA, red squares n=6 mice). **(A)** The number of transitions between the NREM (NR), REM (R), and wake (W) states during a 24 h period. $P<0.05$ in a one-way ANOVA with Bonferroni's post hoc test. **(B)** Analysis of the NREM to wake transition shown in **(A)**, in the theta power range (4-8 Hz). Time '0' indicates awakening. $P=0.0002$ in a two-way ANOVA with Bonferroni's post hoc test. **(C)** Time spent in different vigilance states (wake, NREM and REM sleep) during light and dark periods. $P>0.05$ in a one-way ANOVA with Bonferroni's post hoc test. **(D)** The number of brief awakenings during a 24 h period. $P=0.3441$ in unpaired t test. Data provided by Dr. Verena Mehlfeld and Manuela Brümmer.
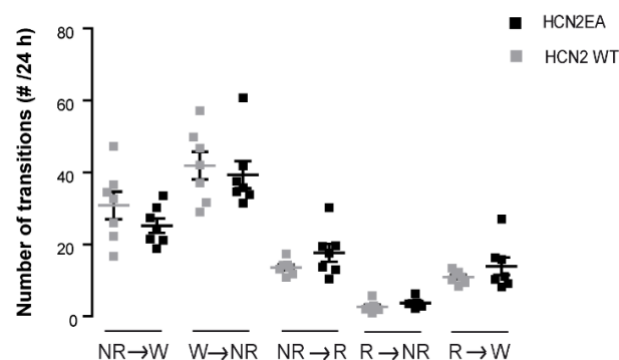
Figure 26. HCN2EA mice do not show a reduced number of transitions from the NREM to wake state. (B) The number of transitions between the NREM (NR), REM (R), and wake (W) states during a 12 h period (HCN2 WT, grey squares n=7 mice; HCN2EA, black squares n=7 mice). $P>0.05$ in one-way ANOVA with Bonferroni's post hoc test. Data provided by Saskia Spahn.

In contrast, HCN2EA mice did not show a significant difference in the number of transitions from the NREM to the wake state, or in any of the transitions in the sleep cycle (Figure 26). It was also observed previously that HCN2EA do not show a difference in the

length of any of the vigilance states (Hammelmann et al., 2019). Taken together, this indicates that CDR of HCN4 regulates the transition from the NREM to the wake state, and this role is distinct from CDR of HCN2.
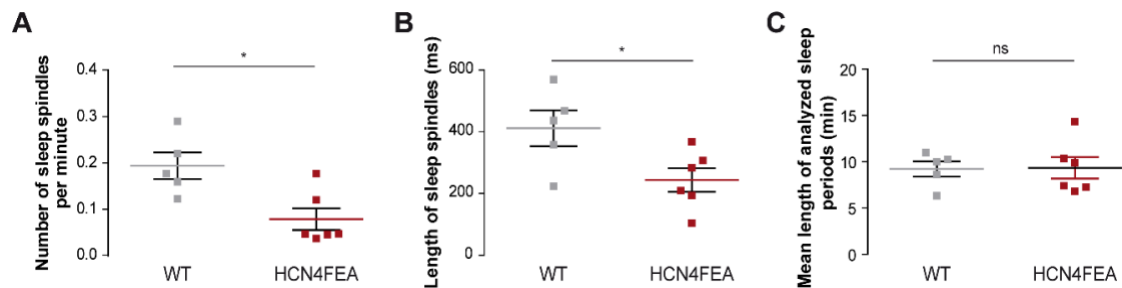
Figure 27. HCN4FEA mice show a decreased number and length of sleep spindles compared to WT. (A) The number of sleep spindles per minute in WT (grey squares, *n*=5) and HCN4FEA (red squares, *n*=6) mice, *P*=0.0118 in two sample t test. **(B)** The length of sleep spindles in WT (grey squares, *n*=5) and HCN4FEA (red squares, *n*=6) mice, *P*=0.0348 in two sample t test. **(C)** Mean length of the analyzed sleep periods in WT (grey squares, *n*=5) and HCN4FEA (red squares, *n*=6) mice, *P*=0.9472 in a two sample t test. ns, not significant. Data provided by Manuela Brümmer.

Sleep spindles are characteristic EEG signatures of stage 2 NREM sleep. In HCN4FEA mice, both the number and the length of sleep spindles was reduced (Figure 27A, B), while the total sleep period was similar (Figure 27C). This indicates that CDR of HCN4 is also a regulator of low-frequency sleep waves particular in the sigma (10-15 Hz) frequency range.

3.5 HCN4FEA mice show anxiety-like behaviours

Previous studies have suggested that HCN4 may play a role in mood and anxiety disorders (Kelmendi et al., 2011; Günther et al., 2019). I hypothesized that CDR of HCN4 may also have a role, and HCN4FEA mice were tested for the presence of anxiogenic behaviours. Mice were placed in the open field apparatus and their locomotion was tracked, with parameters measured at 5 min and 20 min (Figure 28A), HCN4FEA mice appeared to engage less in exploratory behaviour particularly in the inner region compared to WT mice (Figure 28B), while there was no difference observed between HCN2EA mice with their WT littermates (Figure 28C).

Open Field Test

A

Inner Region

Outer Region

Track locomotion and time in inner region

0 min   5 min   20 min

B

WT   HCN4FEA

C

HCN2 WT   HCN2EA
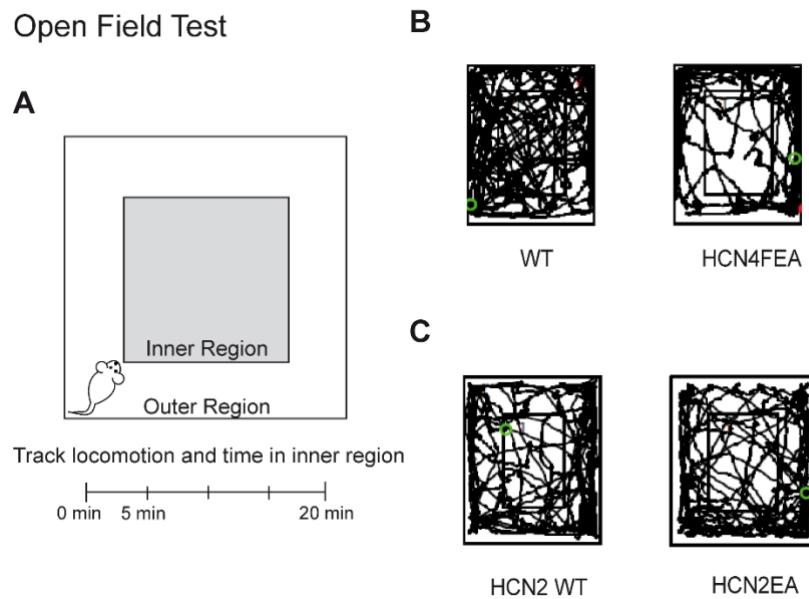
Figure 28. The Open Field Test. **(A)** Experimental scheme of The Open Field Test, The parameters in Figure 29 were tracked and measured at 5 min and 20 min. **(B)** Representative tracks of HCN4FEA mice (*right*) with respective WT littermates (*left*) in the Open Field Test at 5 min. **(C)** Representative tracks of HCN2EA (*right*) and with respective WT littermates (*left*) mice in the Open Field Test at 5 min. Data provided by Dr. Verena Mehlfeld.

There was no difference in the speed or the total distance travelled between WT and HCN4FEA mice (Figure 29A, B) indicating that HCN4FEA mice do not show motor deficits. HCN4FEA mice showed increased latency to first enter the inner region (Figure 29C), and spent less time in the inner region (Figure 29D) compared to WT mice, indicative of anxiety-like behaviour. In contrast, HCN2EA mice did not show any differences in the latency to enter the inner region or the time spent in the inner region (Figure 29H, I), indicating that they do not show anxiety-like behaviour. There was also no difference in the speed of the mice or the distance travelled (Figure 29F, G), indicating that HCN2EA mice also do not show motor deficits.

Figure 29. HCN4FEA mice show increased anxiety-like behaviour compared to WT mice in The Open Field Test. Parameters measured of The Open Field Test described in Figure 28, at 5 min. **(A-E)** HCN4FEA mice (red squares, *n*=12 mice) with respective WT littermates (WT) (grey squares, *n*=11 mice). **(A)** Global speed of the mice; *P*=0.6212 in two sample t test. **(B)** 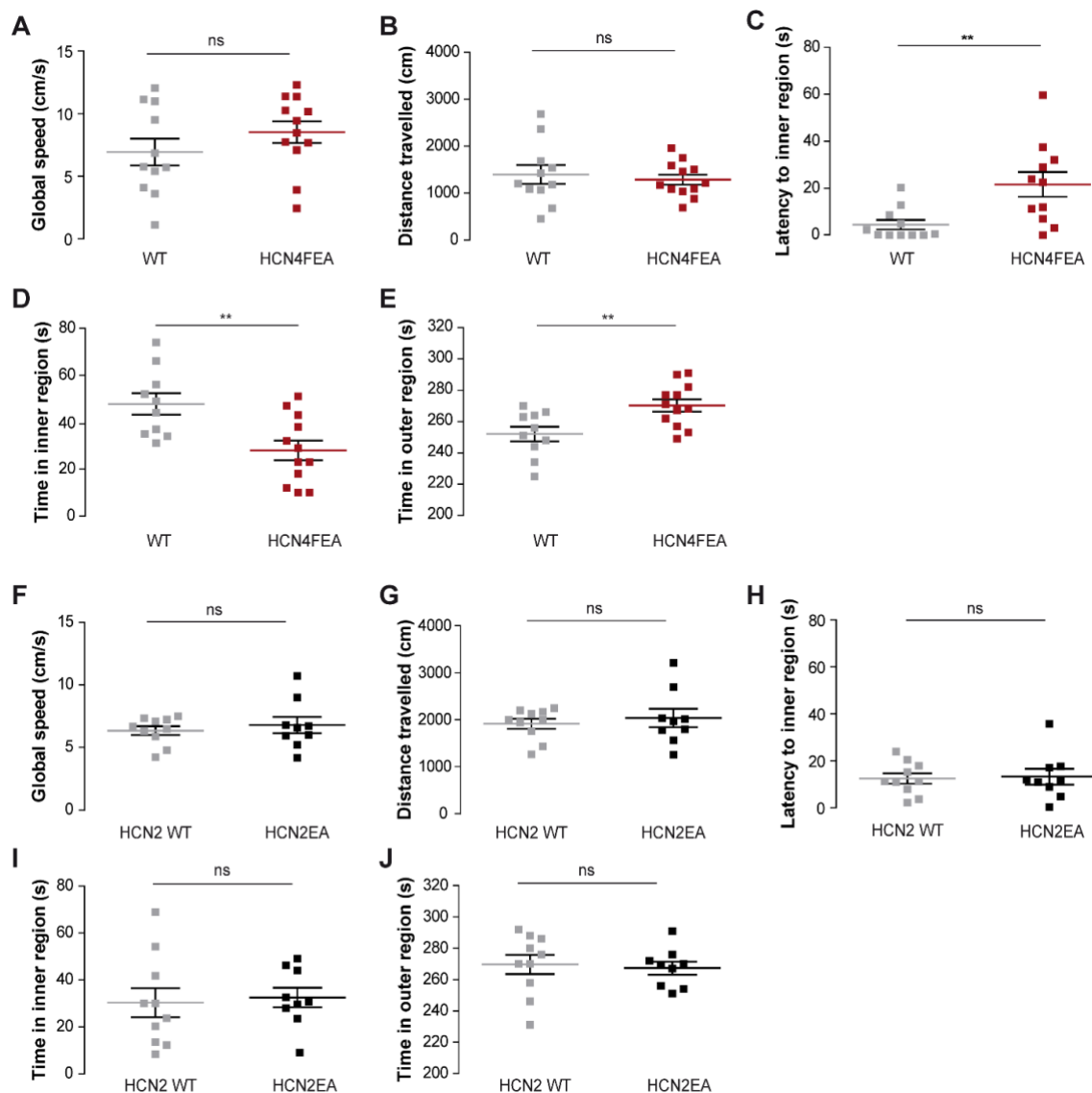The total distance travelled; *P*=0.6218 in two sample t test. **(C)** The latency for the mouse to first enter the inner region; *P*=0.0064 in two sample t test. **(D)** Time spent in the inner region; *P*=0.0044 in two sample t test. **(E)** Time spent in the outer region; *P*=0.0069 in two sample t test. **(A,B)** ns, not significant. **(F-J)** HCN2EA mice (black squares, *n*=9 mice) with respective WT littermates (HCN2 WT) (grey squares, *n*=10 mice). **(F)** Global speed of the mice; *P*=0.5466 in two sample t test. **(G)** The total distance travelled; *P*=0.5789 in two sample t test. **(H)** The latency for the mouse to first enter the inner region; *P*=0.08471 in unpaired t test. **(I)** Time spent in the inner region; *P*=0.7709 in two sample t test. **(J)** Time spent in the outer region; *P*=0.7600 in two sample t test. ns, not significant. Data provided by Dr. Verena Mehlfeld.

The anxiety-like behaviour observed in HCN4FEA mice was further supported in the light-dark transition test (Figure 30). Mice were placed into the dark chamber of a box in which a third of the box composed the dark region, and the other two-thirds of the box composed the light region and the transitions between the two regions were measured (Figure 30A). HCN4FEA mice spent more time in the dark chamber (Figure 30B), showed fewer transitions from the dark chamber to the light chamber (Figure 30C), and travelled a shorter distance in

the light chamber (Figure 30D), which is indicative of bright-space anxiety in mice (Takao and Miyakawa, 2006). However, the latency to enter the light region was not different between HCN4FEA and WT mice (Figure 30E). There was no difference in the speed of the mice in the light chamber (Figure 30F), further indicating that HCN4FEA mice do not show motor deficits. HCN2EA mice did not show a difference in any of the parameters measured (Figure 30H-L), further indicating that HCN2EA mice do not show anxiety-like behaviour or movement deficits. Taken together, these results indicate that CDR of HCN4 but not HCN2, has a role in anxiety-like behaviour.

Light-Dark Test
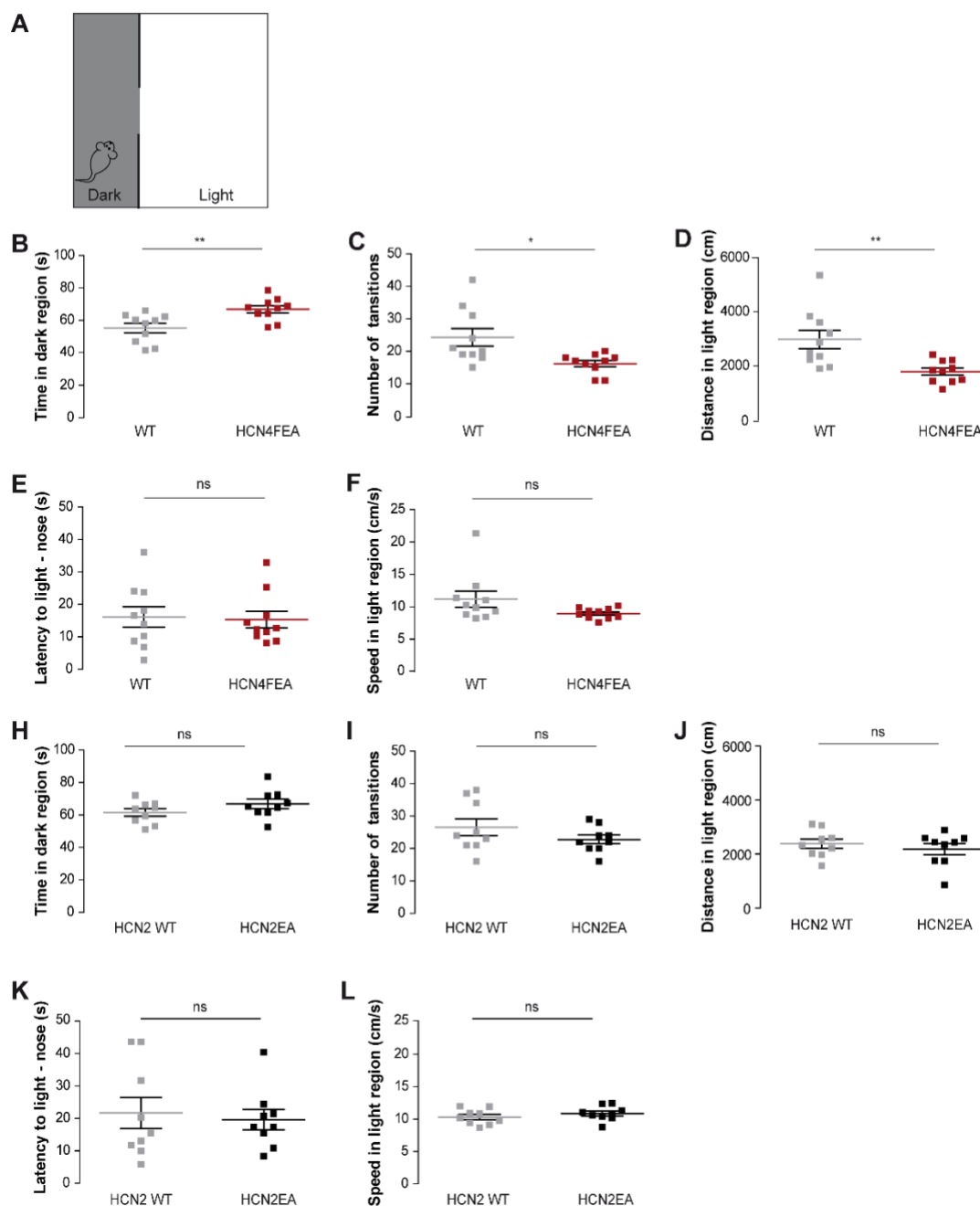
Figure 30. HCN4FEA mice show increased anxiety-like behaviour compared to WT mice in The Light-Dark Test. (A) Experimental scheme, mice were placed into the dark chamber and allowed to move freely between the dark and light chambers for 10 min, and the parameters in **B-F** were tracked. **(A-E)** HCN4FEA mice (red squares, n=10 mice) with respective WT littermates (WT) (grey squares, n=10 mice). **(B)** Length of time spent in the dark region; P=0.0047 in two sample t test. **(C)** The number of transitions between the light and dark regions; P=0.0017 in two sample t test. **(D)** The distance travelled in the light region; P=0.0040 in two sample t test. **(E)** The latency for the nose of the mouse to first enter the light region; P=0.8407 in two sample t test. **(F)** The speed of the mice in the light region; P=0.0948 in two sample t test. **(H-K)** HCN2EA mice (black squares, n=9 mice) with respective WT littermates (HCN2 WT) (grey squares, n=9 mice). **(H)** Length of time spent in the dark region; P=0.1741 in two sample t test. **(I)** The number of transitions between the light and dark regions; P=0.2169 in two sample t test. **(J)** The distance travelled in the light region; P=0.4687 in two sample t test. **(K)** The latency for the nose of the mouse to first enter the light region; P=0.7192 in two sample t test. **(L)** The speed of the mice in the light region; P=0.3416 in two sample t test. ns, not significant. Data provided by Dr. Verena Mehlfeld.

HCN4FEA mice were also tested in a social interaction test with a novel juvenile partner. In this test, mice were placed in a cage with a juvenile male mouse with a protective barrier around the juvenile mouse, and the contact with the juvenile mouse was measured (Figure 31A). HCN4FEA mice did not show a difference in the length of interactions (Figure 31B), suggesting social interaction behaviour with a novel juvenile mouse is not impaired. HCN4FEA mice again did not show a difference in speed compared to WT mice (Figure 31C). HCN2EA mice also did not show a difference in in the length of interactions (Figure 31D) suggesting that HCN2EA mice also do not show an impairment in sociability with a novel juvenile partner.
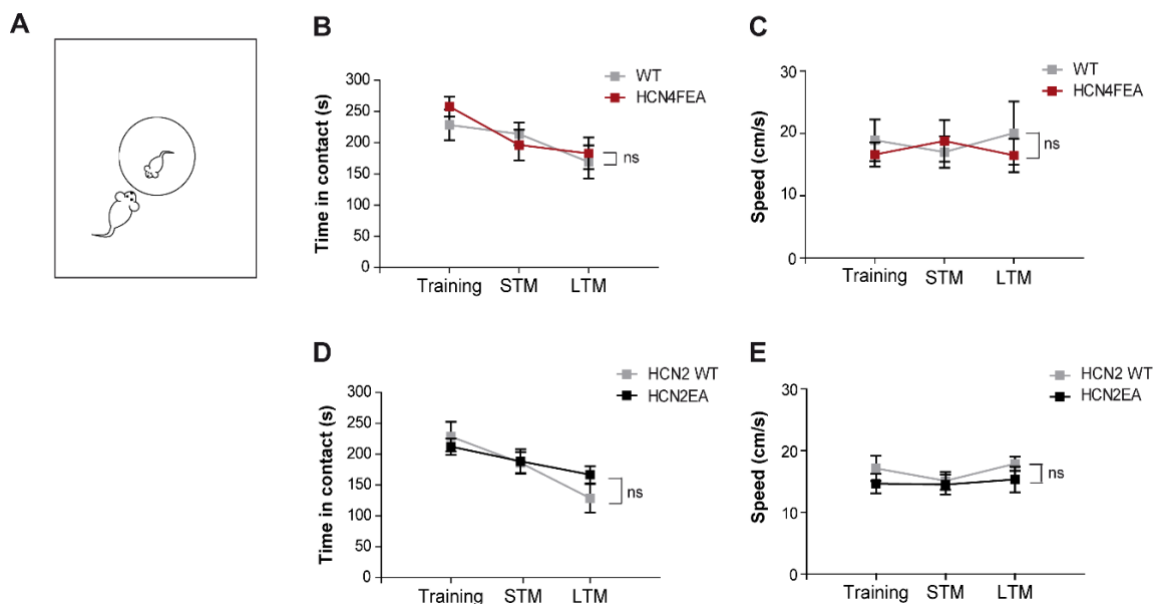
Figure 31. HCN4FEA mice do not show impaired social interaction in The Social Interaction Test. (A) The experimental scheme, a juvenile mouse was placed in the center of the cage in a protective barrier, and the paramenters in **(B-C)** were tracked over a 5 min period, and were measured in three different periods, first during the training period, 1 h later to test STM and 24-hours later to test LTM. **(B-C)** HCN4FEA mice (red squares, n=8 mice) with respective WT littermates (WT) (grey squares, n=8 mice). **(B)** The length of time the mice were in contact; P=0.6529 in two-way ANOVA with Bonferroni's post hoc test. **(C)** Speed of the mice; P=0.6136 two-way ANOVA with Bonferroni's post hoc test. **(D-E)** HCN2EA mice (black squares, n=8 mice) with respective WT littermates (HCN2 WT) (grey squares, n=6 mice). **(D)** The length of time the mice were in contact; P=0.3269 in two-way ANOVA with Bonferroni's post hoc test. (**E**) Speed of the mice; P=0.8122 two-way ANOVA with Bonferroni's post hoc test. ns, not significant. Data provided by Dr. Verena Mehlfeld.

It has previously been shown that HCN2 but not HCN4, is highly expressed in the dLGN which is the main thalamic relay center of the primary visual pathway (Hammelmann et al., 2019). In the visual discrimination test (Figure 32A) which is sensitive to visual information processing via the geniculate pathway, HCN2EA mice showed reduced visual learning during the first two test days which was not due to a defect in retinal function (Hammelmann et al., 2019). Consistent with this result, HCN4FEA mice did not show any differences in visual

learning capability compared to WT mice over all four test days (Figure 32B, C), further indicating that CDR of HCN4 does not contribute to visual learning capability.
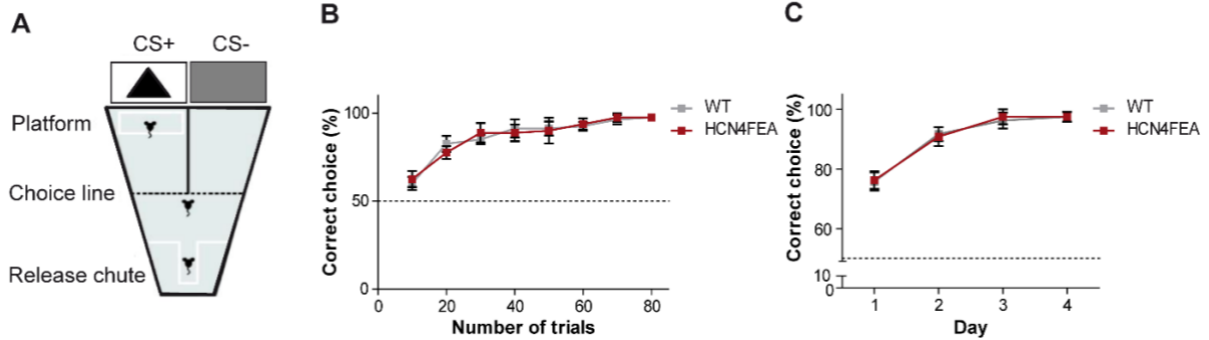
Figure 32. CDR of HCN4 does not affect visual learning in the Visual Discrimination Test. WT (grey squares, n=8 mice) and HCN4FEA mice (red squares, n=8 mice). **(A)** Experimental scheme. CS+, conditioned stimulus. **(B)** The learning curve of WT and HCN4FEA mice for the number of trials. P=0.9722 in two-way ANOVA with Bonferroni's post hoc test. **(C)** The learning curve of WT and HCN4FEA mice over the number of days. P=0.9806 in two-way ANOVA with Bonferroni's post hoc test. Data provided by Dr. Verena Mehlfeld.

4 Discussion

Previous studies have suggested HCN4 as a candidate gene for anxiety disorders. Polymorphisms in the *hcn4* gene have been identified in patients with mood and anxiety disorders including major depressive disorder (MDD), bipolar disorder and obsessive compulsive disorder (OCD) although all located in non-coding regions (Kelmendi et al., 2011; McIntosh 2012). Additionally, knock down of HCN4 in the dorsal hippocampus has been shown to produce anxiety-like behaviour in mice (Günther et al., 2019). However, no study to date has investigated the influence of cAMP binding of the HCN4 channel in the brain. How does CDR of HCN4 affect neuronal networks and behavioural phenotypes? To address this question, the influence of CDR of HCN4 in the thalamus was investigated. In the present study, it was found that CDR of HCN4 regulates a complex pleiotropic neuronal phenotype. On a cellular level, CDR of HCN4 is important in addition to HCN2, in regulating the transition from burst to tonic firing in the VB thalamus. Expression of the predominant 5-HT receptor in the thalamus, the 5-HT_7 receptor, was decreased in HCN4FEA thalamic tissue. In line with this result, decreased responsiveness to 5-HT was also observed from HCN4FEA TC neurons in the VB compared to WT in whole-cell patch clamp experiments. This suggests an imbalance in 5-HT levels in HCN4FEA neurons compared to WT and that CDR of HCN4 mediates responses to 5-HT via the activation of $G_{\alpha s}$ and adenylyl cyclase. On a behavioural level, it was found the CDR of HCN4 regulates a phenotype distinct from CDR of HCN2. HCN4FEA mice but not HCN2EA mice showed an anxiety-like phenotype compared to their respective WT littermates suggesting an HCN4 specific-mediated effect on these anxiogenic behaviours. In the EEG profile, a decrease in the number of transitions between the NREM to wake state in HCN4FEA mice were observed, directly showing a phenotypic consequence of the deficient transition from burst to tonic firing in the presence of cAMP in HCN4FEA neurons. Furthermore, a decrease in the number and length of sleep spindles was also observed. These deficits demonstrate that CDR of HCN4 is a key regulator of thalamic network activity, via the transition of firing modes and mediating cellular responses to neurotransmitters involving the $G_{\alpha s}/G_{\alpha i}$ cAMP-PKA signalling pathway. CDR of HCN4 further has a role in anxiety-like behaviour, and also directly translates to deficits in the sleep architecture.

HCN2 and HCN4 channels regulate distinct cellular functions

While HCN4 and HCN2 channels interact and cooperate in several regards, they also operate in distinct regions and may regulate separate functions. TC neurons of the VB showed attenuated firing properties over a range of current injections, suggesting that both HCN4 and

HCN2 regulate the switch from burst to tonic firing and that neither channel is able to completely compensate for cAMP regulation (or lack thereof), of the other channel. However, the RMP and $V_{0.5}$ was similar between WT and HCN4FEA mice, suggesting that the high co-expression of HCN2 in the VB is able to compensate for any hyperpolarization of the RMP induced by lack of cAMP binding to HCN4. A summary of the cellular roles, contribution to I_h and phenotypes of HCN4 and HCN2 investigated from HCN4FEA mice and HCN2EA mice, is described in Table 2 in the appendix.

In the thalamus of HCN4FEA mice it was found that HCN4 channels are predominantly expressed in dendrites while HCN2 is expressed at higher levels and is somatic and dendritic. The differences in expression also support the notion that the two channels may regulate different cellular functions. These expression patterns are consistent with the expression patterns observed in HCN2EA mice (Hammelmann et al., 2019), and are also consistent with the expression patterns of HCN2 and HCN4 previously observed in the VB of WT and TRIP8b KO mice (Zobeiri et al., 2018).

Previous investigation of I_h properties from HCN4FEA channels and HCN4 WT channels transiently expressed in HEK293 cells revealed that the $V_{0.5}$ of HCN4FEA channels showed an approximate 9 mV shift towards more depolarized potentials. The depolarizing shift was also associated with accelerated activation kinetics compared to HCN4 WT, and the $V_{0.5}$ and activation time constants were not shifted in the presence of cAMP even at high micromolar concentrations (Fenske et al., 2020). This depolarizing shift in the $V_{0.5}$ is due to the Y527F mutation in the C-linker, and was in between the respective values obtained for HCN4 WT channels in the absence and presence of cAMP (Fenske et al., 2020). However, due to the high co-expression of HCN2 in the VB thalamus, the Y527F mutation in HCN4FEA mice did not impact the $V_{0.5}$, as also evidenced by the residual modulation of I_h by cAMP observed in HCN4FEA neurons.

HCN2 and HCN4 channels regulate distinct phenotypes

Further consistent with the hypothesis that CDR of HCN4 and CDR of HCN2 regulates distinct phenotypes, a direct phenotypic consequence of the impaired transition from burst to tonic firing in HCN4FEA TC neurons was detected as HCN4FEA mice showed a significantly fewer number of transitions from NREM to the awake state compared to WT mice during a 24 hour period, although there was no difference in the total length of the vigilance states. Furthermore, in the NREM to wake transition in the theta power range, in HCN4FEA mice the frequency remains high at the time of awakening and also after waking. However, in WT mice there is a decrease as arousal is accompanied by a power shift from high frequency to low

frequency (Akerstedt et al., 2002). In HCN2EA mice there was no difference in the number of transitions from NREM to wake, or in any of the transitions between NREM, REM and wake, demonstrating a distinct role of CDR of HCN4 in the transition from NREM to the awake state.

The thalamus is an integral component of the ascending reticular activating system (ARAS), which is a network of nerve fibers ascending from the brain stem and through associated structures causing activation of the forebrain during waking and REM sleep (Magoun, 1952). At the onset of conscious states, during wakefulness and REM sleep, TC neurons are excited by the action of acetylcholine, NA, histamine and 5-HT, leading to a switch from burst firing seen in the transition from NREM sleep to tonic firing, to faithfully transmit sensory information to the cortex (Brown et al, 2012). This switch in firing, is due to depolarization mediated by several conductances including leak potassium conductance by G_q-coupled receptors (muscarinic $M_{1,3}$, α-adrenergic, histaminergic H1 receptors), and I_h by $G_{\alpha s}$/adenylyl cyclase-coupled receptors (muscarinic $M_{2,4}$, β-adrenergic, $5-HT_{4,6,7,}$ histaminergic H_2 receptors) (Brown et al., 2012). However, in HCN4FEA mice, HCN4 does not bind cAMP and thus is insensitive to a majority of the depolarization induced by $G_{\alpha s}$/adenylyl cyclase-coupled receptors. This results in disrupted transmission from TC neurons to the cortex, and a reduced number of transitions from NREM to wake and sustained theta power even after waking. A model of this mechanism is shown in Figure 32. However, given that other neurotransmitters are also involved in the depolarization inducing waking and that ARAS systems are strongly interconnected, mutually excitatory and converge onto common effector systems at the level of thalamic and cortical neurons, there is considerable redundancy in the system. Inactivation of any individual component of the system can be compensated for by other circuits. A second possibility for the mild phenotype observed in HCN4FEA mice, is that CDR of HCN4 may also not be absolutely necessary for the mechanism of waking.
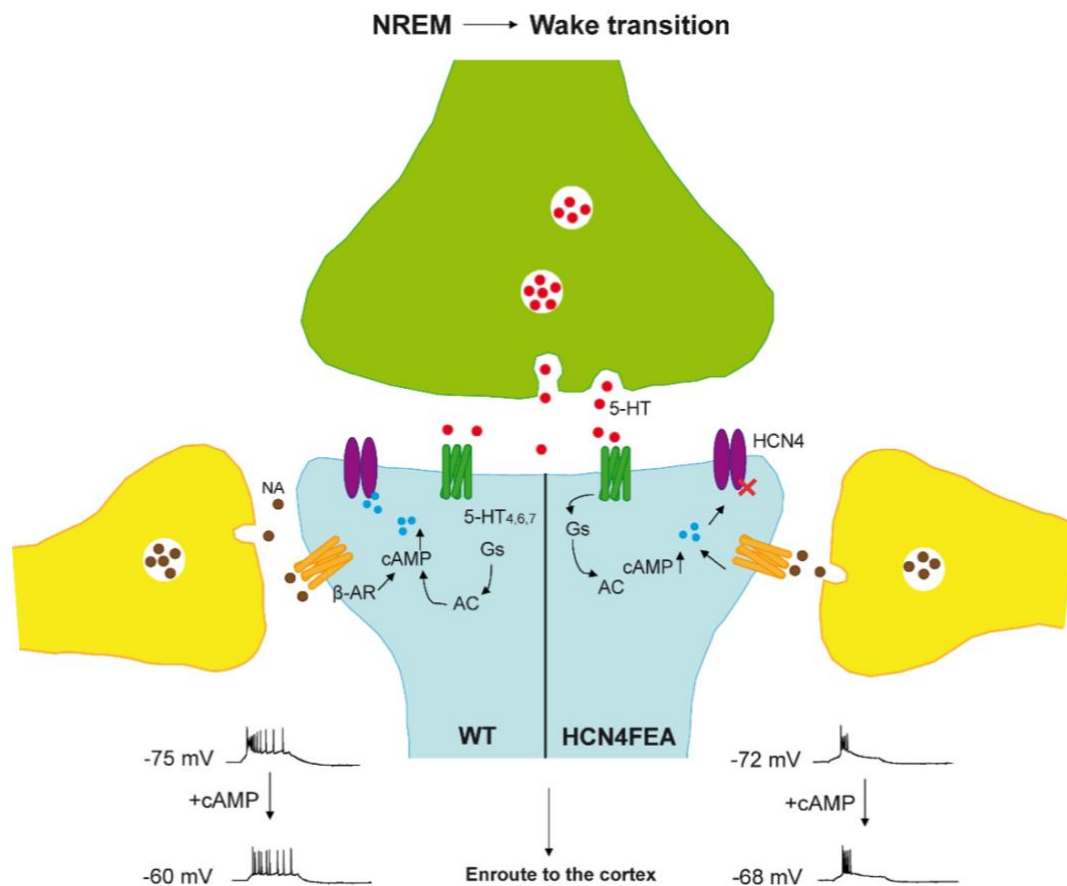
Figure 32. Schematic of the NREM to Wake transition in a TC neuron at the level of the synapse in HCN4FEA compared to WT. At the onset of waking, TC neurons receive several depolarizing inputs from serotonergic (green) and adrenergic (yellow) neurons, and also from cholinergic, histaminergic, and muscarinic neurons (not shown), which activate $G_{\alpha s}$ and $G_{\alpha q}$ coupled receptors. Activation of 5-HT $G_{\alpha s}$ coupled receptors (green) leads to an increase in cAMP levels. In WT TC neurons, cAMP binds to HCN4 channels (purple), leading TC neurons to depolarize to ~-60 mV, and switch from burst to tonic firing. In HCN4FEA TC neurons, cAMP cannot bind HCN4 channels, and TC neurons do not depolarize to the same extent ~-68 mV, and either do not switch to tonic firing or fire with reduced frequency. Abbreviations: AC, adenylyl cyclase; β-AR, β-adrenergic receptor, NA; noradrenaline.

A recent study examined the cellular activity of arousal and attention (CM) and sensory (VB) thalamic nuclei across sleep-wake states. It was found that during global NREM to wake transitions, CM neuron spiking rates were increased compared to VB neurons, and that both CM and VB neuron spike rates increased above that seen during wake maintenance, and returned to baseline values after 10 s (Gent et al., 2018). Additionally, optogenetic activation of CM but not VB neurons induced rapid wakefulness. The authors suggest that CM neurons have a greater role in controlling the NREM to wake transition, but that CM and VB neurons are differentially modulated across sleep-wake states and have distinct functions in regulating cortical excitability (Gent et al., 2018). Taken together, this shows that CDR of HCN4 has a role in the transition from NREM to the waking and is distinct from roles of CDR of HCN2 in the sleep architecture, but that different TC neurons may also have distinct roles in the NREM to wake transition.

HCN4FEA mice also did not show impaired visual learning in the visual discrimination test, which was observed in HCN2EA mice (Hammelmann et al., 2019), indicating that the flow of information between the dLGN and the visual cortex critically relies on CDR of HCN2 but not HCN4. Furthermore, HCN4FEA did not show SWDs and an absence epilepsy phenotype, which was observed in HCN2EA mice (Hammelmann et al., 2019). This finding may be due to the lack of HCN4 expression in the somata, while HCN2 is highly expressed in the somata. Importantly, the RMP was also not altered (hyperpolarized) in HCN4FEA TC neurons, very likely leading to reduced epileptic susceptibility and therefore physiologically, HCN4FEA mice do not show absence seizures.

A brain specific HCN4 KO mouse model (brHCN4-KO) has been previously investigated in the PhD thesis of Anne-Christina Blaich. Whole cell voltage clamp analysis revealed a 50% reduction of I_h in thalamic neurons, and a hyperpolarizing shift in the RMP (~ 5 mV) compared to WT neurons (Blaich, 2008), although far less than the hyperpolarizing shift observed in TC neurons of HCN2KO mice (~ 12 mV) (Ludwig et al., 2003). Consistent with EEG recordings from HCN4FEA mice, brHCN4-KO mice also did not show absence seizures (Blaich, 2008). Additionally, application of the GABAA antagonists picrotoxin and bicuculline, which reduces the inhibition on the TC circuit causing absence seizures in control mice, did not cause absence seizures in brHCN4-KO mice (Blaich, 2008). It was hypothesized that the deletion of HCN4 which eliminates the slow depolarizing Na^+ influx through HCN4 channels, causes neurons to be less excitable leading to an inhibition of the synchronized stimulus transmission and to a resistance to SWDs, and that after the administration of the GABAA antagonists the threshold potential in brHCN4-KO neurons on the axon hillock is only rarely reached (Blaich, 2008). Additionally, a second brain specific HCN4 KO model has previously been examined which revealed a 57% reduction of I_h current amplitude in VB neurons, reduced burst firing, and significantly slower thalamic and cortical oscillations during active wakefulness (Zobeiri et al., 2019). The authors suggest that HCN4 channels are essential in the production of rhythmic oscillations and determine oscillatory activity during alert states in TC neurons (Zobeiri et al., 2019).

In HCN4FEA TC neurons, the voltage dependent functions are preserved and the RMP was similar compared to WT TC neurons, although the membrane potential was impaired compared to WT TC neurons when both hyperpolarizing and depolarizing current injections were applied. The RMP has a crucial role in keeping neurons in the tonic firing mode at depolarized potentials, thus preventing inappropriate switching to burst firing at hyperpolarized potentials and the appearance of absence seizures in HCN4FEA mice. However, the impaired firing of HCN4FEA TC neurons in the presence of cAMP shows that CDR of HCN4 is

nevertheless important for the transition from burst to tonic firing in TC neurons. This effect may not be solely attributed to the RMP, as cAMP has a critical role in the recruitment of HCN channels within the range of physiological membrane potentials. HCN4 channels are the subtype most sensitive to cAMP and can be tuned by upstream cAMP-sensitive signalling effectors such as $G_{\alpha s}/G_{\alpha i}$. HCN4FEA channels cannot bind cAMP and are therefore insensitive to changes in cAMP concentrations induced by cAMP-sensitive signalling effectors. Within the dynamic range of cAMP-sensitive tuning, cAMP can recruit up to three-fold HCN channel activity, while in the absence of cAMP the channel availability is greatly reduced (Hammelmann et al., 2019). The depolarizing inward current produced by activation of HCN4FEA channels towards the threshold for an action potential would therefore be impaired by decreased channel availability. On the synaptic level, the absence of CDR of HCN4 and decreased channel availability in HCN4FEA channels may lead to inhibition of the synchronized stimulus transmission in the TC circuit due to an imbalance between depolarizing inward currents carried by I_h and hyperpolarizing potassium currents and thus be more prone to excitatory or inhibitory influences that could also destabilize the RMP during tonic-burst firing transitions.

Modulation of I_h by 5-HT is impaired in HCN4FEA TC neurons

The high sensitivity of HCN4 to cAMP compared to the other HCN isoforms, and its expression in specific subsets of brain regions related emotional and cognitive functions, positions HCN4 as a key neuromodulator for cellular responses to neurotransmitters which are coupled to cAMP. Electrophysiological analysis of the effect of 5-HT on TC neurons revealed that the reduced expression of the 5-HT$_7$ receptor from HCN4FEA thalamic tissue was associated with decreased responsiveness to 5-HT compared to WT. The depolarizing shift in the $V_{0.5}$ of WT neurons in response to 5-HT is consistent with predominant activation of the 5-HT$_7$ receptor and subsequent increases in cAMP levels. In contrast, in HCN4FEA neurons the small hyperpolarizing shift of the $V_{0.5}$ in response to 5-HT is consistent with the predominant activation of the 5-HT$_{1A}$ and 5-HT$_{1B}$ receptors and the inability of HCN4FEA neurons to bind cAMP. CDR of HCN4 likely has a key role in mediating responses to 5-HT via activation of $G_{\alpha s/\alpha i}$ and corresponding cAMP levels.

Direct effects on I_h by activation of the 5-HT$_7$ receptor have previously been reported in anterodorsal thalamic neurons (Chapin and Andrade, 2001), in chemosensitive neurons in the retrotrapezoid nucleus (Hawkins et al., 2014), in fear retrieval memory in the ventral hippocampus (Ohmura et al., 2016), in a model of neuropathic pain (Santello and Nevian, 2015; Santello et al., 2017), and most recently in PVT neurons in the regulation of feeding

behaviours (Ye and Zhang, 2021). The PVT receives dense GABAergic projections from the ZI to regulate feeding behaviours, and 5-HT signaling is known to inhibit food intake (Ye and Zhang, 2021). It was found that 5-HT depolarized and excited PVT neurons by activating 5-HT_7 receptors to modulate I_h, and also disinhibited PVT neurons by acting on 5-HT1$_A$ receptors to inhibit GABA release from ZI GABA terminals in the PVT (Ye and Zhang, 2021). In line with these results, the reduced expression of the 5HT$_7$ receptor observed from HCN4FEA thalamus compared to WT, and therefore reduced 5-HT signalling, may explain why differences in the feeding behaviour and food intake was not different between WT and HCN4FEA mice. In the ventral hippocampus, it has been shown that microinjection of the 5HT$_7$ receptor antagonist SB269970 (but notably not antagonists for other 5-HT receptors, $_{1A}$, $_{2A}$, $_{2C}$, $_3$, $_4$, and $_6$) suppressed freezing behaviour in rats which is an index of fear memory retrieval (Ohmura et al., 2016). 5HT$_7$ mRNA positive neurons were co-expressed with HCN2 and HCN4 in the ventral hippocampal CA3 region, and the 5HT$_7$ receptor agonist LP44 increased the frequency of action potentials via the action of I_h, as the increase was blocked by the HCN channel blocker ZD7288 (Ohmura et al., 2016). It has also been shown that injection of ZD7288 into the basolateral amygdala increased anxiety-like behaviour in mice in the elevated-plus maze test (Park et al., 2011), and in a model of neuropathic pain it has been shown that the activation of 5-HT$_7$ receptor did not further influence cellular excitability when HCN channels were blocked (Santello and Nevian, 2015). I hypothesize that the reduced firing capability of HCN4FEA TC neurons in the presence of cAMP, may also partially mimic this effect of reduced cellular excitability, as HCN4FEA neurons show significantly attenuated firing frequency, therefore highlighting the cAMP binding capability of HCN4 as a likely regulator in 5-HT$_7$-mediated responses.

Influence of 5-HT$_7$ in anxiogenic behaviours

While the present work does not show a direct link between NA or 5-HT to the anxiogenic behaviours observed in HCN4FEA mice, the probable roles of altered serotonergic and noradrenergic neurotransmission in anxiety disorder studies is widely accepted, and several treatment strategies for anxiety disorders are based on selective serotonin reuptake inhibitors (SSRIs) and serotonin and noradrenaline reuptake inhibitors (SNRIs) (Morilak and Frazer, 2004; Baldwin, 2006; Blier and Mansari, 2007). Of note, there is also growing evidence from pharmacological and genetic tools in animal models, supporting a role for the 5-HT$_7$ receptor in psychiatric diseases including anxiety, OCD, MDD and schizophrenia although with mixed results. For example, SB-269970 and the antipsychotic drug amisulpride which has a high affinity for the 5-HT$_7$ receptor, were effective in attenuating ketamine induced deficits in pre-pulse inhibition of the startle reflex and social interaction test in rats, and were

suggested as a pharmacological approach in the treatment of cognitive deficits and negative symptoms of schizophrenia (Nikiforuk et al., 2013). SB-269970 has also been shown to counteract an anxiogenic-like effect of acute administration of the SSRI fluoxetine, in the open field test and forced swim test in rats, (Mnie-Filali et al., 2011) suggesting a role in regulating anxious or depressive-like behaviour. However, in a 5-HT induced hypothermia assay, doses of SB-269970 and another 5-HT$_7$ receptor antagonist DR-4004, which blocked 5-HT-induced hypothermia, did not display significant anxiolytic-like (elevated plus maze, vogel conflict) or antidepressant-like efficacy (tail suspension test) in mice (Maxwell et al., 2018).

Involvement of CDR of I$_h$ in schizophrenia

Nevertheless, previous studies support the notion that the effect of CDR of HCN4 on neurotransmitter signalling via the cAMP system may have a role in psychiatric diseases. Schizophrenia associates with several genetic alterations that dysregulate cAMP signalling, and deficits in working memory which is mediated by firing of pre-frontal cortex (PFC) neurons, are often a feature of the illness (Weinberger et al., 1986; Arnsten et al., 2007). It has been shown that dysregulation of cAMP signalling in PFC impairs working memory and weakens network connectivity via interactions with HCN channels (Wang et al., 2007; Arnsten et al., 2010). The post-synaptic scaffolding protein disrupted-in-schizophrenia 1 (DISC1), phosphodiesterase 4A (PDE4A), PDE4B, and dopamine receptor 1 (D1R), have been identified as cAMP signalling proteins (Paspalas et al., 2012). DISC1 specifically interacts with PDE4s in response to cAMP levels and translocation of the *disc1* gene is associated with schizophrenia (Millar et al., 2005; Murdoch et al., 2007). DISC1, PDE4A, PDE4B, D1R, and HCN channels, have been identified next to excitatory synapses and the neck of dendritic spines in monkey PFC, where microcircuits for working memory interconnect, and have been suggested to contribute to the impaired PFC function and working memory deficits associated with schizophrenia (Paspalas et al., 2012). HCN channels also co-localize with α2A adrenergic receptors, and it has been found that activation of α2A adrenergic receptors strengthened PFC network firing and improved working memory by inhibiting cAMP and closing HCN channels (Wang et al., 2007). Additionally in electrophysiological studies, activation of α2A adrenergic receptors, inhibition of cAMP signalling or blocking HCN channels (HCN1 channels or HCN1/HCN2 heteromers) enhanced the rate of delay-related firing *in vivo* in monkey PFC neurons (Wang et al., 2007). Furthermore, stress has been shown to impair working memory via high levels of D1R activation and increased cAMP levels, which reduced neuronal firing of PFC neurons, and also increased the open state of HCN channels present on dendritic spines, demonstrating a key role of HCN channel dysregulation in response to neurotransmitter signalling, in the disease (Vijayraghaven et al., 2007; Gamo et al., 2015).

CDR of HCN4 may have an influence in the pathology of schizophrenia

Several phenotypes observed in HCN4FEA mice have also been reported in schizophrenia and CDR of HCN4 may play a role in the pathology of the disease. In addition to the impaired neurotransmitter signalling and impaired tonic firing mode of TC neurons which may be important for cognitive behaviours, anxiety is frequently observed in schizophrenia and may present as a component of the disease or a co-occurring anxiety disorder. One study found that 62% of schizophrenia patients examined were diagnosed with at least one co-morbid anxiety disorder; OCD symptoms and social anxiety symptoms were related to positive symptoms of the disease, and panic and social anxiety were related to suspiciousness and paranoia (Huppert et al., 2005). Altered firing rates associated with an anxiety and depression phenotype and an altered expression of an HCN channel subtype has also been recently demonstrated in two independent studies. In a chronic unpredictable stress mouse model which shows anxiety-like behaviour, nucleus accumbens-projecting dopaminergic neurons in the ventral tegmental area showed a decrease rate of tonic firing (Zhong et al., 2018). I_h was also decreased in these neurons and sh-RNA mediated knockdown of HCN2 in the ventral tegmental area recapitulated anxiety-like behaviour, while over expression of HCN2 largely prevented these behavioural deficits (Zhong et al., 2018). In line with this study, using three mouse models for chronic stress and depression, chronic social defeat stress mice, chronic restrain stress mice, and p11 conditional knockout mice, Cheng and colleagues showed that the rate of tonic firing is decreased in cholinergic interneurons of the nucleus accumbens shell (Cheng et al., 2019). As part of the molecular mechanism, they further showed that expression of HCN2 in these neurons was decreased, and enhancing cholinergic interneuron activity by chemogenetics or over expression of HCN2 in cholinergic interneurons was sufficient to rescue the depressive phenotype (Cheng et al., 2019). These studies demonstrate a clear role for an HCN channel subtype in the altered rates of tonic firing associated with an anxiogenic phenotype.

While HCN2EA mice did not show an anxiogenic phenotype, it is possible that down-regulating expression of HCN2 will have different phenotypic consequences compared to CDR of HCN2. Additionally, targeting distinct anatomical regions which have different functional features and regulate different behaviours will also likely differentially affect anxiogenic phenotypes. In anxiety, it is also known that other cellular pathways also play a crucial role such as oxidative stress pathways (Bouayed et al. 2009). Nevertheless, HCN4FEA mice showed an anxiogenic phenotype in both the OFT and the light-dark test, but not in social behaviour. In the OFT, an increase in the latency to the center region and decreased time spent in the center region was observed. In the light-dark test, HCN4FEA mice spent more

time in the dark region, travelled a shorter distance in the light region, and showed a fewer number of transitions between the dark and light region, indicative of bright space anxiety in mice. Further supporting the role of HCN4 in anxiogenic behaviours, brHCN4-KO mice (discussed above) also showed a decrease in exploration behaviour in the OFT and a decrease in the total distance travelled in the inner region (Blaich, 2007). Additionally, in the light-dark test, brHCN4-KO mice showed a decrease in the distance travelled in the light region (Blaich, 2007). Taken together, both the HCN4FEA and the brHCN4-KO mouse models suggest that HCN4 has a role in anxiogenic phenotypes.

Abnormal sleep is also a common feature in schizophrenia patients and there is accumulating evidence of a marked reduction in sleep spindle activity in schizophrenia patients (Schilling et al., 2017; D'Agostino et al., 2018). Also in line with this phenotype, HCN4FEA mice showed a reduced number of sleep spindles and length of sleep spindles. In a study investigating the correlation of fast and slow sleep spindle activity with cognitive function, it was found that fast spindle density was reduced in patients with schizophrenia and healthy first degree relatives, and was associated with decreased cognitive performance (Schilling et al., 2017). Sleep spindles are generated by the interplay between the reticular thalamic nucleus and other thalamic nuclei in the frequency range of ~11 to 16 Hz, with a duration of 0.5-1.5 seconds during NREM sleep which mediates memory consolidation. In schizophrenia, this correlates with impaired cognition, positive symptoms of the disease, and abnormal thalamic connectivity which therefore impairs gating of sensory information to the cortex (Behrendt and Young, 2004).

In addition, schizophrenia patients often have an increased risk of cardiac dysfunction and it has been shown in genome-wide association studies that variants of voltage-gated Na^+ channels and HCN channels, have qualitatively similar effects on layer V pyramidal cell and sinoatrial node cell excitability (Mäki-Marttunen et al., 2017). Previous investigation of the HCN4FEA mouse model discovered that HCN4FEA mice showed severe sinus bradychardia and sinus dysrhythmia, although the heart rate was preserved (Fenske et al., 2020), confirming a link with cardiac dysfunction.

In summary, CDR of HCN4 is an important mechanism regulating thalamic network activity, via the transition between firing modes and responses to neurotransmitter signalling via the cAMP system. CDR of HCN4 is also a regulator in the control of vigilance states, from the NREM to wake transition state, and in sleep spindle activity. CDR of HCN4 may also be an important regulator of anxiogenic behaviour and may have an influence in the pathology of schizophrenia.

5   Summary

Hyperpolarization-activated cyclic nucleotide-gated (HCN) channels are key regulators of neuronal excitability and are subject to a high degree of modulation by cAMP. The present work aimed to investigate roles of HCN4 in the thalamus, how CDR of HCN4 affects neuronal networks and behavioural phenotypes, and differences in the modulation of HCN4 and HCN2 by cAMP. Here, it was shown for the first time that CDR of HCN4 regulates a complex neuronal phenotype. Using biochemical and electrophysiological methods, it was found that HCN4 is important in addition to HCN2, in regulating the transition from burst to tonic firing in the VB thalamus, and that neither channel is able to completely compensate for cAMP regulation of the other channel. However, the high expression of HCN2 in the thalamus can compensate for the RMP. In addition, investigation of the consequences of CDR of HCN4 in response to neurotransmitters coupled to cAMP using the serotonergic system revealed decreased responsiveness to 5-HT in TC neurons where HCN4 was unable to bind cAMP, suggesting an imbalance in 5-HT levels and that CDR of HCN4 mediates responses to 5-HT via activation of $G_{\alpha s}$ and adenylyl cyclase.

Differences in the modulation of HCN2 and HCN4 by cyclic nucleotides and its consequences on behavioural phenotypes, were dissected using EEG recordings and behavioural experiments. Differences in the roles of CDR of HCN4 and HCN2 were detected in the sleep architecture and the control of vigilance states. It was found that CDR of HCN4 but not HCN2, has a role in regulating the number of transitions from the NREM to wake state, directly showing a phenotypic consequence of the deficient transition from burst to tonic firing observed in TC neurons. Furthermore, CDR of HCN4 also has a role in the number and length of sleep spindles. It was also found that CDR of HCN4 but not CDR of HCN2, has a role in anxiety-like behaviour but neither subtype had a role in affecting social behaviour. These data suggest that while HCN4 and HCN2 interact and are co-expressed, that CDR of HCN4 also regulates distinct cellular functions and neuronal phenotypes

6   Bibliography

Akerstedt T, Billiard M, Bonnet M, Ficca G, Garma L, Mariotti M, Salzarulo P, Schulz H. Awakening from sleep. Sleep Med Rev. 6(4):267-86, 2002.

Aponte Y, Lien CC, Reisinger E, Jonas P. Hyperpolarization-activated cation channels in fast-spiking interneurons of rat hippocampus. J Physiol 574(1):229-243, 2006.

Arnsten AF. Catecholamine and second messenger influences on prefrontal cortical networks of "representational knowledge": a rational bridge between genetics and the symptoms of mental illness. Cereb Cortex Suppl 1:i6-15, 2007.

Atherton JF, Kitano K, Baufreton J, Fan K, Wokosin D, Tkatch T, Shigemoto R, Surmeier DJ, Bevan MD. Selective participation of somatodendritic HCN channels in inhibitory but not excitatory synaptic integration in neurons of the subthalamic nucleus. J Neurosci 30(47):16025-16040, 2010.

Bacqué-Cazenave J, Bharatiya R, Barrière G, Delbecque JP, Bouguiyoud N, Di Giovanni G, Cattaert D, De Deurwaerdère P. Serotonin in Animal Cognition and Behavior. Int J Mol Sci 21(5):1649, 2020.

Baldwin DS. Serotonin noradrenaline reuptake inhibitors: A new generation of treatment for anxiety disorders. Int J Psychiatry Clin Pract. 2006;10 Suppl 2:12-5, 2002.

Balse E, Boycott HE. Ion Channel Trafficking: Control of Ion Channel Density as a Target for Arrhythmias?. Front Physiol 8:808, 2017.

Behrendt RP, Young C. Hallucinations in schizophrenia, sensory impairment, and brain disease: a unifying model. Behav Brain Sci. 2004 Dec;27(6):771-87; discussion 787-830. doi: 10.1017/s0140525x04000184. PMID: 16035402.

Biel M, Wahl-Schott C, Michalakis S, Zong X. Hyperpolarization-activated cation channels: from genes to function. Physiol Rev 89:847-885, 2009.

Blier P, El Mansari M. The importance of serotonin and noradrenaline in anxiety. Int J Psychiatry Clin Pract. 2007;11 Suppl 2:16-23. doi: 10.1080/13651500701388310. PMID: 24926868.

Blaich, AC. Untersuchung der Rolle des Schrittmacherkanals HCN4 im Gehirn adulter Mäuse, 2008.

Bouayed J, Rammal H, Soulimani R. Oxidative stress and anxiety: relationship and cellular pathways. Oxid Med Cell Longev 2(2):63-7, 2009.

Brown, HF, Difrancesco, D, Noble SJ. How does adrenaline accelerate the heart? Nature 280, 235-236, 1979a.

Brown HF, DiFrancesco D, Noble SJ. Adrenaline action on rabbit sino-atrial node [proceedings]. J. Physiol. 290:31-32, 1979b.

Brown RE, Basheer R, McKenna JT, Strecker RE, McCarley RW. Control of sleep and wakefulness. Physiol Rev 92(3):1087-1187, 2012.

Catterall WAF. Ion channel voltage sensors: structure, function, and pathophysiology. Neuron 67(6):915-928 (2010).

Cain SM, Tyson JR, Jones KL, Snutch TP. Thalamocortical neurons display suppressed burst-firing due to an enhanced Ih current in a genetic model of absence epilepsy. Pflugers Arch 467(6):1367-1382, 2015.

Chapin EM, Andrade RJ. A 5-HT(7) receptor-mediated depolarization in the anterodorsal thalamus. II. Involvement of the hyperpolarization-activated current I(h). Pharmacol Exp Ther. 297(1):403-409, 2001.

Chen S, Wang J, Siegelbaum SA. Properties of hyperpolarization-activated pacemaker current defined by coassembly of HCN1 and HCN2 subunits and basal modulation by cyclic nucleotide. J Gen Physiol 117(5):491-504, 2001.

Cheng J, Umschweif G, Leung J, Sagi Y, Greengard P. HCN2 Channels in Cholinergic Interneurons of Nucleus Accumbens Shell Regulate Depressive Behaviors. Neuron 101(4):662-672, 2019.

Ciranna L, Catania MV. 5-HT7 receptors as modulators of neuronal excitability, synaptic transmission and plasticity: physiological role and possible implications in autism spectrum disorders. Front Cell Neurosci 8:250, 2014.

Danober L, Deransart C, Depaulis A, Vergnes M, Marescaux C. Pathophysiological mechanisms of genetic absence epilepsy in the rat. Prog Neurobiol 55(1):27-57, 1998.

D'Agostino A, Castelnovo A, Cavallotti S, Casetta C, Marcatili M, Gambini O, Canevini M, Tononi G, Riedner B, Ferrarelli F, Sarasso S. Sleep endophenotypes of schizophrenia: slow waves and sleep spindles in unaffected first-degree relatives. NPJ Schizophr 4(1):2, 2018.

Diaz SL, Doly S, Narboux-Nême N, Fernández S, Mazot P, Banas SM, Boutourlinsky K, Moutkine I, Belmer A, Roumier A, Maroteaux L. 5-HT(2B) receptors are required for serotonin-selective antidepressant actions. Mol Psychiatry 17(2):154-63, 2017.

DiFrancesco D. A study of the ionic nature of the pace-maker current in calf Purkinje fibres. J Physiol. 314:377-393, 1981.

DiFrancesco D, Tortora P. Direct activation of cardiac pacemaker channels by intracellular cyclic AMP. Nature 351:145-147, 1991.

Doyle DA, Morais Cabral J, Pfuetzner RA, Kuo A, Gulbis JM, Cohen SL, Chait BT, MacKinnon R. The structure of the potassium channel: molecular basis of K^+ conduction and selectivity. Science 280:69–77, 1998.

Faber DS, Pereda AE. Two Forms of Electrical Transmission Between Neurons. Front Mol Neurosci 11:427, 2018.

Gamo NJ, Lur G, Higley MJ, Wang M, Paspalas CD, Vijayraghavan S, Yang Y, Ramos BP, Peng K, Kata A, Boven L, Lin F, Roman L, Lee D, Arnsten AF. Stress Impairs Prefrontal Cortical Function via D1 Dopamine Receptor Interactions With Hyperpolarization-Activated Cyclic Nucleotide-Gated Channels. Biol Psychiatry 78(12):860-870, 2015.

Gauss R, Seifert R, Kaupp, UB. Molecular identification of a hyperpolarization-activated channel in sea urchin sperm. Nature 393:583-587, 1998.

Gent TC, Bandarabadi M, Herrera CG, Adamantidis AR. Thalamic dual control of sleep and wakefulness. Nat Neurosci 21, 974-984, 2018.

Günther A, Luczak V, Gruteser N, Abel T, Baumann A. HCN4 knockdown in dorsal hippocampus promotes anxiety-like behavior in mice. Genes Brain Behav. 2019;18(2):e12550. doi:10.1111/gbb.12550

Hagena H, Manahan-Vaughan D. The serotonergic 5-HT4 receptor: A unique modulator of hippocampal synaptic information processing and cognition. Neurobiol Learn Mem 138:145-153, 2017.

Haidarliu S, Yu C, Rubin N, Ahissar E. Lemniscal and Extralemniscal Compartments in the VPM of the Rat. Front Neuroanat 2:4. doi: 10.3389/neuro.05.004, 2008.

Harden SW, Brogioli D. LJPcalc [Online] 2020. Available: https://swharden.com/software/LJPcalc.

Halliwell JV, Adams PR. Voltage-clamp analysis of muscarinic excitation in hippocampal neurons. Brain Res. 250:71-92, 1982.

Hammelmann V, Zong X, Hofmann F, Michalakis S, Biel M. The cGMP-dependent protein kinase II Is an inhibitory modulator of the hyperpolarization-activated HCN2 channel. PLoS One. 6(2):e17078, 2011.

Hammelmann V, Stieglitz MS, Hülle H, Le Meur K, Kass J, Brümmer M, Gruner C, Rötzer RD, Fenske S, Hartmann J, Zott B, Lüthi A, Spahn S, Moser M, Isbrandt D, Ludwig A, Konnerth A, Wahl-Schott C, Biel M. Abolishing cAMP sensitivity in HCN2 pacemaker channels induces generalized seizures. JCI Insight. 4(9):e126418, 2019.

Harzheim D, Pfeiffer KH, Fabritz L, Kremmer E, Buch T, Waisman A, Kirchhof P, Kaupp UB, Seifert R. Cardiac pacemaker function of HCN4 channels in mice is confined to embryonic development and requires cyclic AMP. EMBO J 27(4):692-703, 2008.

Hawkins VE, Hawryluk JM, Takakura AC, Tzingounis AV, Moreira TS, Mulkey DK. HCN channels contribute to serotonergic modulation of ventral surface chemosensitive neurons and respiratory activity. J Neurophysiol 113(4):1195-1205, 2015.

Hauser SR, Hedlund PB, Roberts AJ, Sari Y, Bell RL, Engleman EA. The 5-HT7 receptor as a potential target for treating drug and alcohol abuse. Front Neurosci 8:448, 2015.

Heine M, Ponimaskin E, Bickmeyer U, Richter DW. 5-HT-receptor-induced changes of the intracellular cAMP level monitored by a hyperpolarization-activated cation channel. Pflugers Arch 443(3):418-426, 2002.

Hennis K, Biel M, Wahl-Schott C, Fenske S. Beyond pacemaking: HCN channels in sinoatrial node function. Prog Biophys Mol Biol. S0079-6107(21)00027-4, 2021.

Herrmann S, Rajab H, Christ I, Schirdewahn C, Höfler D, Fischer MJM, Bruno A, Fenske S, Gruner C, Kramer F, Wachsmann T, Wahl-Schott C, Stieber J, Biel M, Ludwig A. Protein kinase A regulates inflammatory pain sensitization by modulating HCN2 channel activity in nociceptive sensory neurons. Pain 158(10):2012-2024, 2017

Heys JG, Schultheiss NW, Shay CF, Tsuno Y, Hasselmo ME. Effects of acetylcholine on neuronal properties in entorhinal cortex. Front Behav Neurosci 24;6:32, 2012.

Huppert JD, Smith TE. Anxiety and schizophrenia: the interaction of subtypes of anxiety and psychotic symptoms. CNS Spectr 10(9):721-31, 2005.

Fakhfouri G, Rahimian R, Dyhrfjeld-Johnsen J, Zirak MR, Beaulieu JM. 5-HT$_3$ Receptor Antagonists in Neurologic and Neuropsychiatric Disorders: The Iceberg Still Lies beneath the Surface. Pharmacol Rev 71(3):383-412, 2019.

Fenske, S, Hennis K, Rötzer, RD. Brox VF, Becirovic E, Scharr A, Gruner C, Yiegler T, Mehlfeld V, Brennan J, Efimov IR, Pauža G, Moser M, Wotjak CT, Kupatt C, Gönner R, Zhang R, Zhang H, Zong X, Biel M, Wahl-Schott C. cAMP-dependent regulation of HCN4 controls the tonic entrainment process in sinoatrial node pacemaker cells. Nat Commun 11:5555, 2020.

Frere SG, Lüthi A. Pacemaker channels in mouse thalamocortical neurones are regulated by distinct pathways of cAMP synthesis. J Physiol 554: 111-125, 2004.

Isacoff EY, Jan LY, Minor DL Jr. Conduits of life's spark: a perspective on ion channel research since the birth of neuron. Neuron. 80(3):658-674, 2013.

Jiang, D., Tonggu, L., Gamal El-Din, T.M. *et al.* Structural basis for voltage-sensor trapping of the cardiac sodium channel by a deathstalker scorpion toxin. Nat Commun 12:128, 2021.

Jenkins TA, Nguyen JC, Polglaze KE, Bertrand PP. Influence of Tryptophan and Serotonin on Mood and Cognition with a Possible Role of the Gut-Brain Axis. Nutrients 8(1):56, 2016.

Jahnsen H, Llinas R. Electrophysiological properties of guinea-pig thalamic neurones: an in vitro study. J Physiol 349: 205-226, 1984a.

Jahnsen H, Llinas R. Ionic basis for the electro-responsiveness and oscillatory properties of guinea-pig thalamic neurones in vitro. J Physiol 349: 227-247, 1984b.

Kaufman J, Delorenzo C, Choudhury S, Parsey R. The 5-HT$_{1A}$ receptor in Major Depressive Disorder. Eur Neuropsychopharmacol. 26(3):397-410, 2017.

Kelmendi B, Holsbach-Beltrame M, McIntosh AM, et al. Association of polymorphisms in HCN4 with mood disorders and obsessive compulsive disorder. Neurosci Lett 496(3):195-199, 2011.

Kjaerby C, Athilingam J, Robinson SE, Iafrati J, Sohal VS. Serotonin 1B Receptors Regulate Prefrontal Function by Gating Callosal and Hippocampal Inputs. Cell Reports. 17(11):2882-2890, 2016.

Kim DG, Gonzales EL, Kim S, et al. Social Interaction Test in Home Cage as a Novel and Ethological Measure of Social Behavior in Mice. Exp Neurobiol. 2019;28(2):247-260. doi:10.5607/en.2019.28.2.247

Kim JY, Park CS. Potentiation of large-conductance calcium-activated potassium (BK(Ca)) channels by a specific isoform of protein kinase C. Biochem Biophys Res Commun 365(3):459-65, 2008.

Lau C, Hunter MJ, Stewart A, Perozo E, Vandenberg JI. Never at rest: insights into the conformational dynamics of ion channels from cryo-electron microscopy. J Physiol 596(7):1107-1119, 2018.

Lee CH, MacKinnon R. Structures of the human HCN1 hyperpolarization-activated channel. Cell;168(1–2):111–120.e11, 2017.

León-Ponte M, Ahern GP, O'Connell PJ. Serotonin provides an accessory signal to enhance T-cell activation by signaling through the 5-HT7 receptor. Blood 109(8):3139-3146, 2007.

Lesch KP, Waider J. Serotonin in the modulation of neural plasticity and networks: implications for neurodevelopmental disorders. Neuron 76(1):175-191, 2012.

Liu DT, Tibbs GR, Paoletti P, Siegelbaum SA. Constraining ligand-binding site stoichiometry suggests that a cyclic nucleotide-gated channel is composed of two functional dimers. Neuron, 21(1):235–248, 1998.

Llinás RR, Steriade M. Bursting of Thalamic Neurons and State of Vigilance. J Neurophysiol 95(6): 3297-3308, 2006.

Longmore J, Shaw D, Smith D, Hopkins R, McAllister G, Pickard JD, Sirinathsinghji DJ, Butler AJ, Hill RG. Differential distribution of 5HT1D- and 5HT1B-immunoreactivity within the human trigemino-cerebrovascular system: implications for the discovery of new antimigraine drugs. Cephalalgia 17(8):833-842, 1997.

Ludwig A, Zong X, Jeglitsch M, Hofmann F, Biel M. A family of hyperpolarization-activated mammalian cation channels. Nature. 393:587–591, 1998.

Ludwig A, Budde T, Stieber J, Moosmang S, Wahl C, Holthoff K, Langebartels A, Wotjak C, Munsch T, Zong X, Feil S, Feil R, Lancel M, Chien KR, Konnerth A, Pape HC, Biel M, Hofmann F. Absence epilepsy and sinus dysrhythmia in mice lacking the pacemaker channel HCN2. EMBO J 22:216–224, 2003.

Magoun HW. An Ascending Reticular Activating System in the brain stem. Arch NeurPsych 67(2):145-154, 1952.

Männikkö R, Elinder F, Larsson HP. Voltage-sensing mechanism is conserved among ion channels gated by opposite voltages. Nature 837-841, 2002.

Mäki-Marttunen T, Lines GT, Edwards AG, Tveito A, Dale AM, Einevoll GT, Andreassen OA. Pleiotropic effects of schizophrenia-associated genetic variants in neuron firing and cardiac pacemaking revealed by computational modeling. Transl Psychiatry 7(11):5, 2017.

Marazziti, D, Rotondo, A, Presta S, Pancioli-Guadagnucci ML, Palego L, Conti L. Role of serotonin in human aggressive behaviour. Aggressive Behavior 19(5) 347-353, 1993.

Mayer ML, Westbrook GL. A voltage-clamp analysis of inward (anomalous) rectification in mouse spinal sensory ganglion neurones. J Physiol 340:19-45, 1983.

McCormick DA. Neurotransmitter actions in the thalamus and cerebral cortex and their role in neuromodulation of thalamocortical activity. Prog Neurobiol 39(4):337-388, 1992.

McCormick DA, Bal T. Sleep and arousal: thalamocortical mechanisms. Annu Rev Neurosci 20: 185–215, 1997.

McCormick DA, Pape HC. Properties of a hyperpolarization-activated cation current and its role in rhythmic oscillation in thalamic relay neurones. J Physiol 431:291-318, 1990a.

McCormick DA, Pape HC. Noradrenergic and serotonergic modulation of a hyperpolarization-activated cation current in thalamic relay neurones. J Physiol 431: 319-342, 1990b.

McCormick DA, Huguenard JR. A model of the electrophysiological properties of thalamocortical relay neurons. J Neurophysiol 68:1384-1400, 1992.

McCormick DA, Bal T. Sleep and arousal: thalamocortical mechanisms. Annu Rev Neurosci 20:185–215, 1997.

McIntosh AM, Simen AA, Evans KL, Hall J, Macintyre DJ, Blackwood D, Morris AD, Smith BH, Dominiczak A, Porteous D, Deary HI, Thomson PA. Genetic variation in Hyperpolarization-activated cyclic nucleotide-gated channels and its relationship with neuroticism, cognition and risk of depression. Front Genet 3:116, 2012.

Monckton JE, McCormick DA. Neuromodulatory role of serotonin in the ferret thalamus. J Neurophysiol. 87(4):2124-2136, 2002.

Monconduit L, Bourgeais L, Bernard JF, Le Bars D, Villanueva L. Ventromedial thalamic neurons convey nociceptive signals from the whole body surface to the dorsolateral neocortex. J Neurosci 19(20):9063-72, 1999.

Morilak DA, Frazer A. Antidepressants and brain monoaminergic systems: a dimensional approach to understanding their behavioural effects in depression and anxiety disorders. Int J Neuropsychopharmacol 7(2):193-218, 2004.

Mnie-Filali O, Faure C, Lambás-Señas L, El Mansari M, Belblidia H, Gondard E, Etiévant A, Scarna H, Didier A, Berod A, Blier P, Haddjeri N. Pharmacological blockade of 5-HT7 receptors as a putative fast acting antidepressant strategy. Neuropsychopharmacology 36(6):1275-88, 2011.

Much B, Wahl-Schott C, Zong X, Schneider A, Baumann L, Moosmang S, Ludwig A, Biel M. Role of subunit heteromerization and *N*-linked glycosylation in the formation of functional hyperpolarization-activated cyclic nucleotide-gated channels. J Biol Chem 278: 43781-43786, 2003.

Mundo E, Zai G, Lee L, Parikh SV, Kennedy JL. The 5HT1Dbeta receptor gene in bipolar disorder: a family-based association study. Neuropsychopharmacol 25(4):608-613, 2001.

Nolan MF, Malleret G, Lee KH, Gibbs E, Dudman JT, Santoro B, Yin D, Thompson RF, Siegelbaum SA, Kandel ER, Morozov A. The hyperpolarization-activated HCN1 channel is important for motor learning and neuronal integration by cerebellar Purkinje cells. Cell 115(5):551-564, 2003.

Noma, A., and Irisawa, H. Membrane currents in the rabbit sinoatrial node cell as studied by the double microelectrode method. Pflüg Arch 364:45-52, 1976.

Nikiforuk A, Kos T, Fijał K, Hołuj M, Rafa D, Popik P (2013) Effects of the Selective 5-HT7 Receptor Antagonist SB-269970 and Amisulpride on Ketamine-Induced Schizophrenia-like Deficits in Rats. PLoS ONE 8(6): e66695.

Ohmura Y, Yoshida T, Konno K, Minami M, Watanabe M, Yoshioka M. Serotonin 5-HT7 Receptor in the Ventral Hippocampus Modulates the Retrieval of Fear Memory and Stress-Induced Defecation. Int J Neuropsychopharmacol 19(6):pyv131, 2016.

O'Reilly C, Iavarone E, Yi J, Hill SL. Rodent somatosensory thalamocortical circuitry: Neurons, synapses, and connectivity. Neurosci Biobehav Rev 126:213-235, 2021.

Oyrer J, Bleakley LE, Richards KL, Maljevic S, Phillips AM, Petrou S, Nowell CJ, Reid CA. Using a Multiplex Nucleic Acid *in situ* Hybridization Technique to Determine HCN4 mRNA Expression in the Adult Rodent Brain. Front Mol Neurosci 12:211. doi: 10.3389, 2019.

Pan Y, Laird JG, Yamaguchi DM, Baker SA. An N-Terminal ER Export Signal Facilitates the Plasma Membrane Targeting of HCN1 Channels in Photoreceptors. Invest Ophthalmol Vis Sci. 56(6):3514-3521, 2015.

Park K, Yi JH, Kim H, Choi K, Kang SJ, Shin KS. HCN channel activity-dependent modulation of inhibitory synaptic transmission in the rat basolateral amygdala. Biochem Biophys Res Commun. 404(4):952-957, 2011.

Paspalas CD, Wang M, Arnsten AF. Constellation of HCN channels and cAMP regulating proteins in dendritic spines of the primate prefrontal cortex: potential substrate for working memory deficits in schizophrenia. Cereb Cortex 23(7):1643-1654, 2013

Petrovich GD. The Function of Paraventricular Thalamic Circuitry in Adaptive Control of Feeding Behavior. Front Behav Neurosci. 15:671096, 2021.

Petrunich-Rutherford ML, Garcia F, Battaglia G. 5-HT$_{1A}$ receptor-mediated activation of neuroendocrine responses and multiple protein kinase pathways in the peripubertal rat hypothalamus. Neuropharmacology 139(1):173-181sssssssss, 2018.

Pinault D, O'Brien TJ. Cellular and network mechanisms of genetically-determined absence seizures. Thalamus Relat Syst 3(3):181-203, 2005.

Pithadia AB, Jain SM. 5-Hydroxytryptamine Receptor Subtypes and their Modulators with Therapeutic Potentials. J Clin Med Res 1(2):72-80, 2009.

Porro A, Saponaro A, Gasparri F, Bauer D, Gross C, Pisoni M, Abbandonato G, Hamacher K, Santoro B, Thiel G, Moroni A. The HCN domain couples voltage gating and cAMP response in hyperpolarization-activated cyclic nucleotide-gated channels. Elife 8:e49672, 2019.

Raes A, Wang Z, van den Berg RJ, Goethals M, Van de Vijver G, van Bogaert PP. Effect of cAMP and ATP on the hyperpolarization-activated current in mouse dorsal root ganglion neurons. Pflugers Arch 434(5):543-550, 1997.

Rossé G, Schaffhauser H. 5-HT6 receptor antagonists as potential therapeutics for cognitive impairment. Curr Top Med Chem 10(2):207-221.

Santello M., Nevian T. Dysfunction of cortical dendritic integration in neuropathic pain reversed by serotoninergic neuromodulation. Neuron 86:233–246, 2015.

Santello M, Bisco A, Nevian NE, Lacivita E, Leopoldo M, Nevian T. The brain-penetrant 5-HT$_7$ receptor agonist LP-211 reduces the sensory and affective components of neuropathic pain. Neurobiol Dis 106:214-221, 2017.

Santoro B, Liu DT, Yao H, Bartsch D, Kandel ER, Siegelbaum SA, Tibbs GR. Identification of a gene encoding a hyperpolarization-activated pacemaker channel of brain. Cell. 93:717-729, 1998.

Santoro B, Wainger BJ, Siegelbaum SA. Regulation of HCN channel surface expression by a novel C-terminal protein-protein interaction. J Neurosci 24:10750–10762, 2004.

Santoro B, Hu L, Liu H, Saponaro A, Pian P, Piskorowski RA, Moroni A, Siegelbaum SA. TRIP8b regulates HCN1 channel trafficking and gating through two distinct C-terminal interaction sites. J Neurosci 31(11):4074-4086, 2011.

Schilling C, Schlipf M, Spietzack S, Rausch F, Eisenacher S, Englisch S, Reinhard I, Haller L, Grimm O, Deuschle M, Tost H, Zink M, Meyer-Lindenberg A, Schredl M. Fast sleep spindle reduction in schizophrenia and healthy first-degree relatives: association with impaired cognitive function and potential intermediate phenotype. Eur Arch Psychiatry Clin Neurosci 267(3):213-224, 2017.

Schweizer PA, Duhme N, Thomas D, Becker R, Zehelein J, Draguhn A, Bruehl C, Katus HA, Koenen M. cAMP sensitivity of HCN pacemaker channels determines basal heart rate but is not critical for autonomic rate control. Circ Arrhythm Electrophysiol 3(5):542-552, 2010

Seibenhener ML, Wooten MC. Use of the Open Field Maze to measure locomotor and anxiety-like behavior in mice. J Vis Exp. 2015;(96):e52434, 2015.

Seidenbecher T, Pape HC. Contribution of intralaminar thalamic nuclei to spike-and-wave-discharges during spontaneous seizures in a genetic rat model of absence epilepsy. Eur J Neurosci 13(8):1537-1546, 2001.

Shelton J, Bonaventure P, Li X, Yun S, Lovenberg T, Dugovic C. 5-HT7 receptor deletion enhances REM sleep suppression induced by selective serotonin reuptake inhibitors, but not by direct stimulation of 5-HT1A receptor. Neuropharmacol 56(2):448-454, 2008.

Shukla R, Watakabe A, Yamamori T. mRNA expression profile of serotonin receptor subtypes and distribution of serotonergic terminations in marmoset brain. *Front Neural Circuits* 8:52, 2014.

Steriade M, Domich L, Oakson G, Deschenes M. The deafferented reticular thalamic nucleus generates spindle rhythmicity. J Neurophysiol 57:260-273, 1987.

Steriade M, Contreras D, Curro Dossi R, Nunez A. The slow (<1 Hz) oscillation in reticular thalamic and thalamocortical neurons: scenario of sleep rhythm generation in interacting thalamic and neocortical networks. J Neurosci 13: 3284-3299, 1993.

Steriade M, Contreras D, Amzica F. Synchronized sleep oscillations and their paroxysmal developments. Trends Neurosci 17:199-208, 1994.

Stiedl O, Pappa E, Konradsson-Geuken A, Ogren SO. The role of the serotonin receptor subtypes. Front Pharmacol 6:162, 2015.

Tanaka S, Wu N, Hsaio CF, Turman J Jr, Chandler SH. Development of inward rectification and control of membrane excitability in mesencephalic v neurons. J Neurophysiol 89(3):1288-1298, 2003.

Takao K, Miyakawa T. Light/dark transition test for mice. J Vis Exp (1):104, 2006.

Tao X, MacKinnon R. Cryo-EM structure of the KvAP channel reveals a non-domain-swapped voltage sensor topology. *Elife* 8:e52164, 2019.

Tian L, Shipston MJ. Characterization of hyperpolarization-activated cation currents in mouse anterior pituitary, AtT20 D16:16 corticotropes. Endocrinology 141(8):2930-2937, 2000.

Thuault SJ, Malleret G, Constantinople CM, Nicholls R, Chen I, Zhu J, Panteleyev A, Vronskaya S, Nolan MF, Bruno R, Siegelbaum SA, Kandel ER Prefrontal cortex HCN1 channels enable intrinsic persistent neural firing and executive memory function. J Neurosci. 21;33(34):13583-13599, 2013.

Tokimasa T, Akasu T. Cyclic AMP regulates an inward rectifying sodium-potassium current in dissociated bull-frog sympathetic neurones. J Physiol 420:409-429, 1990.

Vaca L, Stieber J, Zong X, Ludwig A, Hofmann F, Biel M. Mutations in the S4 domain of a pacemaker channel alter its voltage dependence. FEBS Lett 479:35–40, 2000.

Vacher H, Trimmer JS. Trafficking mechanisms underlying neuronal voltage-gated ion channel localization at the axon initial segment. Epilepsia 53(Suppl 9):21-31, 2012.

Varela C. Thalamic neuromodulation and its implications for executive networks. Front Neural Circuits 8(69): 1-22, 2014.

Vijayraghavan S, Wang M, Birnbaum SG, Williams GV, Arnsten AF. Inverted-U dopamine D1 receptor actions on prefrontal neurons engaged in working memory. Nat Neurosci 10(3):376-84, 2007.

Wainger BJ, DeGennaro M, Santoro B, Siegelbaum SA, Tibbs GR. Molecular mechanism of cAMP modulation of HCN pacemaker channels. Nature 411:805–810, 2001.

Wang J, Chen S, Nolan MF, Siegelbaum SA. Activity-dependent regulation of HCN pacemaker channels by cyclic AMP: signaling through dynamic allosteric coupling. Neuron 36(3):451-461, 2002.

Wang M, Ramos BP, Paspalas CD, Shu Y, Simen A, Duque A, Vijayraghavan S, Brennan A, Dudley A, Nou E, Mazer JA, McCormick DA, Arnsten AF. Alpha2A-adrenoceptors strengthen working memory networks by inhibiting cAMP-HCN channel signaling in prefrontal cortex.Cell 129(2):397-410, 2007.

Wu X, Ramentol R, Perez ME, Noskov SY, Larsson HP. A second S4 movement opens hyperpolarization-activated HCN channels. Proc Natl Acad Sci U S A. 118(37): e2102036118. 2021.

Weinberger DR, Berman KF, Zec RF. Physiologic dysfunction of dorsolateral prefrontal cortex in schizophrenia. I. Regional cerebral blood flow evidence. Arch Gen Psychiatry 43(2):114-24, 1986.

Yamada R, Kuba H, Ishii TM, Ohmori H. Hyperpolarization-activated cyclic nucleotide-gated cation channels regulate auditory coincidence detection in nucleus laminaris of the chick. J Neurosci 25(39):8867-8877, 2005.

Ye Q, Zhang X. Serotonin activates paraventricular thalamic neurons through direct depolarization and indirect disinhibition from zona incerta. J Physiol. 2021 doi: 10.1113/JP282088. Epub ahead of print. PMID: 34510418.

Zagotta WN, Olivier NB, Black KD, Young EC, Olson R, Gouaux E. Structural basis for modulation and agonist specificity of HCN pacemaker channels. Nature 425:200–205, 2003.

Zhong P, Vickstrom CR, Liu X, Hu Y, Yu L, Yu HG, Liu QS. HCN2 channels in the ventral tegmental area regulate behavioral responses to chronic stress. Elife 7:e32420, 2018.

Zhou L, Siegelbaum SA. Gating of HCN channels by cyclic nucleotides: residue contacts that underlie ligand binding, selectivity, and efficacy. Structure 15:655–670, 2007.

Zobeiri M, Chaudhary R, Datunashvili M, Heuermann RJ, Lüttjohann A, Narayanan V, Balfanz S, Meuth P, Chetkovich DM, Pape HC, Baumann A, van Luijtelaar G, Budde T. Modulation of thalamocortical oscillations by TRIP8b, an auxiliary subunit for HCN channels. Brain Struct Funct 223(3):1537-1564, 2018.

Zobeiri M, Chaudhary R, Blaich A, Rottmann M, Hermann S, Meuth P, Bista P, Kanyshkova T, Lüttjohan A, Narayanan V, Hundehege P, Meuth SG, Romanelli MN, Urbano FJ, Pape HC, Budde T, Ludwig A. The Hyperpolarization-Activated HCN4 Channel is Important for Proper Maintenance of Oscillatory Activity in the Thalamocortical System. Cereb Cortex 29(5):2291-2304, 2019.

Zong X, Zucker H, Hofmann F, Biel M. Three amino acids in the C-linker are major determinants of gating in cyclic nucleotide-gated channels 17(2):353-62, 1998.

7   Appendix

7.1   Primers used for PCR and qPCR experiments

Primers for genotyping

Primer	Sequence 5' - 3'
HCN4_FEA forward	5' CTCAAGGTCTCAGCTGAGG 3'
HCN4_FEA reverse	5' GTAATGTAAGCACACGGTACC 3'

Primers for qPCR

Primer	Sequence 5' - 3'
HCN1 forward	5'-CTGCTGCAGGACTTCCCACCA-3'
HCN1 reverse	5'- ATGCTGACAGGGGCTTGGGC-3'
HCN2 forward	5'-CAGGAACGCGTGAAGTCGGCG -3'
HCN2 reverse	5'-TCCAGGGCGCGGTGGTCTCG-3"
HCN3 forward	5'- TGGCCATGGACCGGCTTCGG-3'
HCN3 reverse	5'-GAGCCAGGCCCCGAACACCAC -3'
HCN4 forward	5'-AGGGCCTTCGAGACGGTTGCGC -3'
HCN4 reverse	5'-GGCCATCTCACGGTCATGCCG -3'
ALAS forward	5'-TCGCCGATGCCCATTCTTATC-3'
ALAS reverse	5'-GGCCCCAACTTCCATCATCT-3'

Primer	Sequence 5'-3'
5HT1A forward	5′-ACC CCA ACG AGT GCA CCA TCA G-3′
5HT1A reverse	5′-GCA GGC GGG GAC ATA GGA G-3′
5HT1B forward	5′-CGA TGC GGT GGA GTA TTC TGC-3′
5HT1B reverse	5′-TAG CGG CCA TGA GTT TCT TCT TTT-3′
5HT3A forward	5′-CAA CGT GGA TGA GAA GAA CCA GG-3′
5HT3A reverse	5′-AGC AAG AGG CTG ACT GCA TAG AAT AAA G-3′
5HT6A forward	5′-CTT TGG ACC GCC TTC GAC GTG ATG TGC T-3′
5HT6A reverse	5′-GGC TGG CCT TCA GGC CTT CCT GCT AT G-3′
5HT7A forward	5′-CCG TGA GGC AGA ATG GGA AAT GTA T-3′
5HT7A reverse	5′-CAC TGC GGT GGA GTA GAT CGT GTA GC-3′
GAPDH forward	5′-GCC GCC TGG AGA AAC CTG CCA AGT-3
GAPDH reverse	5′-TAT TCA AGA GAG TAG GGA GGG CTC-3′

5-HT receptor sequences from León-Ponte et al., 2007

7.2 Antibodies

Primary Antibodies

Antibody	Host	Company	Experiment	dilution
HCN1	rabbit polyclonal	Alomone (APC-056)	IHC	1:300
HCN2	rabbit polyclonal	Alomone (APC-030)	IHC	1:300
			Western blot	1:1000
HCN4	rabbit polyclonal	Alomone (APC-052)	IHC	1:300
			Western blot	1:1000
TRIP8b	mouse polyclonal	NeuroMab (N212_17)	IHC	1:300
			Western blot	1:2000

Secondary Antibodies

Antibody	Host	Company	Experiment	dilution
Cy3 α-rabbit IgG	donkey	Jackson ImmunoResearch (711-165-152)	IHC	1:400
Alexa488 α-rabbit	donkey	Jackson ImmunoResearch (711-545-152)	IHC	1:500
DyLight488 α-mouse	donkey	Jackson ImmunoResearch (715-485-151)	IHC	1:500
α-rabbit HRP	goat	Santa Cruz Biotechnology (sc-2030)	Western blot	1:1000
α-mouse HRP	goat	Santa Cruz Biotechnology (sc-2031)	Western blot	1:1000

7.3   Tables

Subtype	Localization in the brain	Second Messen-ger	Membrane effects	Physiological function	Disease Pathologies	Reference
5-HT$_{1A}$	Dorsal raphe, Hippocampus, Amygdala Thalamus, Cortex, Septal nuclei	Gi/o Increase or decrease in cAMP	Hyperpolarizing Increase in g_K, Decrease in g_{Ca}	Modulation of release of other neurotransmitters (oxytocin, ACTH), Slow wave sleep	Anxiety, MDD, Schizophrenia, Parkinson's disease	Kaufman et al., 2017 Marazziti et al., 1994 Petrunich-Rutherford et al., 2015
5-HT$_{1B}$	Hippocampus, Globus pallidus, Substantia nigra, Amygdala, Thalamus, Lateral septum Basal ganglia	Gi/o, decrease in cAMP	Hyperpolarizing	Nerve terminal autoreceptor; modulation of release of other neurotransmitters, Slow wave sleep, Food intake	MDD, Anxiety, migraine	Monti, 2011 Kjaerby et al., 2016 Pithadia and Jain, 2009
5-HT$_{1D}$	Dorsal raphe, Heart, Basal ganglia, Trigeminal ganglia and nerves, Cranial blood vessels	Gi/o, decrease in cAMP	Unknown, likely hyperpolarizing	Autoreceptor, Food intake, Sensorimortor function	Migraine, Bipolar disorder	Mundo et al., 2001, Longmore et al., 1997
5-HT$_{2A}$	Cortex, Basal ganglia, Septal nuclei, Hippocampus, Amygdala Thalamus, Hypothalamus	Gq/11	Depolarizing (decrease in g_K)	Possible role in learning and memory, Wakefulness, Slow wave sleep	Depression, Schizophrenia, Addiction	Monti, 2011
5-HT$_{2B}$	Cerebellum, Lateral septum, Hypothalamus, Amygdala, Heart	Gq/11	Depolarizing	Food intake; behaviour	Anxiety, Feeding disorders, Cardiac valvulopathies	Diaz et al., 2012
5-HT$_{2C}$	Choroid plexus, Hippocampus, Habenula, Substantia nigra Raphe nuclei, Amygdala, Thalamus, Hypothalamus	Gq/11	Depolarizing	Food intake, neuroendocrine regulation, Wakefulness Slow wave sleep	Feeding disorders; Cognitive impairment, Schizophrenia	Monti, 2011
5-HT$_3$	Hippocampus, Entorhinal cortex, Frontal cortex, Amygdala, Substantia nigra, Ventral tegmental area	None: direct gating of channel	Fast depolarization (increase in g_{Na} and g_K)	Pre-synaptic modulation of transmitter release	Anxiety; Schizophrenia; Cognitive impairment	Fakhfouri et al., 2019
5-HT$_4$	Colliculi, Hippocampus, Peripheral tissues,	Gs Increase in cAMP	Slow depolarization (decrease in g_K)	Modulation of transmitter release, Memory enhancement, cognition	Alzheimer's, Cardiac arrhythmia	Hagena et al., 2017
5-HT$_6$	Striatum, Amygdala, Nucleus accumbens, Hippocampus, Cortex, Olfactory tubercle, Thalamus, Hypothalamus	Gs Increase in cAMP	Depolarizing	Modulation of acetylcholine transmission, food inake	Cognitive impairment	Monti, 2011 Rossé and Schaffhauser, 2010
5-HT$_7$	Cerebral cortex, Thalamus, Hypothalamus, Suprachiasmatic nucleus, Portine nuclei, Amydala, Ventral tegmental area, Nucleus accumbens	Gs, Increase in cAMP	Slow depolarization (increase of I_h)	Control of circadian rhythms, Enhances suppression of REM sleep, Thermoregulation, Mood and behaviour	Schizophrenia, Cognitive impairment Migraine, Nociception, MDD, anxiety	Stiedl et al., 2015, Shelton et al., 2009 Monti, 2011 Hauser et al., 2015

Table 1. Broad overview of the known roles and effects of 5-HT receptors. The localization in the brain, second messenger activation, effects on the membrane, agonists and antagonists, physiological functions, and implicated disease pathologies of 5-HT receptors are summarized. The 5-HT1$_E$, 5-HT1$_F$, 5-HT5$_A$, and 5-HT5$_B$ receptors are not included.

	HCN4	HCN2
Cellular Expression	Dendritic	Somatic and dendritic
Role in transition from burst to tonic firing	Yes	Yes
Role in regulating the RMP	No	Yes
$V_{0.5}$ shift in the presence of cAMP in VB neurons	WT $\Delta V_{0.5}$= +14.31 mV HCN4FEA $\Delta V_{0.5}$= +10.54 mV	WT $\Delta V_{0.5}$= +5.56 mV HCN2EA $\Delta V_{0.5}$= +3.59 mV
Modulation of I_h by 5-HT receptors coupled to $G_{\alpha s}/G_{\alpha i}$	Important	-
Role of CDR in sleep spindles	Yes	-
Role of CDR in the transition from NREM to wake state	Yes	No
Role in absence seizures	No	Yes
Role of CDR in NREM sleep	No	Yes
Role of CDR in an anxiety-like phenotype	Yes	No
Role of CDR in impaired social interaction phenotype	No	No
Role in dLGN-visual pathway	No	Yes
Role in movement deficits	No	No

Table 2. Summary of the neuronal roles of CDR of HCN4 and HCN2. The cellular roles, contribution to I_h, and neuronal phenotypes of HCN2 and HCN4, observed from HCN4FEA mice and HCN2EA mice, are listed. Note: the modulation of I_h by 5-HT receptors coupled to $G_{\alpha s}/G_{\alpha i}$ and the role of CDR in sleep spindles in HCN2EA mice were not investigated and are not known,

7.4   List of Figures

Figure 1. The structure of HCN channels.
Figure 2. Overview of the key features and primary pathways of the somatosensory TC circuit in rodents.
Figure 3. The mechanism of firing modes of TC neurons.
Figure 4. Main neuroanatomical structures which receive afferent 5-HT projections in the rodent brain.
Figure 5. Schematic of the HCN4 channel depicting the 'FEA' mutation.
Figure 6. HCN4 channel co-expression with HCN2 in the VB thalamus.
Figure 7. Expression of HCN channels in the brain.
Figure 8. Lack of cAMP modulation of HCN4 does not alter expression levels of HCN isoforms in the thalamus of WT and HCN4FEA mice.
Figure 9. Interaction of HCN channels in the brain.
Figure 10. HCN channel co-expression with TRIP8b in the VB.
Figure 11. Impaired cAMP dependent regulation of I_h in TC neurons expressing HCN4FEA.
Figure 12. The voltage dependence of activation of I_h shows impaired cAMP dependent modulation in TC neurons expressing HCN4FEA
Figure 13. Activation time constants of HCN4FEA TC neurons in the VB.
Figure 14. The resting membrane potential of HCN4FEA TC neurons in the VB.
Figure 15. I_h density of HCN4FEA TC neurons in the VB.
Figure 16. Impaired cAMP dependent regulation of the HCN4 channel alters firing properties of TC neurons in the VB.
Figure 17. The effect of the RMP on firing properties of WT and HCN4FEA TC neurons in the VB.
Figure 18. HCN4FEA TC neurons display suppressed burst firing.
Figure 19. Time course of 5-HT treatment of WT and HCN4FEA TC neurons.
Figure 20. The voltage dependence of activation of I_h shows a depolarizing shift in the presence of 5-HT in WT but not HCN4FEA TC neurons.
Figure 21. The $V_{0.5}$, RMP and tau of WT and HCN4FEA TC neurons in the VB after 5-HT treatment.
Figure 22. HCN4FEA mice show decreased expression of the 5-HT_7 receptor and α2B adrenergic receptor in the thalamus.
Figure 23. Contribution of the 5-HT_7 receptor to the shift in $V_{0.5}$ of I_h in response to 5-HT.
Figure 24. Power spectra of HCN4FEA mice.
Figure 25. HCN4FEA mice show a reduced number of transitions from the NREM to wake state.
Figure 26. HCN2EA mice do not show a reduced number of transitions from the NREM to wake state.
Figure 27. HCN4FEA mice show a decreased number and length of sleep spindles compared to WT.
Figure 28. The Open Field Test.
Figure 29. HCN4FEA mice show increased anxiety-like behaviour compared to WT mice in The Open Field Test.
Figure 30. HCN4FEA mice show increased anxiety-like behaviour compared to WT mice in The Light-Dark Test.
Figure 31. HCN4FEA mice do not show impaired social interaction in The Social Interaction Test.
Figure 32. CDR of HCN4 does not affect visual learning in the Visual Discrimination Test.
Figure 33. Schematic of the NREM to Wake transition in a TC neuron at the level of the synapse in HCN4FEA compared to WT.

7.5   List of Abbreviations

aa	amino acid
ATP	adenosine triphosphate
ALAS	5'-Aminolevulinate Synthase
APS	ammonium persulfate
a.m.	ante meridiem
aCSF	artificial cerebrospinal fluid
ARAS	ascending reticular activating system
$BaCl_2$	barium chloride
cAMP	3',5'-cyclic adenosine monophosphate
cGMP	3',5'-cyclic guanosine monophosphate
CDR	cAMP dependent regulation
$CaCl_2$	calcium chloride
cm	centimeter
CM	centromedial thalamic nucleus
cGKII	cGMP-dependent protein kinase II
cDNA	complementary DNA
CNBD	cyclic nucleotide binding domain
CNG	cyclic nucleotide-gated
COOH	cytosolic C-terminus
Co-IP	co-immunoprecipitation
°C	degrees celcius
DNA	deoxyribonucleic acid
dNTP	deoxyribose nucleotide triphosphate
dLGN	dorsal lateralgeniculate nucleus
ddH_2O	double distilled water
DRN	dorsal raphe nuclei
EEG	electroencephalography
EM	electron microscopy
EMG	electromyogram
IgG	immunoglobulin G
I_h	Hyperpolarization-activated cation current
GABA	γ-aminobutyric acid
gDNA	genomic deoxyribonucleic acid
GAPDH	glyceraldehyde 3-phosphate dehydrogenase
GPCR	G-protein-coupled receptors
g	gram
GTP	guanosine triphosphate
h	hour
HCl	hydrochloric acid
HCN channel	hyperpolarization-activated-cyclic nucleotide-gated channel
HEPES	4-(2-Hydroxyethyl)piperazine-1-ethanesulfonic acid, N-(2 Hydroxyethyl)piperazineN'-(2-ethanesulfonic acid)
HRP	horseradish peroxidase
Hz	hertz
KO	knock out
L	liter
LDT	light dark test
LTM	long term memory
T_m	melting temperature
$MgCl_2$	magnesium chloride
MDD	major depressive disorder
MFB	medial frontal bundle

MRN	median raphe nuclei
mRNA	messenger RNA
μg	microgram
μL	microliter
μm	micrometer
μM	micromolar
mA	milliampere
mg	milligram
mL	milliliter
mm	millimeter
mM	millimolar
mOsm	milliosmole
min	minute
ms	millisecond
mV	millivolt
M	molar
NaH_2PO_4	monosodium phosphate
NA	noradrenaline
NREM	non rapid eye movement
OCD	obsessive compulsive disorder
O/N	over night
qPCR	quantitative real-time PCR
pA	picoampere
pF	picofarad
PFA	paraformaldehyde
PBS	phosphate buffered saline
pA	picoampere
PCR	polymerase chain reaction
P	postnatal day
pH	potential hydrogen
KCl	potassium chloride
$KMeSO_4$	potassium methane sulfonate
PFC	prefrontal cortex
PKA	Protein Kinase A
RIPA	radio immunoprecipitation assay buffer
REM	rapid eye movement
REM	rapid eye movement
RMP	resting membrane potential
nRT	reticular thalamic nucleus
rpm	revolutions per minute
RNA	ribonucleic acid
5-HT	serotonin
s	second
STM	short term memory
$NaHCO_3$	sodium bicarbonate
NaCl	sodium chloride
SDS	sodium dodecyl sulfate
NaOH	sodium hydroxide
SSC	somatosensory cortex
SWD	spike-and-wave
SEM	Standard error of the mean
TBST	TBS-tween 20
TC	thalamocortical
TEMED	Tetramethylethylenediamine
TPR	tetratricopepide repeat

TRIP8b	Tetratricopeptide repeat-containing Rab8b interacting protein
TTX	tetrodotoxin
EGTA	ethylenglycol-bis(aminoethylether)-N,N,N',N'-tetraacetic acid
TBS	tris buffered saline
Tris	tris(hydroxymethyl)aminomethane
w/v	weight by volume
WT	wildtype
V	volt
$V_{0.5}$	voltage dependence of activation
VPM	ventral posteromedial nucleus
VPL	ventral posterolateral nucleus
VB	ventrobasal
VGlut2	vesicular glutamate transporter type 2
VGCCs	voltage gated calcium channels

7.6 Publications

Cain SM, Bernier LP, Zhang Y, Yung A, **Kass J**, Bohnet, B, Yi Y, Gopaul R, Kozlowski P, MacVicar B, Snutch TP. Hyperexcitable Superior Colliculus and Fatal Brainstem Spreading Depolarization in a Model of SUDEP. Brain Communications 2021. (Accepted Manuscript)

Hammelmann V, Stieglitz MS, Hülle H, Le Meur K, **Kass J**, Brümmer M, Gruner C, Rötzer RD, Fenske S, Hartmann J, Zott B, Lüthi A, Spahn S, Moser M, Isbrandt D, Ludwig A, Konnerth A, Wahl-Schott C, Biel M. Abolishing cAMP sensitivity in HCN2 pacemaker channels induces generalized seizures. JCI Insight 4(9), 2019.

Shimell JJ, Shah BS, Cain SM, Thouta S, Kuhlmann N, Tatarnikov I, Jovellar DB, Brigidi GS, **Kass J**, Milnerwood AJ, Snutch TP, Bamji SX. The X-Linked Intellectual Disability Gene Zdhhc9 Is Essential for Dendrite Outgrowth and Inhibitory Synapse Formation. Cell Rep (8):2422-2437, 2019.

Garcia-Caballero A, Zhang FX, Hodgkinson V, Huang J, Chen L, Souza IA, Cain S, **Kass J**, Alles S, Snutch TP, Zamponi GW. T-type calcium channels functionally interact with spectrin (α/β) and ankyrin B. Mol Brain 11(1):24, 2018.

Thomas SA, Nandan D, **Kass J**, Reiner NE. Countervailing, time-dependent effects on host autophagy promotes intracellular survival of leishmania. J Biol Chem 293(7):2617-2630, 2017.

7.7 Acknowledgements